Signal Acquisition and Tracking for Fixed Wireless Access Multiple Input Multiple Output Orthogonal Frequency Division Multiplexing

A Thesis
Presented to
The Academic Faculty

by

Apurva N. Mody

In Partial Fulfillment
of the Requirements for the Degree
Doctor of Philosophy

School of Electrical and Computer Engineering
Georgia Institute of Technology
October 2004

Signal Acquisition and Tracking for Fixed Wireless Access Multiple Input Multiple Output Orthogonal Frequency Division Multiplexing

Approved by:

Dr. Gordon L. Stüber,
Advisor and Committee Chair
Electrical and Computer Engineering

Dr. Ye (Geofferey) Li
Electrical and Computer Engineering

Dr. Douglas B. Williams,
Electrical and Computer Engineering

Dr. Nikil S. Jayant,
Electrical and Computer Engineering

Dr. Alfred Andrew,
Mathematics

Date Approved: 9 November 2004

To,

My father, Narendra and my mother, Jyotsna

for their patience and support for all these years.

PREFACE

This thesis is an attempt to provide a holistic solution to the receiver implementation for the broadband fixed wireless access (BFWA) multiple-input multiple-output (MIMO) orthogonal frequency division multiplexing (OFDM) systems.

OFDM has been adopted into several wire-line and wireless standards for telecommunications. This is due to its ease in implementation and its robustness to the multi-path wireless channels. In addition, OFDM allows adaptive bit loading which can utilize the channel in an efficient manner.

OFDM and MIMO form a strong companionship and complement each other in their capabilities. MIMO systems are slowly obtaining a wider acceptability because of the increasing capabilities of the digital signal processing (DSP) chips, application specific integrated circuits (ASICs) and field programmable gate array(FPGA)s, rendering the implementation of advanced signal processing algorithms no longer a difficult task. In addition, a strong demand for high-speed wireless applications has breathed a new life into research in these areas.

In spite of all its advantages, such systems suffer from implementation and complexity issues which must be addressed before their successful deployment. MIMO systems require sophisticated algorithms and accurate system modeling for an efficient implementation. The implementation algorithms must focus on signal acquisition and tracking problems. Signal acquisition consists of time and radio frequency (RF) oscillator synchronization, sampling frequency (SF) offset estimation and correction, phase noise estimation and correction and finally channel estimation. Signal tracking consists of tracking all these parameters. In addition, a bench mark is needed to test the performance of these algorithms and this is can be obtained by deriving the Cramér-Rao bounds for such systems.

So far, most authors have focussed on these issues individually and for single-input single-output (SISO) OFDM systems. Most of these problems are inter-connected and need

joint estimation for an efficient system implementation. Hence in this thesis we first try and understand this problem by developing a comprehensive system model for a MIMO-OFDM system under all these impairments [66], and later attempt to provide a solution to estimate the various parameters. We believe that this is just a starting point for this research and it will serve as a beginning for many more contributions in the future.

ACKNOWLEDGEMENTS

First and foremost, I wish to express my deepest sense of gratitude to my advisor, Dr. Gordon L. Stüber, for being my mentor in all respects of education and research. He has provided me with invaluable guidance and support, throughout the course of my Ph. D. studies. But for his keen interest and support, this thesis would not have taken the present form.

I wish to sincerely thank Dr. Nikil S. Jayant, my Ph. D. proposal committee chair, who has been a constant source of advice and encouragement during my Ph. D. studies. I would like to extend my heartfelt thanks to Dr. Douglas B. Williams for his tremendous help and support in and outside of my research. I would like to thank Dr. Ye (Geofferey) Li for being on my reading committee and for his invaluable suggestions throughout the course of my Ph. D. studies. I would like to thank Dr. Alfred Andrew from the School of Mathematics at Georgia Tech for willingly agreeing to serve as my external committee member. The courses that I took under you have helped my research to a great extent.

I was privileged to have worked with Dr. John R. Barry, Dr. Steven W. McLaughlin, Dr. Ian Akyildiz, Dr. Mary Ann Ingram, Dr. Raghupathy Sivakumar and their students. It was indeed a great pleasure to take courses and learn from you. I would like to thank Marilou Mycko who has become one my best friends and a well wisher. I would like to offer my special thanks to Raviv Raich who has been a long time friend now, for patiently going through my thesis and providing me with useful suggestions. I am grateful to all the teachers and professors who have taught me so far, and made this accomplishment possible. I would like to thank the Yamacraw initiative of the State Government of Georgia and the National Science Foundation (NSF) for funding my research project.

I would like to thank all my colleagues for their support, co-operation and kindness. It has been a privilege to have known y' all and I look forward to visiting y' all wherever you might be on this earth. I am deeply and sincerely grateful to all my friends, roommates

and house-mates. You supported me, taught me, fed me, encouraged me and without y' all my Ph. D. studies would have been like a rainbow without any colors. I will never forget the fantastic experiences which inspired me to write so many poetries about you.

I would like to thank my sister Ami for her immense love and affection, my uncle Kiran, my aunt Alka and my cousin sisters Shivani, Eshani and her husband Nilesh, who have supported me through thick and thin. I would like to acknowledge, the support and love of my other aunt Nimisha, my uncle Kiran and the two sweetest cousin sisters Jui and Jill. I would like to thank Shirishbhai' s family for hosting me when I came to Atlanta. I will never forget all the families in Atlanta, and especially my music teacher Kakali Bandhyopadhyaya and her husband Dibyendu for their constant affection, support and taunts to finish my Ph. D. fast so that I can get married and settle down in life. I would like to deeply and sincerely thank all my relatives for constantly sending me words of encouragement, for all their love and kindness. A lot of my inspiration has come from my grandmother, Shashiba' s struggle with old age and arthritis. Even at such an old age I am always amazed with her alertness and mental agility. Finally, I attribute all the successes in my life to the values imbibed in me by my parents, to whom I would like to dedicate my thesis. I am immensely indebted to my father, Narendra and my mother, Jyotsna who, in spite of all their hardships and sufferings have taught me the values of truth, endurance and patience and who always encouraged me to pursue my goals. I would not be what I am today, without the unfaltering faith and love of all of you.

TABLE OF CONTENTS

LIST OF TABLES

LIST OF FIGURES

LIST OF ABBREVIATIONS

A/D	analog to digital
ADSL	asymmetric digital subscriber loop
ASIC	application specific integrated circuit
AWGN	additive white Gaussian noise
BER	bit error rate
BPSK	binary phase shift keying
BFWA	broadband fixed wireless access
BLAST	Bell labs layered space-time
CP	cyclic prefix
CPE	customer premises equipment
CRB	Cramér-Rao bound
D/A	digital to analog
DAB	digital audio broadcasting
DMT	discrete multi-tone
DL	downlink
DSL	digital subscriber loop
DSP	digital signal processing
DVB	digital video broadcasting
FCC	federal communications commission
FDMA	frequency division multiple access
FDE/FEQ	frequency domain equalizer
FFT	fast Fourier transform
FPGA	field programmable gate array
FWA	fixed wireless access
ICI	inter-carrier interference
ISI	inter-symbol interference

IFFT	inverse fast Fourier transform
ITU	international telecommunications union
LDPC	low density parity check
LS	least squares
MBWA	mobile broadband wireless access
MCM	multi-carrier modulation
MIMO	multiple-input multiple output
ML	maximum likelihood
MMSE	minimum mean squared error
MRRC	maximal ratio receive combining
MSE	mean squared error
NC-DLL	non-coherent delay locked loop
OFDM	orthogonal frequency division multiplexing
QAM	quadrature amplitude modulation
QPSK	quaternary phase shift keying
PAM	pulse amplitude modulation
ppm	parts per million
RF	radio frequency
rms	root mean squared
SF	sampling frequency
SISO	single-input single-output
SMMR	spectral max to min ratio
SNR	signal to noise ratio
STBC	space-time block code
STC	space-time code
SVD	singular value decomposition
TDE/TEQ	time domain equalizer
TDMA	time division multiple access
UL	uplink

UNII	United States national information infrastructure
WLAN	wireless local area network
WMAN	wireless metropolitan area network
ZF	zero-forcing

SUMMARY

The general objective of this proposed research is to design and develop signal acquisition and tracking algorithms for multiple input multiple output orthogonal frequency division multiplexing (MIMO-OFDM) systems for fixed wireless access applications. The algorithms are specifically targeted for systems that work in time division multiple access (TDMA) and frequency division multiple access (FDMA) frame modes. In our research, we first develop a comprehensive system model for a MIMO-OFDM system under the influence of the radio frequency (RF) oscillator frequency offset, sampling frequency (SF) offset, RF oscillator phase noise, frequency selective channel impairments and finally the additive white Gaussian noise (AWGN). We then develop the acquisition and tracking algorithms to estimate and track all these parameters. The acquisition and tracking algorithms are assisted by a preamble consisting of one or more training sequences and pilot symbol matrices. Along with the signal acquisition and tracking algorithms, we also consider design of the MIMO-OFDM preamble and pilot signals that enable the suggested algorithms to work efficiently.

Signal acquisition as defined in our research consists of time and RF synchronization, SF offset estimation and correction, phase noise estimation and correction and finally channel estimation. Signal tracking consists of RF, SF, phase noise and channel tracking. Time synchronization, RF oscillator frequency offset, SF oscillator frequency offset, phase noise and channel estimation and tracking are all research topics by themselves. A large number of studies have addressed these issues, but usually individually and for single-input single-output (SISO) OFDM systems. In the proposed research we present a complete suite of signal acquisition and tracking algorithms for MIMO-OFDM systems along with Cramér-Rao bounds for the SISO-OFDM case. In addition, we also derive the Maximum Likelihood (ML) estimates of the parameters for the SISO-OFDM case.

Our proposed research is unique from the existing literature in that it presents a complete

receiver implementation for MIMO-OFDM systems and accounts for the cumulative effects of all possible acquisition and tracking errors on the bit error rate (BER) performance. The suggested algorithms and the pilot/training schemes may be applied to any MIMO OFDM system and are independent of the space-time coding techniques that are employed.

CHAPTER I

INTRODUCTION

In this chapter we introduce multiple-input multiple-output orthogonal frequency division multiplexing (MIMO-OFDM) systems. In Section 1.1, we introduce the OFDM transmission technique, cite its advantages, application and implementation. In Section 1.2 we introduce a typical MIMO system and give examples of the existing MIMO-OFDM systems. In our work in [66], we have introduced a new and comprehensive model for a MIMO-OFDM system under the influence of the radio frequency (RF) oscillator frequency offset, sampling frequency (SF) offset, RF oscillator phase noise, frequency selective channel and finally the additive white Gaussian noise (AWGN). Hence in Section 1.3, we define the MIMO-OFDM system model and the problem statement for this thesis.

Throughout this thesis, we will be using the following notations to represent the various entities. *Notation:* Bold upper case letters denote matrices, and upper case letters with an underline denote vectors; $(\cdot)^*$, $(\cdot)^T$ and $(\cdot)^H$ denote conjugate and transpose and conjugate transpose operations, respectively; E[·] and Var(·) are the expectation and variance operators; $||\cdot||$ stands for the norm of a vector; $\odot$ refers to the Schur-Hadamard [33] product or an element by element multiplication between the two vectors; $\Re\{\cdot\}$ refers to the real part of an entity; $\mathbf{I}_K$ stands for an identity matrix of size K; Tr[·] denotes the trace of a matrix; Diag(·) denotes a diagonal matrix. Most of the times, *Upper* case letters are used to represent the entities in the frequency domain and the *lower* case letters are used to represent the entities in the time domain.

1.1 Orthogonal Frequency Division Multiplexing

Orthogonal frequency division multiplexing (OFDM) has become a popular data transmission technique over wired and wireless media. It has been adopted in several wireless standards, including digital subscriber loops (DSL) [8], digital audio broadcast (DAB) [28],

digital video broadcast (DVB) [27] the IEEE 802.11 wireless local area network (WLAN) standard [35] and the IEEE 802.16a [37] wireless metropolitan area network (WMAN) standard which is also referred to as broadband fixed wireless access (BFWA). Future applications include mobile broadband wireless access (MBWA) (IEEE 802.20) [38] mobile wireless dedicated short range communications (DSRC) in the 5.850 5.925 GHz band, fourth generation (4G) mobile and the residential power line communications. Figure 1 shows the channelization of the OFDM spectra for different users in the 5.15-5.85 GHz UNII band.

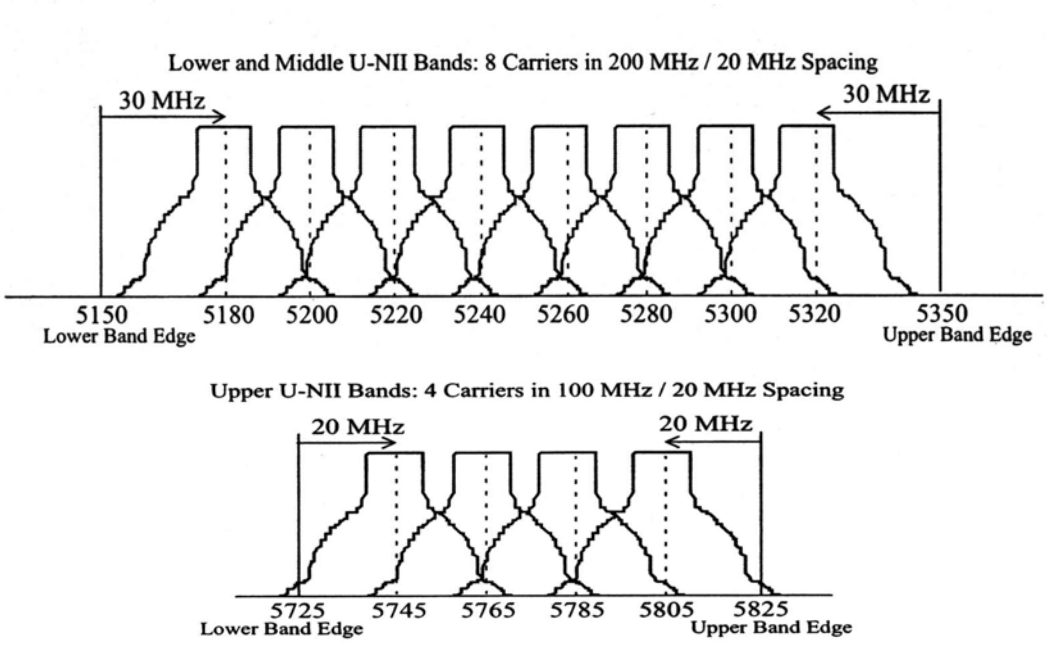

Figure 1: Spectrum allocation for the systems operating using the IEEE 802.11a Standard in the UNII band [37].

OFDM is a type of a multi-carrier modulated (MCM) system. MCM consists of dividing a wide-band channel into a number of narrow-band sub-channels and modulating each subcarrier separately depending upon its signal to noise ratio (SNR, E_s/N_0). This is also called as the adaptive bit loading principle. The sub-carriers are made orthogonal to each other so that they can be demodulated without any inter-channel or inter-carrier interference (ICI). The main advantages of MCM are its high spectral efficiency due to the closely packed orthogonal sub-carriers, adaptive data loading depending upon the available signal

to noise ratio per subcarrier and resilience to the inter-symbol or inter-block interference (ISI) [71]. Another major advantage of MCM is that it converts a frequency selective channel into a number of independent flat-faded sub-channels which can be individually modulated. This allows a simpler receiver implementation since a single tap frequency domain equalizer (FEQ/FDE) may be used at each of the sub-carrier to undo the effects of the channel instead of a complicated time-domain equalizer (TEQ/TDE) that is needed for the traditional single-carrier (SC) systems.

Figure 2 (a) and (b) show the OFDM spectra in frequency non-selective and frequency selective channels respectively. In frequency selective channels it is possible to perform adaptive bit loading on the OFDM sub-carriers provided that the knowledge of the channel is available at the transmitter. Sub-channels with a lower attenuation are modulated with a larger constellation to transmit more data on them.

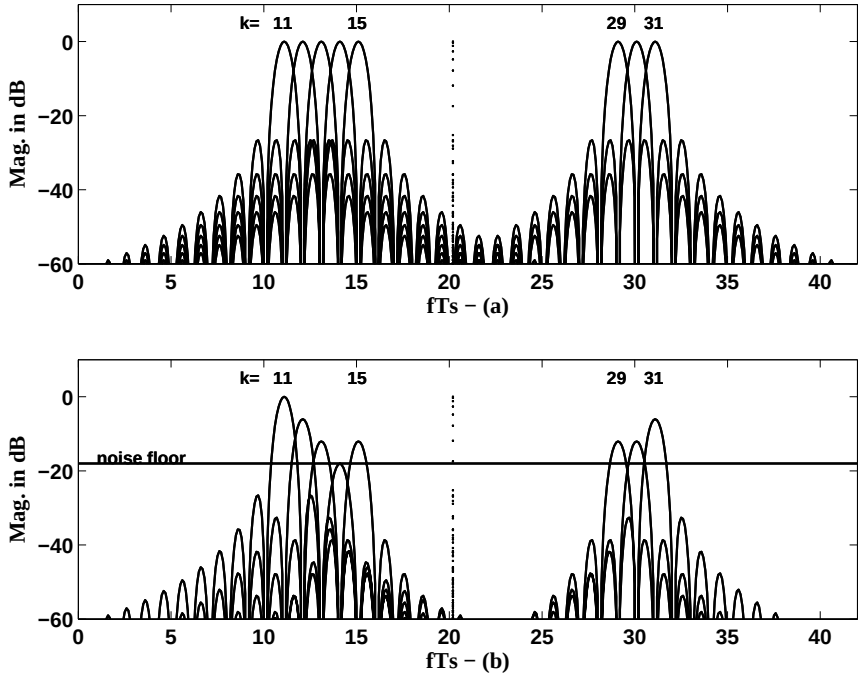

Figure 2: OFDM spectrum in (a) frequency non-selective and (b) frequency-selective channels

The sub-channel bandwidths of the OFDM must be kept much smaller than the coherence bandwidth; where coherence bandwidth is defined as the reciprocal of the maximum

multi-path delay spread (T_m) of the channel [77]. In other words, the symbol period (T_s) of an MCM signal should be kept much *larger* than T_m. Hence, each of the individual sub-channels experiences nearly flat fading and the distortions introduced due to the channel can be corrected individually for each of the sub-carriers by using a simple one tap equalizer [14, 85].

When a serial data train is transmitted in parallel, it results in a symbol whose period is much longer than the maximum delay spread of the channel. This dramatically reduces the effect of time dispersion or multi-path on the transmitted symbols. However, keeping data rate the same and increasing the symbol period requires increase in the number of sub-carriers (N). This results in an increase in the maximum end-to-end transmission delay and the computational complexity of the system in terms of processing power and memory. At the same time, increasing the symbol period makes OFDM signal sensitive to the time selective fading of the channel. This results in a loss of orthogonality between the sub-carriers and causes ICI [80, 91, 93]. Hence, the symbol period of an MCM signal needs to be kept much *smaller* than the coherence time of the channel and can not be increased indefinitely. Coherence time is defined as the reciprocal of the maximum Doppler frequency (f_m) [77]. As mentioned above, a long time-domain symbol is resilient to multi-path channel. However, the length of the OFDM symbol can not be increased indefinitely. Hence, a guard interval, or a cyclic prefix of time duration T_g or G samples is inserted in front of the OFDM symbol. The length of this cyclic prefix should be ideally greater than or equal to the maximum delay spread of the channel. As long as the cyclic prefix has a duration greater than T_m, it would maintain orthogonality between the sub-carriers and eliminate ISI at a cost of a rate loss and power loss by a factor proportional to $G/(N+G)$.

1.1.1 Continuous Time Representation of OFDM

An OFDM signal with a guard interval of time duration T_g can be represented as [7]

$$s(t) = \sum_{d=-\infty}^{\infty} \sum_{k=0}^{N-1} S_k^d \Psi_k^d(t) \tag{1}$$

where S_k^d is the information symbol for the d^{th} OFDM symbol and the k^{th} carrier. $\Psi_k^d(t)$ form the orthogonal basis which can be represented as

$$\Psi_k^d(t) = g_k(t - dT_s) \tag{2}$$

$$g_k(t) = \begin{cases} e^{j2\pi f_k t} & -T_g \leq t \leq T_u \\ 0 & \text{otherwise,} \end{cases} \tag{3}$$

where

$$f_k = f_0 + k/(T_u) \quad 0 \leq k \leq (N-1) \tag{4}$$

are the N subcarriers which are separated by a distance of the reciprocal of the useful symbol time $T_u = T_s - T_g$, and T_s is the total symbol time.

The basis $\Psi_k^d(t)$ are orthogonal and satisfy the conditions

$$\int_{-\infty}^{\infty} \Psi_k^d(t) \Psi_{k'}^{d'*}(t) = 0 \quad d \neq d' \;\; k \neq k' \tag{5}$$

and

$$\int_{-\infty}^{\infty} |\Psi_k^d(t)|^2 dt = T_u + T_g = T_s. \tag{6}$$

Suppose $h(t)$ is the channel impulse response and $*$ operation denotes linear convolution, the received signal $r(t)$ can be expressed as $r(t) = h(t) * s(t)$.

At the receiver, the received OFDM signal $r(t)$ can be demodulated using

$$R_k^d = \frac{1}{T_u} \int_{-\infty}^{\infty} r(t) \Psi_k^{d'*}(t) dt \tag{7}$$

where R_k^d would equal S_k^d in absence of noise, and any other distortion. $\Psi_k^{d'*}(t)$ are the modified basis after the removal of the guard such that

$$\Psi_k^{d'}(t) = g_k^{'}(t - iT_s) \tag{8}$$

$$g_k^{'}(t) = \begin{cases} e^{j2\pi f_k t} & 0 \leq t \leq T_u \\ 0 & \text{otherwise.} \end{cases} \tag{9}$$

1.1.2 Discrete Time Representation of OFDM

In the previous section we described the continuous time description for the implementation of an OFDM system. However, commercial OFDM systems are implemented in the discrete time in a slightly different manner. In 1971, Weinstein and Ebert [112] suggested that a multi-carrier system can be efficiently implemented in discrete time using an inverse fast Fourier transform (IFFT) to act as a modulator and a fast Fourier transform (FFT) as a demodulator. The actual data to be transmitted, now represent "frequency" domain coefficients of the signal and the samples at the output of the IFFT stage are in the "time" domain. This method considerably simplifies the implementation of a multi-carrier system and has made it a popular transmission technique for wireless applications, digital subscriber lines, broadcasting etc. [43].

Let $\{S_k^d\}_{k=0}^{N-1}$ be the input symbols to the N-point IFFT for q^{th} transmit antenna. *Capital* letter in S_k^d is used to emphasize that input symbols are in the frequency domain. The output sequence of the IFFT is

$$s_n^d = \frac{1}{\sqrt{N}} \sum_{k=0}^{N-1} S_k^d \exp\left(j\frac{2\pi nk}{N}\right) \quad 0 \leq n \leq N-1. \tag{10}$$

A cyclic prefix is inserted in front of the IFFT output sequence as shown in the Figure 7. The time length of the cyclic prefix should be greater than the maximum delay spread of the channel. The main function of the cyclic prefix is to guard the OFDM symbol against inter-symbol interference. Hence, this cyclic prefix is called the guard interval of the OFDM symbol and has a time duration $T_g = GT$, where G is the number of samples in the cyclic prefix and $1/T$ is the sampling frequency at the output of the cyclic prefix inserter. The guard-inserted sequence is applied to a pair of balanced D/A converters, up-converted to radio frequency, and transmitted over the channel. The received sequence for the $(dT_s)^{\text{th}}$ time instant after the removal of the guard interval is given by

$$r_n^d = \sum_{m=0}^{M-1} h_{d(N+G)+n}(m) s_{(n-m)_N}^d + w_n^d, \tag{11}$$

where $h_{d(N+G)+n}(m)$ is the channel impulse response for the m^{th} tap at the $(d(N+G)+n)^{\text{th}}$ instant and T_s is the OFDM symbol period including the guard interval. The w_n^d are complex

additive white Gaussian noise samples with $\mathrm{E}[|w_n^d|^2] = N_0$. The received sample sequence $\{r_n^d\}_{n=0}^{N-1}$ is demodulated as

$$\begin{aligned} R_k^d &= \mathrm{FFT}\{\underline{r}^d\}(k) \\ &= H_k^d S_k^d + W_k^d \end{aligned} \tag{12}$$

where [80]

$$H_k^d = \sum_{m=0}^{M-1} H_m^d(0) \exp\left(\frac{-j2\pi km}{N}\right) \tag{13}$$

and where

$$H_m(0) = \frac{1}{N} \sum_{n=0}^{N-1} h_{(N+G)+k}(m). \tag{14}$$

This is the discrete-time system representation of the OFDM system.

Figures 3 and 4 show the implementation of an OFDM modulator and demodulator for a system operating using the IEEE 802.16a Standard with a block-size of 256 sub-carriers. These figures show the sub-carrier allocations for the IEEE 802.16a system. As shown in

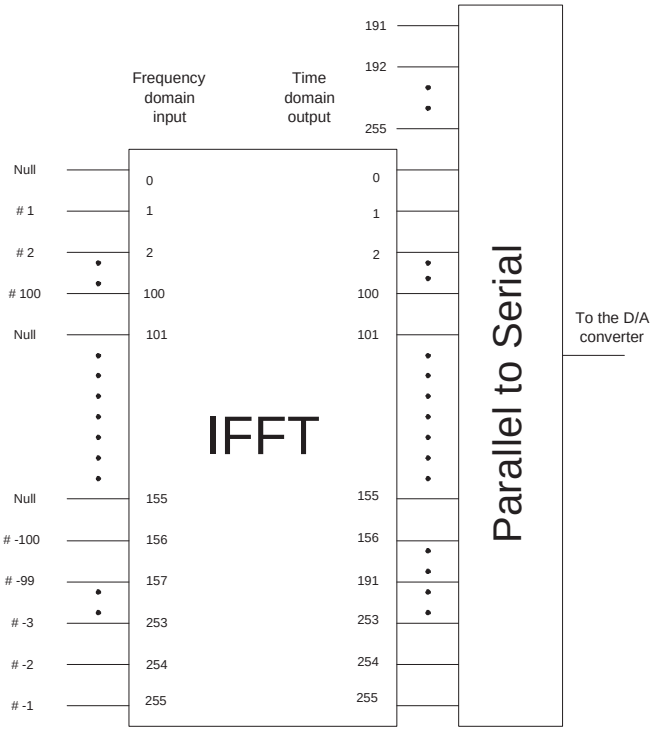

Figure 3: Implementation of the IEEE 802.16a OFDM modulator.

the figure, out of the 256 sub-carriers, the dc sub-carrier and 55 other sub-carriers at the

band edges are set to zero [37]. Therefore, the number of used sub-carriers, $N_u = 200$; or in other words, $[1 \ldots 100\ 156 \ldots 255]$, are used. The 55 sub-carriers at the band-edges are

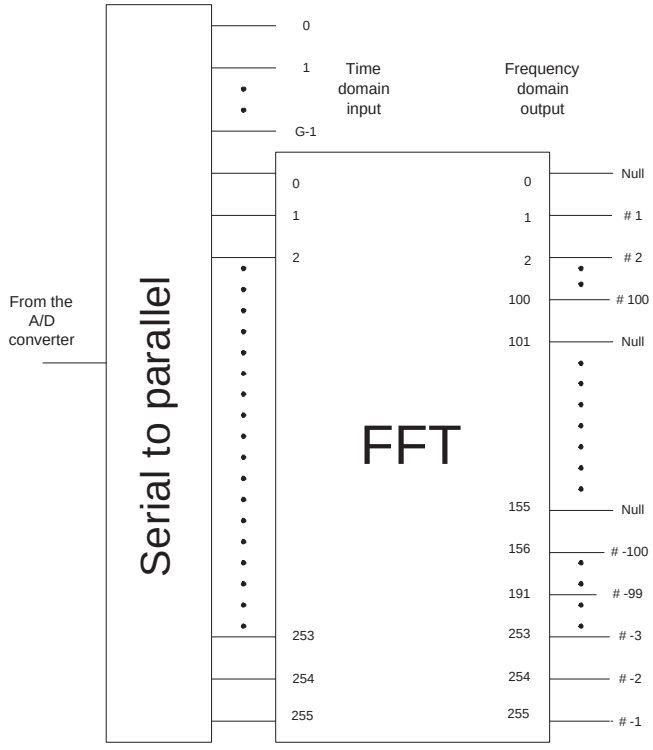

Figure 4: Implementation of the IEEE 802.16a OFDM demodulator.

termed as virtual sub-carriers and are nulled to prevent adjacent channel/user interference and ease in the implementation of the analog/ digital filters at the receiver.

1.2 Multiple Input Multiple Output Systems

To further exploit the spatial diversity of the wireless channel, OFDM systems may employ multiple antennas at the transmitter and the receiver to create a MIMO channel. A typical diagram of a MIMO-OFDM system is shown in Figure 5.

To exploit the benefits of a MIMO channel, the in-coming data is arranged in a manner such that it forms a specific pattern over space and time. Such space-time codes enable the receiver to extract the benefits of increased channel capacity and diversity gains. Diversity gain enables the improvement of the BER performance of the system. It increases the slope of the BER curve when plotted versus the E_s/N_0 available per each receiver branch. A

receiver with L receive antennas can provide an L-fold diversity gain [113].

Furthermore, a MIMO system can employ more than one transmit antenna to increase the net system capacity. A system with Q transmit antennas can push Q-times the amount of data as compared to a system with a single transmit antenna and hence provides a Q-fold increase in channel capacity [29,30,101]. The detector that minimizes the probability of error for such a scheme is the maximum likelihood (ML) detector. However, the implementation complexity of such a detector increases exponentially with the number of transmit antennas.

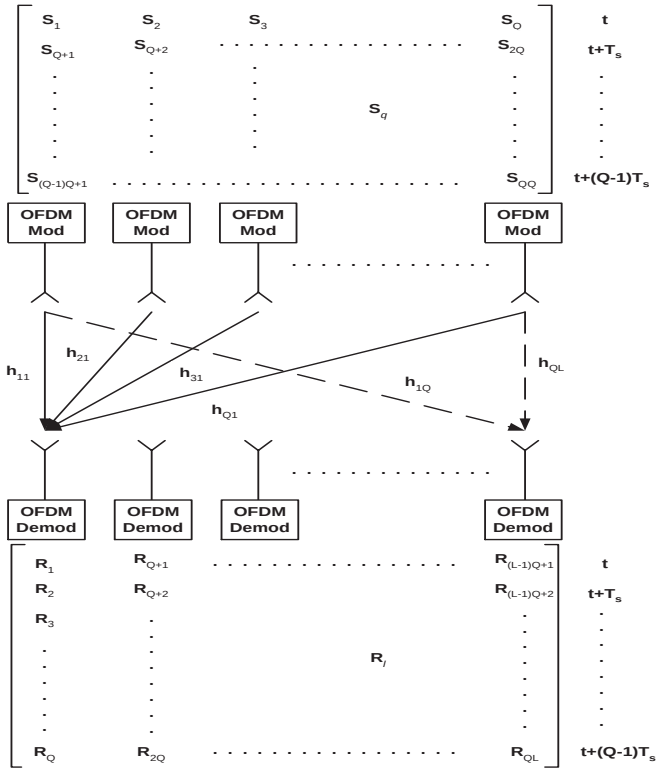

Figure 5: A generic diagram of a MIMO-OFDM system with Q-Transmit antennas and L-Receive antennas.

Sometimes it is necessary to reduce the number of receiver RF chains at the customer premises equipment (CPE) and to keep the decoding complexity of the space-time structures low to reduce the system costs. In order to achieve this, multiple transmitters are employed at the transmitter instead of the receiver [6, 99, 100, 114]. Such a system results in the formation of space-time structures where the elements of these structures are constructed by linearly combining the in-coming symbols over space and time. These structures are termed

as space-time codes (STC) and when these extend over several symbols, they are termed as space-time block-codes (STBC). For example, for $Q = 2$ transmit antennas, Alamouti' s [6] space-time structure has gained a lot of popularity and has been incorporated into several wireless standards [35–37]. It is given by

$$\mathbf{S}_k = \frac{1}{\sqrt{2}} \begin{bmatrix} S_k^1 & S_k^2 \\ -S_k^{2*} & S_k^{1*} \end{bmatrix}, \tag{15}$$

where k is the sub-carrier index and the rows indicate the space dimension and the columns indicate the time. Since in the Alamouti' s scheme, two symbols are transmitted over two time slots, this code is referred to as a full-rate or rate-1 STBC. Likewise for $Q = 4$ two structures exist. One, when the alphabet used to construct the STC uses one dimensional constellation points such as binary phase shift keying (BPSK) and M-ary pulse amplitude modulation (M-PAM) [12, 77]. The signal transmission matrix for $Q = 4$ transmit antennas is given by [100]

$$\mathbf{S}_k = \frac{1}{\sqrt{4}} \begin{bmatrix} S_k^1 & S_k^2 & S_k^3 & S_k^4 \\ -S_k^2 & S_k^1 & -S_k^4 & S_k^3 \\ -S_k^3 & S_k^4 & S_k^1 & -S_k^2 \\ -S_k^4 & -S_k^3 & S_k^2 & S_k^1 \end{bmatrix}. \tag{16}$$

The above STBC is once again a rate-1 STBC. For a two dimensional alphabet such as quadrature phase shift keying (QPSK), and M-ary quadrature amplitude modulation (M-QAM), a rate-1 STC with full diversity gain does not exist. For example, for $Q = 3$ Transmit antennas, one of the example of a rate-3/4 code with full diversity gain is

$$\mathbf{S}_k = \frac{1}{\sqrt{4}} \begin{bmatrix} S_k^1 & S_k^2 & \frac{S_k^3}{\sqrt{2}} \\ -S_k^{2*} & S_k^{1*} & \frac{S_k^3}{\sqrt{2}} \\ \frac{S_k^{3*}}{\sqrt{2}} & \frac{S_k^{3*}}{\sqrt{2}} & \frac{-S_k^1 - S_k^{1*} + S_k^2 - S_k^{2*}}{2} \\ \frac{S_k^{3*}}{\sqrt{2}} & -\frac{S_k^{3*}}{\sqrt{2}} & \frac{S_k^2 + S_k^{2*} + S_k^1 - S_k^{1*}}{2} \end{bmatrix}, \tag{17}$$

and for $Q = 4$ transmit antennas, an example of a rate-3/4 STBC with full diversity is

$$\mathbf{S}_k = \begin{bmatrix} S_k^1 & S_k^2 & \frac{S_k^3}{\sqrt{2}} & \frac{S_k^3}{\sqrt{2}} \\ -S_k^{2*} & S_k^{1*} & \frac{S_k^3}{\sqrt{2}} & -\frac{S_k^3}{\sqrt{2}} \\ \frac{S_k^{3*}}{\sqrt{2}} & \frac{S_k^{3*}}{\sqrt{2}} & \frac{(-S_k^1 - S_k^{1*} + S_k^2 - S_k^{2*})}{2} & \frac{(-S_k^2 - S_k^{2*} + S_k^1 - S_k^{1*})}{2} \\ \frac{S_k^{3*}}{\sqrt{2}} & -\frac{S_k^{3*}}{\sqrt{2}} & \frac{(S_k^2 + S^{2*}{}_k + S_k^1 - S_k^{1*})}{2} & -\frac{(S_k^1 + S_k^{1*} + S_k^2 - S_k^{2*})}{2} \end{bmatrix}. \tag{18}$$

The main advantage of STBCs suggested by Alamouti and Tarokh is that the complexity of the ML detection algorithms for these codes increases only linearly and not exponentially with the number of transmit antennas. The simplicity in decoding of the STBCs comes from the orthogonality of its columns. For example for the Alamouti' s transmit diversity scheme, the ML decoding metric to be minimized is

$$\sum_{l=1}^{Q} \left(\left| R_k^{1,l} - H_k^{1,l} S_k^1 - H_k^{2,l} S_k^2 \right|^2 + \left| R_k^{2,l} + H_k^{1,l} S_k^{2*} - H_k^{2,l} S_k^{1*} \right|^2 \right) \tag{19}$$

The above decoding metric can be seperated into a term containing only S_k^1 as

$$\left| \left[\sum_{l=1}^{L} \left(R_k^{1,l} H_k^{1,l*} + R_k^{2,l*} H_k^{2,l} \right) \right] - S_k^1 \right|^2 + \left(-1 + \sum_{l=1}^{L} \sum_{q=1}^{2} \left| H_k^{q,l} \right|^2 \right) \left| S_k^1 \right|^2 \tag{20}$$

and a term containing only S_k^2 as

$$\left| \left[\sum_{l=1}^{L} \left(R_k^{1,l} H_k^{2,l*} - R_k^{2,l*} H_k^{1,l} \right) \right] - S_k^2 \right|^2 + \left(-1 + \sum_{l=1}^{L} \sum_{q=1}^{2} \left| H_k^{q,l} \right|^2 \right) \left| S_k^2 \right|^2. \tag{21}$$

In the similar fashion we can obtain the seperable ML decoding for the signals for other codes. It is found that a code with Q transmit and L receive antennas provides the same performance as a system with $Q \times L$ maximal ratio receive combining (MRRC) [113, 114].

In essence, OFDM converts a frequency selective channel into a number of individually flat sub-channels, whereas, a MIMO system provides either a diversity gain or increase in the system capacity or both. Hence MIMO and OFDM form an ideal choice for a high data rate wireless communication systems of the future.

1.3 MIMO-OFDM System Description and Modeling

This section describes the comprehensive system model that we developed in our work in [66], which includes the effects of the RF oscillator frequency offset, SF offset, RF oscillator

phase noise, frequency selective channel and finally the AWGN. This model also lays out the ground work for the problem statement for this thesis.

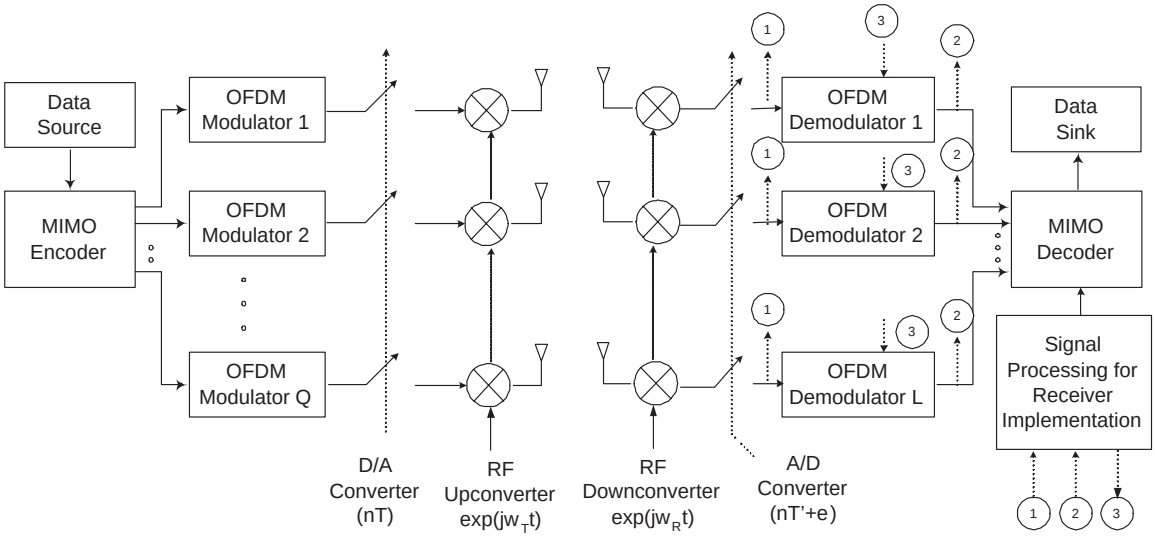

Figure 6: Q-Transmit L-Receive MIMO OFDM system.

Figure 6 shows a MIMO-OFDM system with Q transmit and L receive antennas. The individual OFDM modulators and demodulators are implemented using an N-point IFFT and FFT, respectively. A block of N data symbols specifies the frequency domain coefficients input to the IFFT. The block of N time domain coefficients at the IFFT output constitute an OFDM block. Let $q; 1 \leq q \leq Q$ index the transmit antenna and let $d = 0, 1, \ldots$ be the running OFDM symbol index. Then the time-domain samples are

$$s_n^{d,q} = \frac{1}{\sqrt{N}} \sum_{k'=0}^{N-1} S_{k'}^{d,q} \exp\left\{j2\pi nk'/N\right\},\ 0 \leq n \leq N-1\ , \tag{22}$$

where $S_{k'}^{d,q}$ is the data symbol transmitted from the q^{th} antenna, for the d^{th} OFDM symbol at the k'^{th} sub-carrier. The total average energy transmitted from all Q antennas, E_s, is normalized to unity such that $E_s = \frac{1}{2}\mathrm{E}\left\{\sum_{q=1}^{Q}\left|s_n^{d,q}\right|^2\right\} = 1,\ \forall d,\ n$.

To mitigate the effects of channel delay spread, a cyclic prefix (CP) consisting of the last G coefficients are inserted in front of the OFDM block to form an OFDM symbol as shown in the Figure 7. To fully remove ISI the cyclic prefix duration, $T_g = GT$, must equal or exceed the maximum delay of the channel, T_m, where $1/T$ is the sample rate. The time required

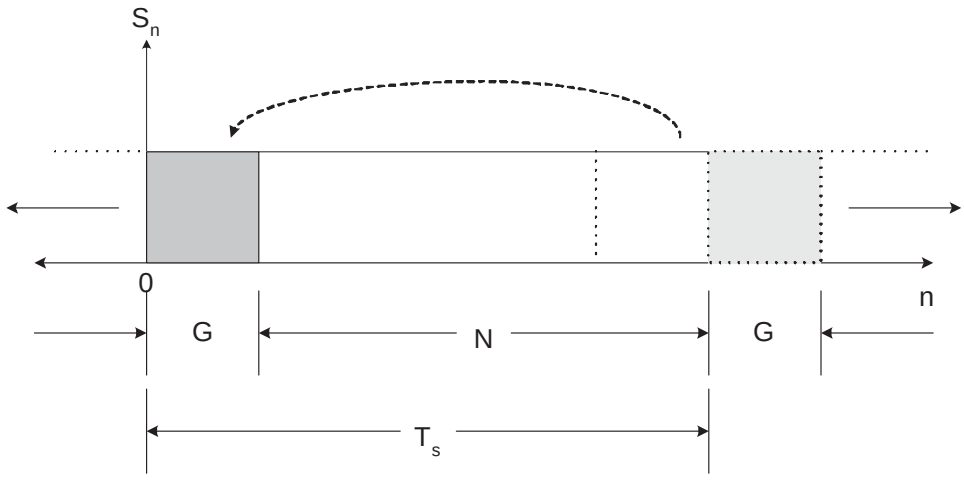

Figure 7: Cyclic prefix (CP) insertion in OFDM to avoid the inter-symbol interference (ISI).

to transmit one OFDM symbol is the OFDM symbol time, $T_s = GT + NT = GT + T_u$, where $T_u = NT$. For each antenna, the corresponding real and imaginary components of the OFDM symbol samples are applied to a pair of D/A converters operating at a sampling frequency of $1/T$ Hz to generate the set of complex envelopes. The set of complex envelopes on the interval $(dT_s, (d+1)T_s)$ is

$$s^{d,q}(t) = \sum_{k'=0}^{N-1} S_{k'}^{d,q} \cdot \exp\left\{ j\frac{2\pi k'}{T_u}(t - (d+1)GT - dNT) \right\}, q = 1, \ldots, Q. \tag{23}$$

The complex envelopes are up-converted to RF with a carrier frequency of f_T Hz. It is assumed that the same RF oscillator is used for all Q RF chains. Similarly, all D/A converters in the transmitter are driven by a common sampling frequency oscillator. The same assumptions are made for the RF and sampling frequency oscillators at the receiver.

The waveforms are transmitted over a $Q \times L$ MIMO channel characterized by the time-variant impulse responses

$$h(\tau, t)^{(q,\ell)} = \sum_{m=0}^{M-1} h_m^{(q,\ell)}(t)\delta(\tau - \tau_m^{(q,\ell)}), \tag{24}$$

where $\{h_m^{(q,\ell)}(t)\}$ are the time varying complex path gains between the q^{th} transmit and the ℓ^{th} receive antenna, $\{\tau_m^{(q,\ell)}\}$ are the corresponding path time delays, and M is the total number of paths for each channel. Assuming that the channel is static for at least one

OFDM symbol duration, the channel transfer functions are given by

$$\tilde{H}_{d,k'}^{(q,\ell)} = \sum_{m=0}^{M-1} h_m^{(q,\ell)}(dT_s) \exp\left\{-j2\pi\tau_m^{q,l}k'/T_u\right\}, k' = 0, \ldots, N-1. \tag{25}$$

The received bandpass signals are down-converted to complex baseband using a local oscillator with carrier frequency f_R Hz. Since the transmitter and the receiver RF oscillators have different frequencies, the received complex envelope is affected by an RF oscillator frequency offset of $\Gamma + \gamma = (f_R - f_T)T_u$ sub-carrier spacings, where Γ and γ refer to the integer and the fractional components of the RF oscillator frequency offset in the units of sub-carrier spacings, respectively. The received complex envelope is also affected by RF oscillator phase noise $\vartheta(t)$. Since Γ has the net effect of shifting the down-converted OFDM signal by an integer number of sub-carrier spacings, it is ignored for the time being in the system equation. We later show a way to estimate and correct this integer offset. The ℓ^{th} received complex baseband signal can be expressed as

$$r^{\ell}(t) = \frac{1}{\sqrt{N}} \sum_{q=1}^{Q} \sum_{k'=0}^{N-1} S_{k'}^{(d,q)} \tilde{H}_{d,k'}^{q,\ell} \exp\left\{\frac{j2\pi k't}{T_u}\right\} \exp\left\{j\left(\frac{2\pi\gamma t}{T_u} + \vartheta(t)\right)\right\} + w^{\ell}(t), \tag{26}$$

where $w^{\ell}(t)$ represents the complex AWGN with a variance of N_0. The real and imaginary components of the received complex baseband waveform are applied a pair of balanced A/D converters with a sampling frequency of $1/T'$ Hz. To counteract the aliasing introduced by the frequency offsets, and for improved parameter estimation, the waveforms are over-sampled by factor of u followed by a uN-point FFT which acts as an OFDM demodulator. Since the sampling frequencies at the transmitter and receiver differ, the received discrete-time samples are affected by the normalized SF offset coefficient $\beta = (T' - T)/T$.

The RF oscillator frequency offset γ drifts slowly with time and, hence, we assume it stays constant for a frame duration. However, the sampling clock and the phase noise suffer from jitters and vary more rapidly than γ. We assume that β and ϑ take on new values every Q OFDM symbols. The n^{th} sample for the d^{th} OFDM symbol may be obtained from $r^{\ell}(t)$ by substituting $t = du(N+G)T'/u + nT'/u + \epsilon = d(N+G)(\beta+1)T + n(\beta+1)T/2 + \epsilon$, where u is the up-sampling factor at the receiver and ϵ is the unknown phase component of the A/D converter. Afterwards, the guard interval is removed and a uN-point FFT

is applied to the samples $\{r_n^\ell\}_{n=0}^{uN-1}$ for the d^{th} OFDM symbol. Assuming that the time synchronization window is accurate, the demodulated samples at the k^{th} sub-carrier are

$$\begin{aligned} R_k^{d,\ell} &= \frac{1}{u\sqrt{N}^2}\sum_{q=1}^{Q}\sum_{k'=0}^{N-1}\sum_{n=0}^{uN-1} S_{k'}^{d,q}\tilde{H}_{k'}^{q,\ell} \\ &\quad \exp\left\{\frac{j2\pi k'}{N}\left[d(N+G)(\beta+1)+n(\beta+1)/u+\epsilon\right]\right\} \\ &\quad \exp\left\{\frac{j2\pi\gamma}{N}\left[d(N+G)(\beta+1)+n(\beta+1)/u+\epsilon\right]\right\} \\ &\quad \exp\left\{\frac{-j2\pi nk}{uN}\right\}\exp\left\{j\vartheta^d\right\}+W_k^{d,\ell} \\ &= \sum_{q=1}^{Q}\left(\sum_{k'=0}^{N-1} S_{k'}^{(d,q)}H_{k'}^{q,\ell}\exp\left\{\frac{j2\pi}{N}\left[d(N+G)(k'\beta+\gamma+\gamma\beta)\right]\right\}\right) \\ &\quad \frac{1}{uN}\frac{\sin[\pi(k'+k\beta+\gamma+\gamma\beta-k)]}{\sin[\frac{\pi}{uN}(k'+k\beta+\gamma+\gamma\beta-k)]}\exp\left\{j\pi(k'+k\beta+\gamma+\gamma\beta-k)(1-\frac{1}{uN})\right\} \\ &\quad \exp\left\{j\vartheta^d\right\}+W_k^{d,\ell} \end{aligned} \tag{27}$$

where $W_k^{d,\ell}$ is the AWGN term in the frequency domain. The above equation can be separated into the useful terms when $k'=k$ and the inter-carrier interference (ICI) terms when $k'\neq k$. This gives

$$\begin{aligned} R_k^{d,\ell} &= \sum_{q=1}^{Q} S_k^{(d,q)}H_k^{q,\ell}\exp\left\{\frac{j2\pi}{N}\left[d(N+G)(k\beta+\gamma+\gamma\beta)\right]\right\} \\ &\quad \frac{1}{uN}\frac{\sin[\pi(k\beta+\gamma+\gamma\beta)]}{\sin[\frac{\pi}{uN}(k\beta+\gamma+\gamma\beta)]}\exp\left\{j\pi(k\beta+\gamma+\gamma\beta)(1-\frac{1}{uN})\right\}\exp\left\{j\vartheta^d\right\} \\ &\quad +W_{k\neq k'}^{d,\ell\ \text{ICI}}+W_k^{d,\ell}, \end{aligned} \tag{28}$$

If the RF oscillators are stable and the phase noise fluctuations are relatively small then the approximation $\exp\left\{j\vartheta^d\right\}\approx 1+j\vartheta^d$ may be made [10], where the imaginary part of the phase noise $j\vartheta^d$ introduces additional noise $W_k^{d,\ell\ \text{PN}}$ into the system. From (28), any residual RF oscillator and SF offsets cause a linear increase in the phase of the received OFDM symbols with time, whereas the phase noise causes random fluctuations of the phase. All these, if not removed, may result in an excessive BER degradation. For example, Figure 8 shows the real and imaginary (I-Q) plot of the received demodulated 16-QAM constellation, for a 4×4 system, with β=0, and frame length F=80 OFDM symbols at bit energy per noise ratio (E_b/N_0) of 10 dB. Figure 9 shows I-Q plot of the same system in presence of an SF offset of $\beta = 10$ parts per million (ppm). Finally, Figure 10 shows the effect of the SF offset on the

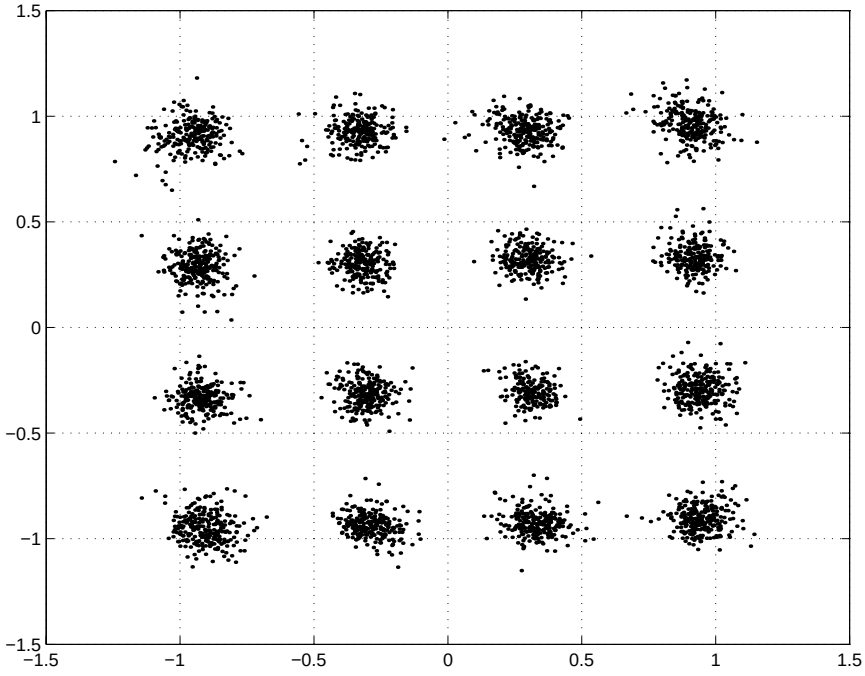

Figure 8: I-Q plot of the received demodulated 16-QAM constellation, for a 4×4 system, with β=0 ppm, frame length=80 OFDM symbols.

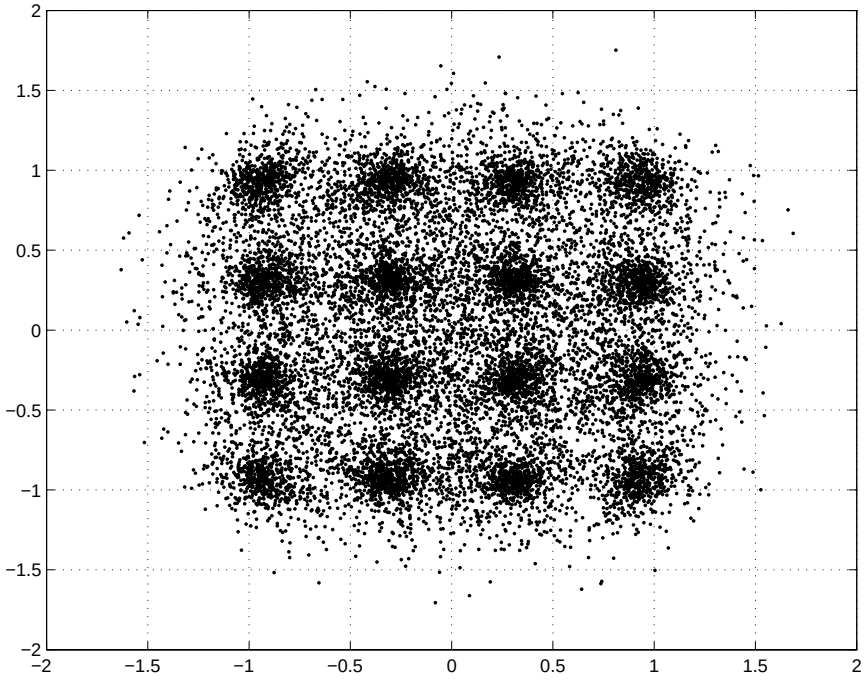

Figure 9: I-Q plot of the received demodulated 16-QAM constellation, for a 4×4 system, with β=10 ppm, frame length F=80 OFDM symbols.

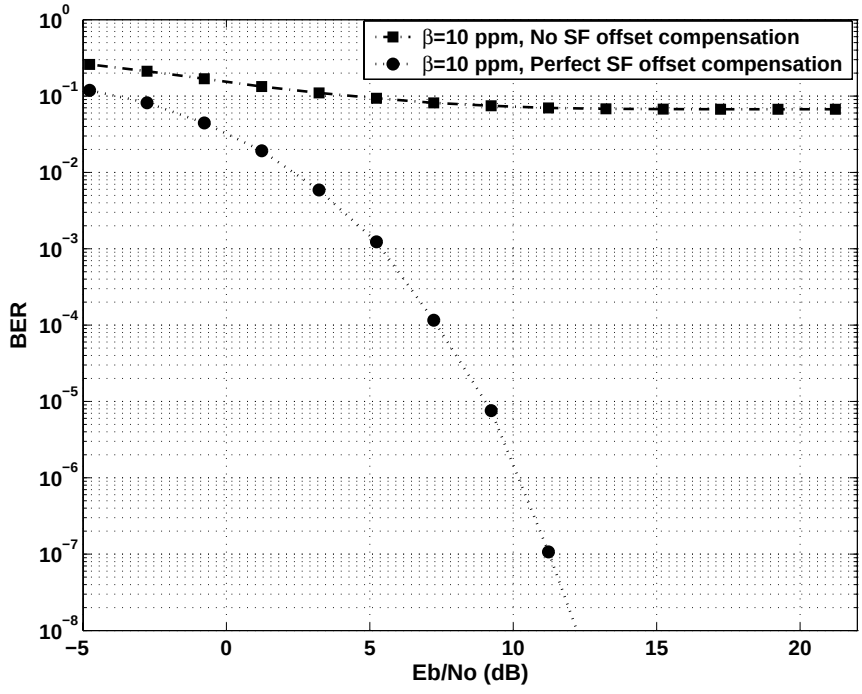

Figure 10: BER as a function of E_b/N_0 ratio for a 4×4 system using 16-QAM constellation, and the STBC suggested by Tarokh (18), with β=10 ppm and frame length F=80 OFDM symbols. The plot shows the BER curves using no SF offset compensation and perfect SF offset compensation.

BER performance of a 4×4 system using 16-QAM constellation, and the STBC suggested by Tarokh (18), with β=10 ppm and frame length F=80 OFDM symbols. The plot shows the BER degradation when no SF offset compensation is present.

The SNR per receive branch, or the E_s/N_0 per receiver branch for the figures and this entire thesis is defined as

$$[E_s/N_0]_\ell = \sum_{q=1}^{Q} \mathrm{E}[|H_k^{q,\ell}|^2]/(QN_0). \tag{29}$$

and bit energy to noise ratio, or the E_b/N_0 per receiver branch is defined as

$$[E_b/N_0]_{\mathrm{dB}} = (E_s/N_0)_{\mathrm{dB}} - 10\ \log_{10}(m \cdot R_{\mathrm{st}}), \tag{30}$$

where where m is the number of bits per constellation symbol and and R_{st} denotes the STC rate. Hence for a 16-QAM alphabet $m = 4$. Suppose the frame structure of the

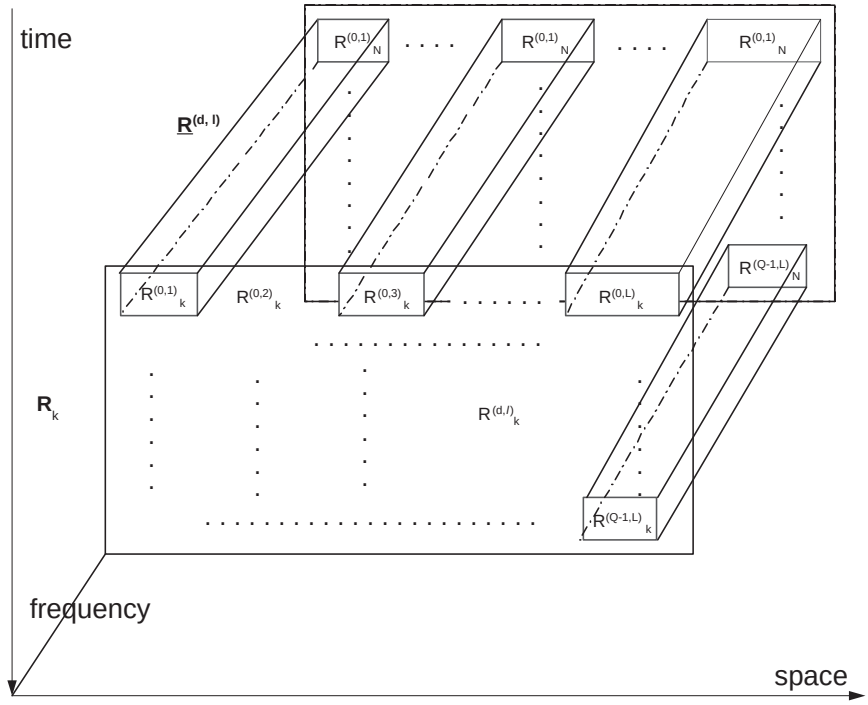

Figure 11: 3-Dimensional representation of the matrix $\mathbf{R}_k$

MIMO-OFDM system is organized into groups of Q OFDM symbols. Starting with the d^{th} OFDM symbol and extending to the $(d+Q-1)^{\mathrm{th}}$ OFDM symbol, (28) has the matrix

representation [65, 66]

$$\mathbf{R}_k^d = A_k^d C_k \mathbf{\Lambda}_k \mathbf{S}_k^d \cdot \mathbf{H}_k^d + \mathbf{W}_k, \tag{31}$$

where

$$A_k^d = \exp\left\{ j \left[2\pi(k\beta + \gamma) d(1 + G/N) + \vartheta^d \right] \right\} \tag{32}$$

is a scalar function of d, β, γ and ϑ;

$$C_k = \frac{1}{uN} \frac{\sin[\pi(k\beta + \gamma + \gamma\beta)]}{\sin[\frac{\pi}{uN}(k\beta + \gamma + \gamma\beta)]} \exp\{j\pi(k\beta + \gamma + \gamma\beta)(1 - 1/uN)\} \tag{33}$$

is a scalar function of β and γ only;

$$\mathbf{\Lambda}_k(\beta) = \begin{bmatrix} \exp\{j2\pi(k\beta + \gamma)0(N + G)/N\} & 0 & \dots \\ 0 & \ddots & \vdots \\ \vdots & \dots & \exp\{j2\pi(k\beta + \gamma)(Q - 1)(N + G)/N\} \end{bmatrix},$$

is a $Q \times Q$ diagonal matrix that is also a function of β and γ;

$$\mathbf{S}_k^d = \begin{bmatrix} S_k^{d,1} & \dots & S_k^{d,Q} \\ \vdots & \dots & \vdots \\ S_k^{d+Q-1,1} & \dots & S_k^{d+Q-1,Q} \end{bmatrix}$$

is the $Q \times Q$ signal transmission matrix, where the $(d, q)^{\text{th}}$ element represents the symbol transmitted from the q^{th} transmit antenna, for the d^{th} OFDM symbol, at the k^{th} sub-carrier. The channel matrix $\mathbf{H}_k^d$ has dimensions $Q \times L$

$$\mathbf{H}_k^d = \begin{bmatrix} H_k^{1,1} & \dots & H_k^{1,L} \\ \vdots & \dots & \vdots \\ H_k^{Q,1} & \dots & H_k^{Q,L} \end{bmatrix},$$

and its $(q, \ell)^{\text{th}}$ element represents the frequency domain channel coefficient between the q^{th} transmit and ℓ^{th} receive antenna, at the d^{th} OFDM symbol and k^{th} sub-carrier. Note that the channel is assumed to be static over a period of Q OFDM symbols. Finally, $\mathbf{W}_k$ is the noise matrix representing the effects of the AWGN, ICI, and ISI.

Finally, each of these structures may be represented as either a collection of N, $Q \times L$ matrices or $Q \times L$ vectors of length-N as shown in the Figure 11.

1.4 Concluding Remarks

In this chapter we laid out a basic ground work for a MIMO-OFDM system and our research. After explaining the principles of an OFDM system, we gave a brief overview of MIMO systems. We then formulated a comprehensive model for a MIMO-OFDM systems incorporating RF oscillator frequency offset, SF offset, phase noise and channel impairment. We also described the effects of all these parameters on a MIMO-OFDM system.

CHAPTER II

PROBLEM STATEMENT AND PREVIOUS WORK

2.1 Problem Statement

In Chapter 1 we saw how MIMO-OFDM systems have become extremely popular and are being considered for a number of different standards and technologies for the future. Using OFDM as a backbone of a MIMO system helps to reduce its net implementation complexity since only a single tap frequency domain equalizer (FEQ/FDE) is needed to undo the effects of each MIMO sub-channel. However from 142, we also saw that a typical MIMO-OFDM system has a number of system parameters which must be estimated and corrected before the advantages of a MIMO system can be realized. Typically, these parameters and processes include frame synchronization also referred to as time synchronization, RF oscillator frequency offset estimation and correction which is also referred to as frequency synchronization, SF offset estimation and correction, phase noise estimation and correction and finally channel estimation. First of all these parameters must be estimated and next, they must be tracked since they are constantly changing. Hence a MIMO-OFDM receiver has in general two modes of operation: signal acquisition and signal tracking.

A MIMO-OFDM receiver operating in the acquisition mode must perform time synchronization, radio frequency (RF) oscillator offset estimation and correction, sampling frequency (SF) offset estimation and correction, phase noise estimation and correction and finally channel estimation. Acquisition may be aided by a preamble containing known training sequences or may be blind. After time and frequency alignment, the receiver performs phase noise and initial channel estimation. After the acquisition phase, the receiver enters the tracking mode. In the tracking mode the receiver needs to track the SF and the phase noise jitters. Finally, even in low mobility WLAN and WMAN systems, the channel needs to be constantly tracked because of the variations in the effective channel due the SF and phase noise jitters and because of the accumulation in the parameter estimation

errors. Hence in this chapter we study the published contributions on signal acquisition and tracking for OFDM systems.

2.2 Previous Work

Commercial OFDM systems must accommodate a number of users within a fixed allocated spectrum. This requires that the available BW be shared by the users either in time referred to as time division multiple access (TDMA) or the frequency referred to as frequency division multiple access (FDMA) and the parameters for the receiver implementation need to be acquired for each user within a short time.

OFDM signal acquisition and tracking are either assisted by the use of a preamble consisting of one or more training sequences, or may be carried out blindly, such that the required parameters are estimated from the signal containing the data itself. Generally blind estimators require more time for parameter estimation and are slightly more complex. They may be used for parameter estimation when the overhead of the preamble or the pilot symbols can not be tolerated [11, 72].

Time synchronization, RF oscillator frequency offset estimation and tracking, channel estimation and tracking, and sampling frequency offset estimation and tracking are all research topics by themselves. Also, the design of an efficient preamble/ pilot tones and the training sequences which constitute them is another research area on which different authors have contributed. Most of the authors have addressed these issues individually and usually for single-input single-output (SISO) OFDM systems. The following is a brief background summary on all these topics.

2.2.1 Time and Radio Frequency (RF) Oscillator Synchronization

Time synchronization is a process of finding the start of the OFDM frame from the received complex baseband samples. Time synchronization is normally divided into coarse time synchronization and fine time synchronization. Coarse time synchronization consists of estimating the approximate range of samples over which the OFDM frame is likely to start, whereas fine time synchronization consists of locking the receiver onto the most dominant component of the received OFDM signal.

RF oscillator frequency synchronization consists of estimation and correction of the RF oscillator frequency offset between the transmitter and the receiver. Since OFDM signal consists of parallel sub-channels in the frequency domain, the RF oscillator frequency offset can be expressed in terms of the number subcarrier spacings. Most approaches consider the RF oscillator frequency offset estimation and correction in baseband, using signal processing algorithms. It generally consists of fractional and integer frequency offset estimation. Fractional frequency offset estimation estimates the offset of up to $\pm 1/2$ subcarrier spacings and integral frequency offset estimation estimates the offset of an integer number of subcarrier spacings.

Most methods suggested for coarse time synchronization and estimation of the fractional portion of the RF oscillator frequency offset rely on some inherent transmitted periodicity in the OFDM signal. Moose [67] has proposed a popular technique for robust frequency offset estimation in the time domain based on the transmission of two identical OFDM symbols. J. J. van de Beek *et al.* [83, 106, 107] have used the periodicity on OFDM signal due to the presence of the CP and proved it to be a maximum likelihood (ML) estimator. In their method, the estimate of the frequency offset is obtained from the phase of the autocorrelation function and the estimation range is $\pm 1/2$ subcarrier spacings. They have also addressed time and frequency synchronization in multiuser OFDM systems in [105]. Schmidl and Cox [87] have combined the methods of Moose and Classen [20], for time and frequency synchronization for SISO OFDM systems by introducing a special symbol with a periodicity of one half OFDM symbol to achieve synchronization and frequency offset estimation. Santella [84] uses a null symbol to perform initial time synchronization and feedback loops to control the local oscillator and sampling clock oscillator frequencies. Coulson [22] has modified the method suggested by Schmidl such that only one training symbol is required instead of two for a narrow-band flat fading SISO OFDM system. J. Li [47] suggests a non-linear least squares approach for frequency offset estimation in IEEE 802.11a systems using short and long training symbols and Minn [59] suggests the use of a pilot symbol with identical parts containing customized $\{+, -\}$ patterns for time and frequency synchronization. Finally Müller-Weinfurtner has analyzed the various metrics

proposed in the literature for time synchronization based on the CP in OFDM systems. He proves that a simple threshold comparison between the autocorrelation of the sampled received complex envelope and the energy of the complex envelope over the autocorrelation window yields an ML estimate and is an adequate metric to obtain the coarse time synchronization instant. Some other work on OFDM time and frequency synchronization can be found in [59, 110, 111].

Once coarse time synchronization and fractional RF oscillator frequency offset estimation and correction are completed, the receiver needs to check for any residual integer frequency offset and then perform fine time synchronization. Generally if N is the block-size of the IFFT and $N_I = N/I$ is the spacing between the periodicity in the time domain signal then the receiver can estimate the frequency offset of $\pm I/2$ subcarrier spacings based on the autocorrelation of the received complex base-band samples at a distance of N_I from each other. Hence, when $I = 1$ the CP-based methods for fractional frequency offset estimation can estimate offsets of up to $\pm 1/2$ subcarrier spacings. In order to overcome this limitation, Schmidl and Cox [87] introduce an extra symbol after their special symbol containing a differentially modulated pseudo-noise (PN) sequence on even frequencies to extend the range of the frequency offset estimation. On the other hand, Zou [121] proposes an interesting technique of estimating the integer frequency offset of a SISO-OFDM system in the frequency domain.

Fine time synchronization involves initial aligning of the receiver clock to the most dominant path of the signal. Since coarse time synchronization algorithms give a range of samples over which the system may be synchronized, fine time synchronization is necessary to determine the exact synchronization instant [90]. Contrary to the single carrier (SC) systems, OFDM systems have a range of samples which can be considered for the fine time synchronization instant. These samples span from the ISI free zone in the guard interval to the start of the useful portion of the OFDM symbol. If the channel is non-causal the ISI from the next OFDM symbol must also be taken into account to determine the location of the fine time synchronization instant. A number of different methods have been suggested in literature for fine time synchronization. Speth [90] has suggested an

approach for time synchronization based on the frequency domain pilot tones, where a performance metric is minimized by choosing an appropriate time synchronization instant. Larsson [45] has suggested a similar approach, however, he jointly estimates the channel as well as the synchronization instant. Zou [121] has suggested a method of fine time synchronization in the frequency domain by measuring the phase difference between the two adjacent pilot subcarrier symbols. Yang *et al.* [118] have proposed a method of converting the channel estimates from the frequency domain to the time domain and finding the most dominant path of the channel over a number of measurements. This method requires an even distribution of the pilot tones and a channel that remains fixed for a sufficiently long time. Finally, if the communication system uses a preamble then one of the simplest and the most effective methods is to perform cross-correlation of the received complex base-band samples with the transmitted time domain sequences stored at the receiver [86, 104]. For such a method, increasing the sampling rate at the receiver improves the resolution of the fine time synchronization instant. However such a correlation method is susceptible to the presence of any residual RF oscillator frequency and sampling frequency offsets in the system.

2.2.2 Channel Estimation

Digital communication systems require accurate channel estimates for coherent detection [77]. In literature on channel estimation for SISO and MIMO-OFDM systems, most of the papers estimate the channel in the frequency domain followed by some post-processing to enhance the channel estimates. Channel estimation is generally aided by the preamble consisting of training sequences or pilot tones inserted at specific frequency locations. Almost all existing literature assumes that time and frequency synchronization has been previously achieved. Some of the work on channel estimation for MIMO-OFDM systems can be found in [24, 42, 52, 57, 79, 117]. Mignone [57] has suggested the use of LS estimation of the channel using pilot tones followed by noise reduction in time domain. Edfors *et al.* [24], obtain the initial channel estimates using the LS approach followed by mean squared error (MSE) reduction using the frequency domain channel correlation matrix and the noise variance.

They have further suggested a low-rank approximation of the estimator using singular value decomposition (SVD) of the channel correlation matrix. Raleigh and Jones [78, 79], have suggested channel estimation for MIMO-OFDM system using a training structure consisting of independent and orthogonal training sequences from various transmit antennas. The structure is composed such that no two transmit antennas send a training symbol on the same subcarrier. Yang [117] suggests the use of windowing in the frequency domain before processing the channel estimates in the time domain to reduce the spectral leakage. Li [52] has derived a channel estimator for an OFDM system with transmitter diversity based on the minimum MSE (MMSE) principle using both the time and frequency domain correlations of the channel. A significant tap catching (STC) approach is suggested to reduce the computational complexity of this estimator. Li has made further contributions on channel estimation for MIMO-OFDM systems in [50], [53] and [51]. Finally, Kotecha [42] has worked on optimal signal design for estimation of correlated MIMO channels.

2.2.3 Sampling Frequency Offset Estimation

Some authors have studied the effects of SF offset and timing jitter on the performance of OFDM systems [89, 120]. Speth [90] measures the sampling frequency offset for a SISO-OFDM system based on the phase rotation of the pilot tones between two consecutive OFDM symbols. Coulson [22] has derived a single shot estimator of the timing offset based on MMSE. Coulson, however, does not perform tracking of the timing offset. Most other literature on time and frequency synchronization either does not address this issue or perform it in the time tracking process [118].

2.2.4 Phase Noise Estimation

A number of authors have analyzed the impact of RF oscillator phase noise on SISO and MIMO OFDM systems. These include the ones by Armada [10], Narasimhan [69], Costa [21], Ryu [81, 82], Wu [116], Piazzo [74], Tomba [103] etc. In general, most authors assume the phase noise to be small which makes its analysis simpler using small error analysis. Also, the analysis of the phase noise depends on how fast it varies. When it varies much faster than the OFDM symbol period, then it must be treated as an ICI noise source.

When it varies slowly as compared to the OFDM symbol period, then it may be estimated based on the pilot tones.

Some authors have made contributions to estimate and correct the phase noise effects in OFDM systems. These include the one by Zelst [108], Wu [115], Jianhua [39] etc. Zelst assumes the phase noise to remain constant for a number of OFDM systems and he estimates the same based on the pilot tones that are inserted in the OFDM data stream. However, it is difficult to analyze the performance of this estimator. Others treat phase noise effects in OFDM as an addition of an ICI noise and try to suppress it in different manners.

2.2.5 Parameter Tracking

Depending upon the system needs, the receiver needs to track the RF oscillator frequency offset, SF offset, phase noise variations and channel coefficients. Generally, RF oscillator frequency offset changes slowly with time, but in systems with long frames, it must be tracked continuously. SF offset and phase noise suffer from jitters and may need to be tracked continuously. SF offset tracking and correction is also referred to as time tracking. For the WLAN and WMAN applications, the channel will change little from frame to frame and, therefore, channel estimate is generally estimated only once per frame. However, even in low mobility WLAN and WMAN systems, the channel needs to be constantly tracked because of the variations in the effective channel due the SF and phase noise jitters and because of the accumulation in the parameter estimation errors.

For MBWA systems, the change in the effective channel due to the terminal mobility is greater than due to the SF offset and phase noise jitters. Hence, SF offset estimation needs to be carried out once in the acquisition phase and the channel at the pilot tones needs to be tracked for every OFDM symbol.

Among papers related to the tracking of synchronization parameters, Speth [90] has suggested the tracking of RF oscillator and sampling frequency offset derived from the one shot estimator using a proportional integral (PI) tracking loop. The tracking and correction of the parameters is carried out at baseband. Santella [84] uses a phase discriminator and a frequency discriminator for the symbol and frequency synchronization loops repectively.

The frequency synchronizer directly controls the the RF oscillator frequency and the phase synchronizer controls the sampling frequency oscillator. Yang [118] has suggested a non-coherent delay locked loop (NC-DLL) to track the sampling frequency offset. The method requires an initial lock of 1/2 sample during the time acquisition phase and later uses early and late generators for sampling frequency offset tracking. J. J. van de Beek *et al.* [105] suggest a symbol timing and RF oscillator frequency offset tracking method for multiuser OFDM systems based on CP and exponential weighted averaging with a simple one pole infinite impulse response (IIR) filter having a forgetting factor of α.

Channel tracking is needed when a long burst of data is transmitted such as in the DAB and DVB [27, 28] applications or for channels that change rapidly such as in the MBWA environments. In general, two approaches have been suggested for channel tracking. One is the pilot-aided method and the other is the decision-directed method. Pilot-aided method is normally preferred for commercial OFDM systems. Among the contribution on pilot-aided channel tracking, Li has suggested channel estimation and tracking for SISO-OFDM based wireless systems [49]. He uses an MMSE interpolation to obtain channel estimates at all the tones. Since an MMSE interpolator requires the knowledge of time and frequency domain statistics of the channel, two-dimensional (2-D) FFT and IFFT are suggested to form a simplified interpolation scheme. A similar method for transform domain interpolation has been suggested in [119]. Mignone [57] has suggested a decision-directed approach for channel estimation and tracking in fixed and mobile receivers. Wookon and Zhu [46] have also suggested a pilot-aided decision directed approach that is processed both in time and frequency domains whereas Necker and Stüber have suggested a totally blind approach for channel estimation in fast-varying mobile channels [70].

2.2.6 Preamble/ Pilot Structures and Training Sequences

Preamble/ pilot-aided parameter estimation requires that the structures and sequences used must be efficient. The general properties required to form an efficient preamble are that the preamble should effectively aid in performing accurate time synchronization and RF oscillator frequency offset estimation over a wide range, it should help to estimate the SF

offset coefficient and the RF phase noise, it should also be ideal for channel estimation and, finally, it should add minimum overhead.

Commercial wireless systems use preamble structures that are often times pretty long and add a large overhead to the system. Of course larger preamble results in a better synchronization and parameter estimation performance. For example, Figure 12, shows the preamble format for the IEEE 802.11a [35] OFDM systems. This preamble consists of a number of short periodic sequences of a total length of two OFDM symbols, followed by long training sequence of the type CP+$N+N$ where $N = 64$. The short training sequences are used for rapid time synchronization and coarse RF oscillator frequency offset estimation, automatic gain control (AGC) and diversity selection in case of multiple receiver antennas. The long training sequences are used for fine RF oscillator frequency offset estimation and channel estimation. Similarly, the preamble for the IEEE 802.16a Standard has initial

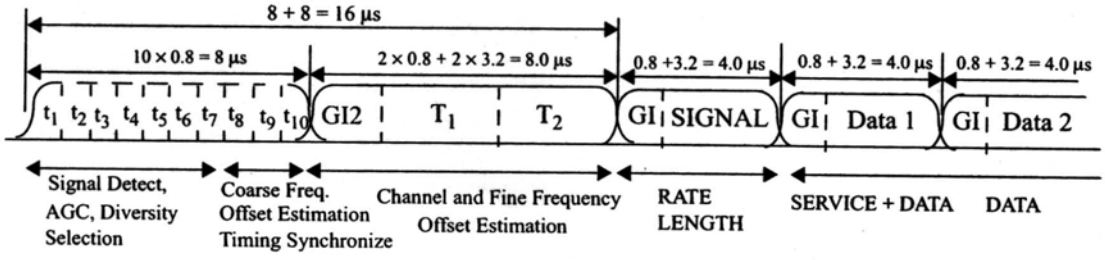

Figure 12: Preamble structure for IEEE 802.11a systems [35].

short sequences of the type CP+4×64 followed by CP+2×128 for similar purposes. These preambles are designated for the SISO-OFDM systems. The preambles for MIMO-OFDM systems are expected to be even longer. Such long preambles are not always needed and they result in an un-necessary overhead in the data throughput.

Some work has optimized the preamble sequences and structures for OFDM systems [44, 48, 55, 102]. Preamble sequences must have desirable properties in both the time and frequency domains. These include constant envelope properties in the frequency domain, good autocorrelation properties in the frequency and time domain, and low peak-to-average power ratio (PAPR) in the time domain [98]. Some contributions on the families of ideal

or near-ideal training sequences include the ones by Milewski [58], Ng [73], Suehiro [95], Frank-Zadoff [31], Chu [18], etc. Out of these, the Frank-Zadoff and the Chu sequences have been accepted to be used in the IEEE 802.16a Standard in their SC mode with an FDE. Another example of an ideal training sequence is the chirp sequence. In the time domain, it is given by

$$s_n = \cos\left(\pi n^2/N\right) + j\sin\left(\pi n^2/N\right),\ n = 0, 1, \ldots, N-1. \tag{34}$$

Figures 13 and 14 show the autocorrelation functions of the chirp and the IEEE 802.11a

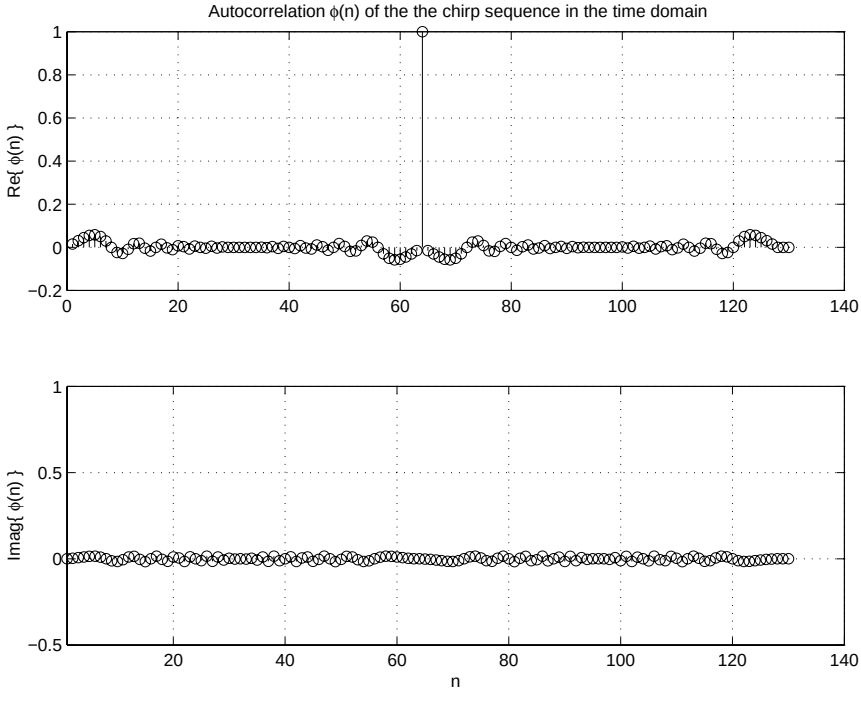

Figure 13: Autocorrelation of the chirp sequence

long sequence. As can be seen, the chirp sequence has cleaner autocorrelation function with a higher main lobe to side lobe energies which makes it more suitable as a training sequence.

Often the preamble sequence is designed in the frequency domain, converted to the time domain, and stored for direct modulation [35, 37]. This could be because of the ease in its implementation and also, since in commercial OFDM systems, certain sub-carrier frequencies at the band-edges are masked in order to avoid adjacent channel interference (ACI). Chen and Mitra [15] prove that time domain channel estimation achieves a superior

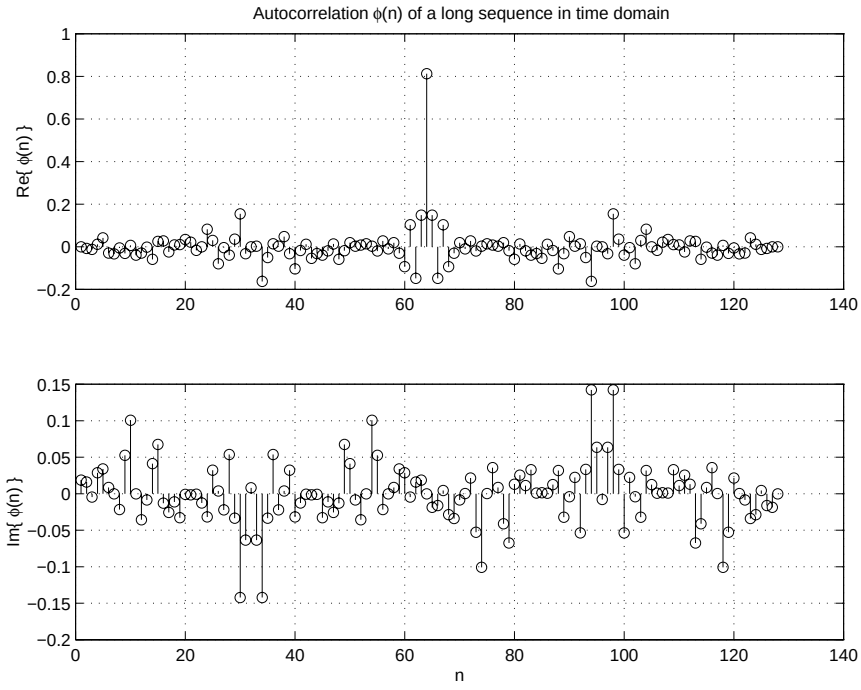

Figure 14: Autocorrelation of IEEE 802.11a Standard' s long sequence.

MSE performance as compared to the frequency domain method. However for OFDM systems, time domain channel estimation is generally complex and cumbersome. Hence frequency domain channel estimation is more popular for system implementation. For the best frequency domain channel estimation performance, the sequences must have a flat spectrum, where the spectral flatness is measured using the spectral max-min ratio (SMMR) given by

$$\Xi(\underline{S}) = \frac{\{\max|\underline{S}_k| : 0 \leq k \leq N\}}{\{\min|\underline{S}_k| : 0 \leq k \leq N\}}, \tag{35}$$

[102]. In simulations we show that if an ideal sequence such as a chirp sequence with PAPR of 1, and good correlation properties is used to construct the training sequence then the performance of our acquisition algorithms can be improved to within 1 dB from the ideal BER curve. As mentioned before, more practical OFDM systems such as the ones based on the IEEE Standards, IEEE 802.11a [35] and IEEE 802.16a [37] construct their training sequences by modulating the sub-carriers with a sequence from a known alphabet and taking their IFFT. This makes the training sequence construction easy to implement.

For example, the IEEE 802.16a Standard [37] has recommended the use of the following frequency domain sequence to construct the preamble. $S_k = \sqrt{2}[0\ 0\ -1\ 0\ -1\ 0\ 1\ 0\ -1\ 0\ -1\ 0\ 1\ 0\ 1\ 0\ -1\ 0\ 1\ 0\ 1\ 0\ 1\ 0\ -1\ 0\ -1\ 0\ -1\ 0-1\ 0\ -1\ 0\ 1\ 0\ -1\ 0\ -1\ 0\ -1\ 0\ -1\ 0\ -1\ 0\ 1\ 0\ 1\ 0\ 1\ 0\ -1\ 0\ 1\ 0\ -1\ 0\ 1\ 0\ 1\ 0\ -1\ 0\ 1\ 0\ 1\ 0\ 1\ 0\ -1\ 0\ -1\ 0\ -1\ 0\ -1\ 0\ 1\ 0\ -1\ 0\ -1\ 0\ 1\ 0\ -1\ 0\ -1\ 0\ 1\ 0\ -1\ 0\ -1\ 0\ 1\ 0\ -1\ \{55\ 0s\}\ -1\ 0\ 1\ 0\ 1\ 0\ 1\ 0\ 1\ 0\ -1\ 0\ -1\ 0\ 1\ 0\ -1\ 0\ -1\ 0\ 1\ 0\ -1\ 0\ 1\ 0\ -1\ 0\ 1\ 0\ -1\ 0\ 1\ 0\ 1\ 0\ -1\ 0\ -1\ 0\ 1\ 0\ -1\ 0\ -1\ 0\ -1\ 0\ 1\ 0\ 1\ 0\ 1\ 0\ -1\ 0\ 1\ 0\ 1\ 0\ 1\ 0\ -1\ 0\ 1\ 0\ 1\ 0\ -1\ 0\ -1\ 0\ -1\ 0\ 1\ 0\ 1\ 0\ 1\ 0\ 1\ 0\ 1\ 0\ 1\ 0\ 1\ 0]$

For MIMO systems, ideally, the sequences transmitted from different antennas should be orthogonal in time [56, 96] and must have good correlation properties. Finally, LS estimation of the channel and the sampling frequency offset for MIMO-OFDM systems require that the sequences that constitute the preamble be arranged in a certain manner. Barhumi [11] suggests that to obtain a MMSE channel estimate, the pilot sequences must be equi-powered, equi-spaced and phase-shift orthogonal. He also suggests that for multiple transmit antennas and low Doppler, the channel parameters may be estimated over multiple OFDM symbols.

2.3 Concluding Remarks

In this chapter, we laid out the problem statement of our research and conducted a literature search of the same. Our search focussed on the published contributions in the areas of signal acquisition and tracking for OFDM systems. In particular, these included time and frequency synchronization, SF offset estimation and tracking, phase noise estimation and tracking and finally channel estimation and tracking. We also identified the strengths and the weaknesses of the previous contributions and the potential areas of focus for our research.

CHAPTER III

SIGNAL ACQUISITION AND TRACKING FOR FIXED WIRELESS ACCESS MIMO-OFDM

In this chapter we present a complete suite of acquisition and tracking algorithms for a BFWA MIMO-OFDM system. This work has been submitted for a journal publication [66] and was presented in parts in [61, 63–65]. In Section 3.1, we present the preamble and pilot matrix structure that aid our algorithms to work efficiently. Section 3.2 overviews the signal acquisition process, while Section 3.3 investigates the parameter tracking. Our residual RF oscillator, phase noise, and SF offset estimators are novel and we undertake a mean squared error (MSE) analysis for better insight into their behavior. Finally, Section 3.4 presents some representative simulation results and Section 3.5 concludes the chapter.

3.1 Preamble and Pilot Structures

3.1.1 Generalized MIMO-OFDM Preamble

Figure 15 shows a generalized MIMO-OFDM frame structure that is appropriate for WLAN and WMAN applications [64, 65], consisting of a preamble followed by F OFDM symbols. The preamble consists of at least Q sub-sequences of length $GT + T_I$ where $GT \leq T_I \leq NT$. The time interval T_I corresponds to the transmission of N_I samples, where $N_I = N/I$ and I is some integer that divides N. The length-N_I time-domain preamble sub-sequence $\underline{s}^{d,q}$ is constructed in the frequency domain by placing a known symbol at every I^{th} coordinate of the vector $\underline{S}^{d,q}$, and setting the remaining coordinates to zero. Then $\underline{s}^{d,q}$ is obtained by taking an N-point IFFT of $\underline{S}^{d,q}$ and retaining the first N_I samples, i.e.,

$$s_n^{d,q} = 1/\sqrt{N} \sum_{k=0}^{N-1} S_k^{d,q} \exp\left\{j2\pi nk/N\right\}, \ 0 \leq n \leq N_I - 1. \tag{36}$$

The choice of the parameter I affects the capabilities and performance of the various acquisition functions. Sometimes, both short and long sub-sequences are used in the preamble to

gain the benefits of both. Of course this might lead to a longer preamble. For example, the IEEE 802.16a standard [37] uses short sequences of the form CP $+ 4 \times 64$ followed by long sequences of the form CP $+ 2 \times 128$. In addition to the preamble, known pilot symbols are inserted at certain sub-carriers in the data symbols to estimate and track the parameters.

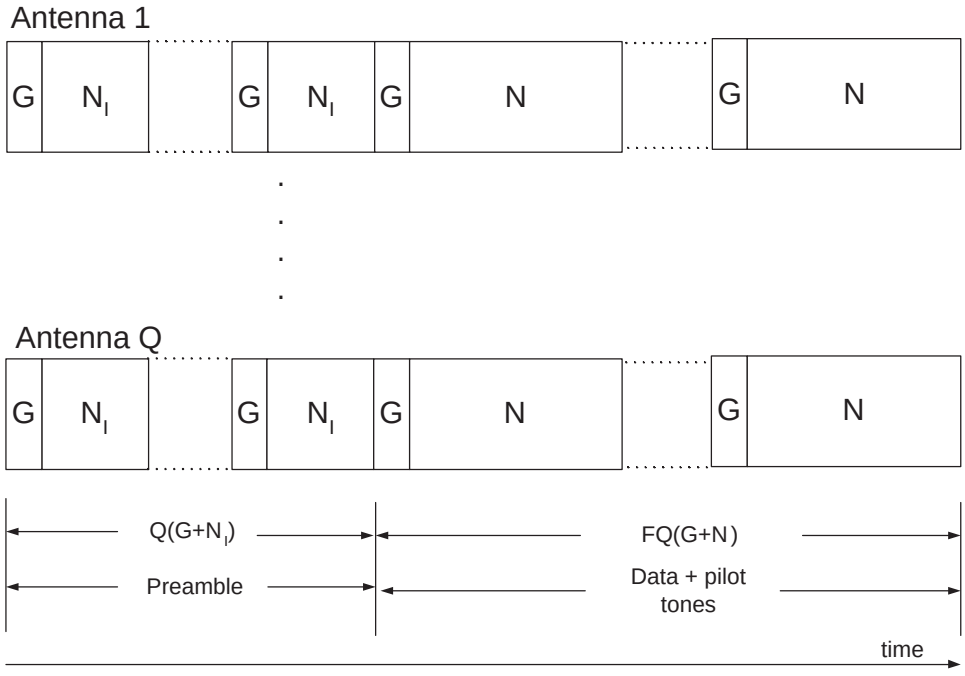

Figure 15: Frame structure for the $Q \times L$ MIMO OFDM system.

3.1.2 MIMO-OFDM Pilot Matrix Structures

The signal transmission matrices $\mathbf{S}_k$, for the preamble and pilot sub-carriers may assume different forms ranging from diagonal to unitary. The IEEE 802.16a standard specifies the preamble and pilot tone matrix structure for 2×2 OFDM systems using Alamouti' s [6] space-time code. In the IEEE 802.16a [37] standard, a training sequence of the form CP $+ 2 \times 128$ (similar to the case when $I = 2$ in this part of our research) is transmitted from one antenna at a time, to maintain medium access control (MAC) conformity and co-existence with SISO-OFDM systems. This results in a diagonal signal transmission matrix for the preamble. Since a diagonal structure does not utilize the diversity advantage of a MIMO channel, we instead choose a unitary structure that is based on orthogonal designs

for binary space-time block codes. The orthonormal property of the transmission matrix has the advantage of being readily invertible and transmission of the signal from all the antennas for Q OFDM symbols improves the parameter estimation performance. For $Q = 2$, we can use the Alamouti [6]' s signal transmission matrix [61]

$$\mathbf{S} = \frac{1}{\sqrt{2}} \begin{bmatrix} \underline{S}_1 & \underline{S}_1 \\ -\underline{S}_1 & \underline{S}_1 \end{bmatrix}. \tag{37}$$

Likewise for $Q = 4$ [61] the signal transmission matrix may have a unitary form,

$$\mathbf{S} = \frac{1}{\sqrt{4}} \begin{bmatrix} \underline{S}_1 & \underline{S}_1 & \underline{S}_1 & \underline{S}_1 \\ -\underline{S}_1 & \underline{S}_1 & -\underline{S}_1 & \underline{S}_1 \\ -\underline{S}_1 & \underline{S}_1 & \underline{S}_1 & -\underline{S}_1 \\ -\underline{S}_1 & -\underline{S}_1 & \underline{S}_1 & \underline{S}_1 \end{bmatrix}. \tag{38}$$

where $\underline{S}_1$ is a length-N vector. When the number of transmit antennas is not of the form $Q = 2^i$ for some i, e.g., $Q = 3$, then a diagonal matrix may be used. or Gram-Schmidt ortho-normalization procedure can be used to obtain the signal transmission matrix [61]. This procedure is explained in Appendix A. However, this procedure yields transmitted symbols in the frequency domain that are not from a finite alphabet.

The IEEE 802.16a standard for $N = 256$ recommends the insertion of $P = 8$ pilot tones at fixed positions of [12 36 60 84 172 196 220 244] as shown in Fig. 16. Fig. 16 also shows the method for generating pilot sequences in the frequency domain for the standard. At the beginning of each frame, the Downlink (DL) and Uplink (UL) shift register is initialized with sequences shown in the figure. A '0' at the output P_d is mapped to +1 and a '1' is mapped to -1. For example, in the DL, the shift register output is given by the sequence [11111111111000000000110 . . .], where the 3$^{\text{rd}}$ 1, i.e. $P_3 = 1$ is used to generate the pilot tones for the first DL OFDM symbol following the preamble. The pilot matrix elements of each OFDM symbol in the DL are initialized as, $\mathbf{S}_{60}^{1,1} = \mathbf{S}_{84}^{1,1} = \mathbf{S}_{172}^{1,1} = \mathbf{S}_{220}^{1,1} = 1 - 2P_d$ and $\mathbf{S}_{12}^{1,1} = \mathbf{S}_{36}^{1,1} = \mathbf{S}_{196}^{1,1} = \mathbf{S}_{244}^{1,1} = 1 - 2\bar{P}_d$, where $\bar{P}_d$ is the complement of P_d. For the UL, the pilot tones are assigned as $\mathbf{S}_{12}^{1,1} = \mathbf{S}_{36}^{1,1} = \mathbf{S}_{60}^{1,1} = \mathbf{S}_{84}^{1,1} = \mathbf{S}_{172}^{1,1} = \mathbf{S}_{220}^{1,1} = 1 - 2P_d$ and $\mathbf{S}_{196}^{1,1} = \mathbf{S}_{244}^{1,1} = 1 - 2\bar{P}_d$. A similar format is defined for the UL in the IEEE 802.16a

Standard. For MIMO-OFDM, the pilot symbols are inserted as known signal transmission matrices $\mathbf{S}_k^p$, where the value of P_d determines the entire pilot matrix when $Q = 2^i$ for some i.

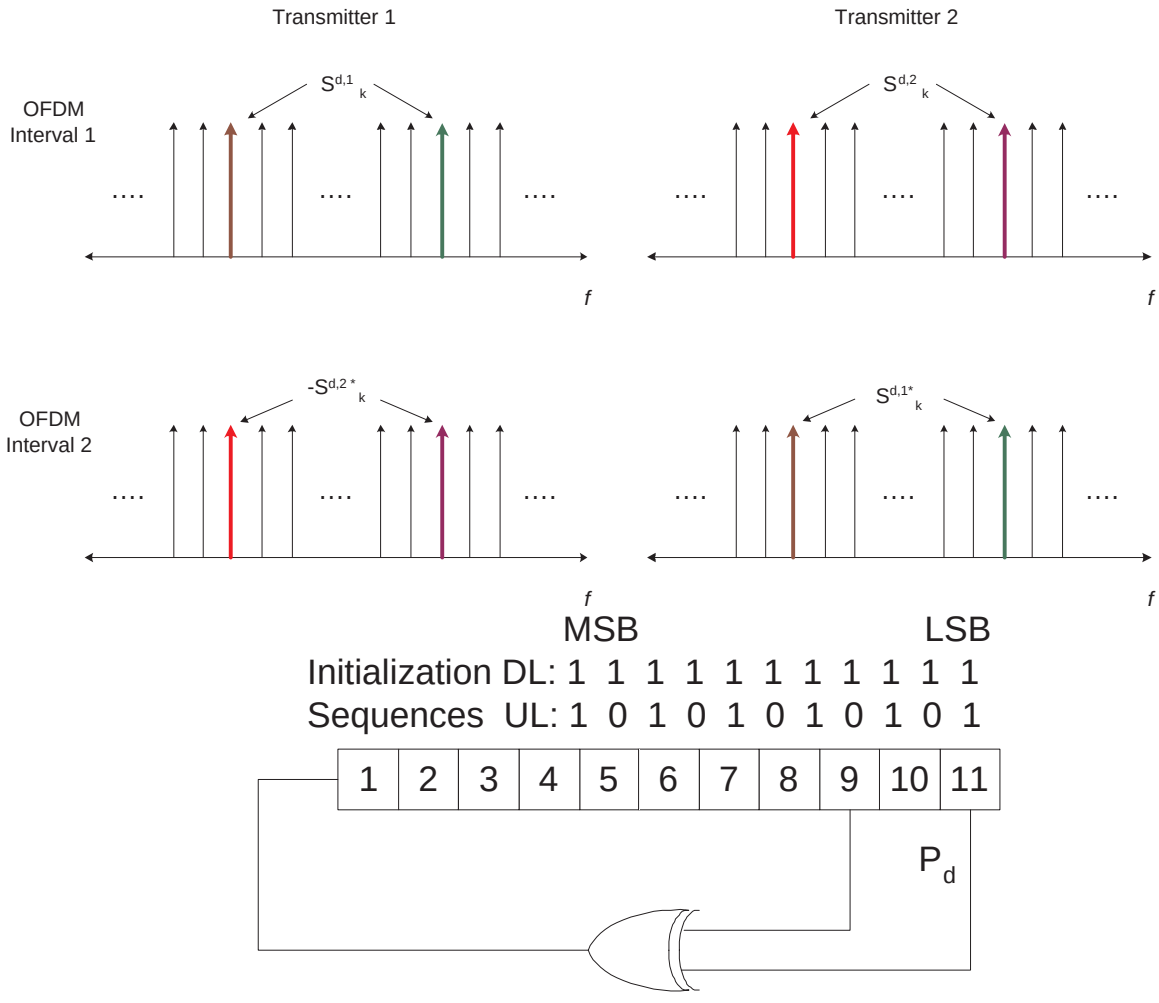

Figure 16: An example of pilot mapping for a $2 \times L$ OFDM system and pilot generation using a shift register [37].

3.2 Acquisition Mode - Step A.

Signal acquisition as defined in this research consists of time synchronization, RF oscillator frequency offset estimation and correction, sampling frequency offset estimation and correction, phase noise estimation and correction and finally, channel estimation [64]. In the proposed method, time synchronization and RF oscillator frequency offset estimation

are performed first, followed by sampling frequency offset estimation and, finally, channel estimation.

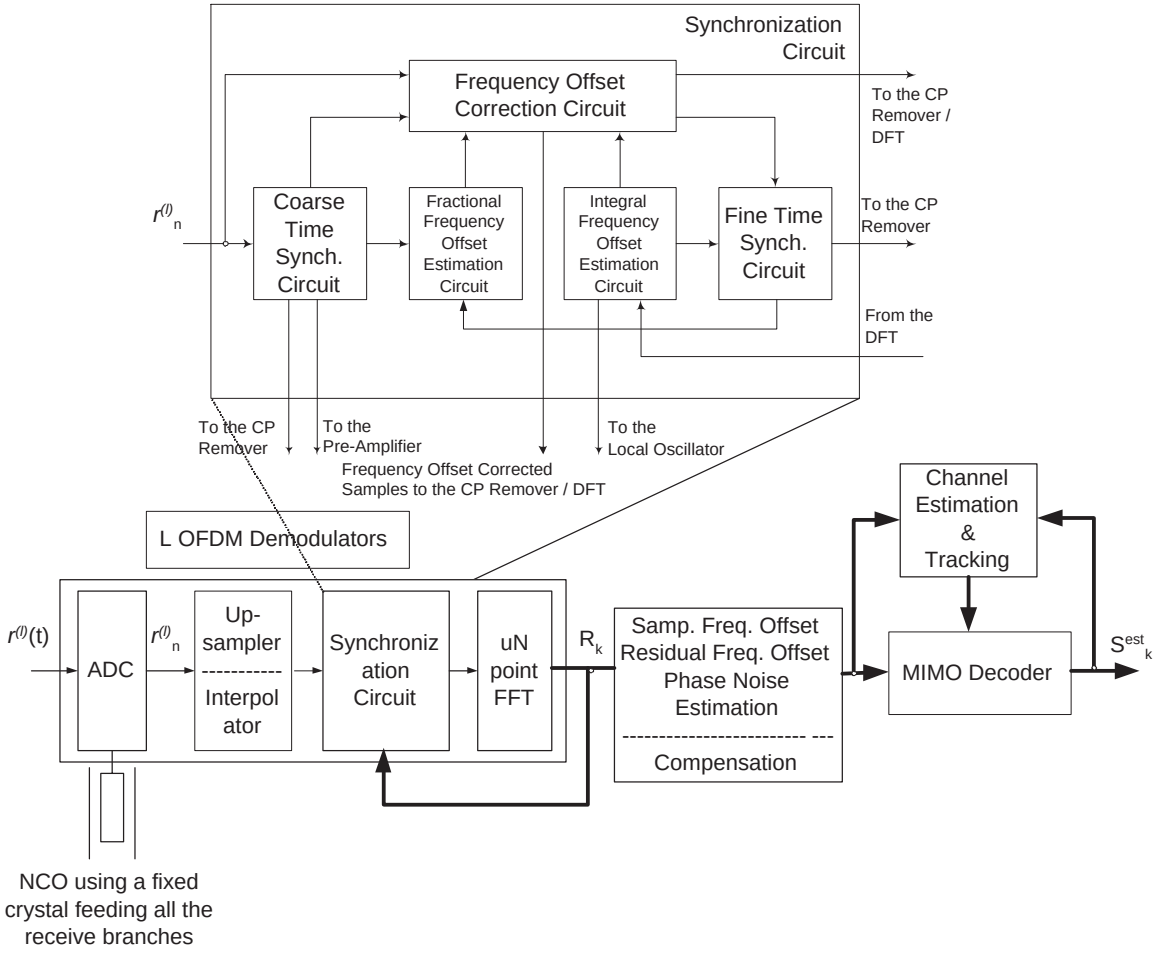

Figure 17: Receiver Implementation for the MIMO OFDM System.

3.2.1 Time Synchronization and RF Frequency Offset Estimation-

Figure 17 depicts the overall synchronization functionality of the MIMO-OFDM system. The MIMO OFDM receiver first performs coarse time synchronization to obtain an approximate range of samples over which the OFDM frame is likely to begin. This is followed by the fractional and the integer RF oscillator frequency offset estimation and correction. Finally, fine time synchronization determines the optimal sampling instant to within a small range of samples.

Step IA. Coarse Time Synchronization- Due to the presence of the RF oscillator frequency offset which is initially unknown at the receiver, coarse time acquisition is performed by exploiting the repeated samples in the guard interval. The discrete autocorrelation of the sampled received complex envelope is computed over a window of G samples that are at a distance of N_I from each other [64,65]. Müller-Weinfurtner [68], has analyzed the various metrics proposed in the literature for OFDM time synchronization based on the cyclic prefix. A simple threshold comparison between the autocorrelation of the sampled received complex envelope and the energy of the complex envelope over the autocorrelation window yields an ML estimate and is an adequate metric to obtain the coarse time synchronization instant. A threshold ρ_{coarse} is introduced which must be exceeded to reduce the probability of false alarm (P_{FA}). We perform autocorrelation over all the receive branches and our coarse time synchronization metric is

$$n^{\ell}_{\text{coarse}} = \left\{ \arg \underbrace{\max}_{n} \left\{ \phi^{\ell}_{n} \right\} : |\phi^{\ell}_{n}| \geq \rho_{\text{coarse}} \cdot (P^{\ell}_{n} + P^{\ell}_{n+uN_I}) \right\}. \tag{39}$$

where

$$\phi^{\ell}_{n} = \sum_{k=0}^{uG-1} (r^{\ell\ *}_{n+k} \cdot r^{\ell}_{n+k+uN_I}) \tag{40}$$

is the autocorrelation function and

$$P^{\ell}_{n} = \sum_{k=0}^{uG-1} |r^{\ell}_{n+k}|^2 \tag{41}$$

is the signal energy calculated over uG samples where u is the over-sampling factor. We empirically choose the threshold ρ_{coarse} as 10% of the incoming signal energy over the correlation window.

Step IIA. Frequency Offset Estimation in the Time Domain - Frequency offset estimation can be carried out based on the inherent periodicity in the OFDM signal and the preamble due to the cyclic prefix. Cyclic prefix and the last G samples of the useful part of the OFDM symbol are exactly the same in the absence of a frequency offset and affected by the channel in a similar fashion. Commercial OFDM systems are expected to have an RF oscillator frequency drift and sampling frequency drift of approximately 20 parts per

million (ppm) at the customer premises equipment (CPE) [37]. If any frequency offset exists between the transmitter and receiver RF oscillators, it is reflected in the cyclic prefix and the posterior part of the OFDM symbol as a proportional phase shift $\theta = 2\pi\gamma N_I/N$, where γ is the fractional portion of the RF frequency offset. A relative frequency offset estimate of up to $\pm I/2$ subcarrier spacings can be generated based on the phase of the autocorrelation function ϕ_n^ℓ at time instant n_{coarse}^ℓ as [64]:

$$\hat{\gamma}^\ell = \frac{I}{2\pi}\angle\{\phi^\ell_{n^\ell_{\text{coarse}}}\}, \tag{42}$$

where $I = N/N_I$. Moose [67] showed this to be an ML estimator for the frequency offset which was extended to MIMO-OFDM systems by Mody [63] and Zelst et al. [108]. The MSE for such an estimator is given by

$$MSE_\gamma = N_0/\{(2\pi)^2 GL\}. \tag{43}$$

The frequency offset can then be removed from the received sample stream at the ℓ^{th} receive antenna by multiplying it by $\exp\left\{-j2\pi\hat{\gamma}^\ell[(d-1)(N+G)+n]/N\right\}$. Reducing the length of the preamble sub-sequences by a factor of I increases the frequency offset estimation range by a factor of I, at a penalty in the MSE performance.

Step IIIA. Integer Frequency Offset Estimation - Time domain frequency offset estimation is followed by post-FFT processing to obtain the frequency offset estimate of an integral number of subcarrier spacings. In this method a A frequency offset of an integral number of subcarrier spacings may still exist and it must be removed. Since the signal transmission matrix is constructed such that the same sequence is transmitted from all the transmit antennas for $d = 1$, a cyclic cross-correlation of the demodulated OFDM symbol with the original sequence can be performed to estimate the residual frequency offset Γ [121]. To use this method for MIMO OFDM systems with Q =2, 4 and 8, the first preamble sub-sequence $\{s_1\}_{n=0}^{N_I-1}$ must be identical for all Q transmit antennas in order for cross-correlation to be accurate and successful. The received frequency corrected time domain sequence from the first stage of frequency offset compensation $\{r_n^{1,\ell\ c}\}_{n=0}^{uN_I-1}$ is repeated I times and its uN-point FFT yields the sequence $\{R_k^{1,\ell\ c}\}_{k=0}^{uN-1}$. Then the cyclic

cross-correlation (in the frequency domain) with the known transmitted sequence is

$$\chi_k = \sum_{\ell=1}^{L} \left| \sum_{n=0}^{uN-1} S^{1,1\ *}_{(k+n)_{uN}} R^{1,\ell\ c}_{n} \right| \quad k = 0, 1, \ldots, uN-1, \tag{44}$$

and frequency offset of integral number of subcarrier spacings is estimated as

$$\hat{\Gamma} = \text{argmax}\{\chi_k\}. \tag{45}$$

In summary, the fractional part of the relative frequency offset within $\pm I/2$ sub-carrier spacings is estimated in the time domain, while the integer part beyond $\pm I/2$ sub-carrier spacings is estimated in the frequency domain.

Step IVA. Fine Time Synchronization - Fine time acquisition consists of finding the start of the useful portion of the OFDM frame to within a few samples. Once the frequency offset is removed, fine time synchronization can be performed by cross-correlating the frequency compensated received samples of the complex envelope with the transmitted time domain preamble sequences [41]. Performing fine time synchronization in the time domain rather than the frequency domain is more appropriate for MIMO OFDM systems as compared to other frequency domain methods suggested in the literature. Fine time synchronization ensures detection of the training sequence, especially when $I = 1$, and reduces P_{FA}. For a MIMO OFDM system with Q transmitters, Q cross-correlators are employed for each receive antenna and their magnitudes are summed to achieve fine time synchronization. The The fine time synchronization metric is set as

$$n^{\ell}_{\text{fine}} = \left\{ \arg \underbrace{\max}_{n} \left\{ \psi^{\ell}_{n} \right\} : \psi^{\ell}_{n} \geq \rho_{\text{fine}} \cdot P^{\ell}_{n} \right\}, \tag{46}$$

where the cross-correlation sequence is

$$\psi^{\ell}_{n} = \sum_{q=1}^{Q} \left| \sum_{k=0}^{uN_I-1} s^{1,q\ *}_{k} \cdot r^{\ell\ c}_{n+k} \right|, \tag{47}$$

$$P^{\ell}_{n} = \sum_{k=0}^{uN_I-1} |r^{\ell\ c}_{n+k}|^2 \tag{48}$$

and the $r^{\ell\ c}_{n+k}$ are the received frequency offset corrected samples. If the same sequences are transmitted from all antennas then only one cross-correlator is needed per receiver antenna. Once again, the threshold ρ_{fine} is set at 10% of the energy contained in the N_I

received samples. Since fine time synchronization is a computationally expensive process, it is conducted for a small window centered around the coarse time synchronization instant n^{ℓ}_{coarse}. The task can be simplified for DSP implementation by approximating the transmitted and received sequence with $\{+1, -1\}$. The net time synchronization instant is chosen as $n_{\text{opt}} \sum_{\ell=1}^{L} \alpha_{\ell} n^{\ell}_{\text{fine}}$ where non-equal weights may be applied to put more emphasis on the stronger signal. Finally, a negative offset of a few samples is applied to n_{opt} to ensure that the fine time synchronization instant lies within the guard interval.

3.2.2 Step *VA*- Sampling and Residual RF Oscillator Frequency Offset Estimation

Although most of the RF oscillator frequency offset was removed in the time and frequency domains as explained earlier, a small residual error (γ_e) might still remain. Also, if the phase noise is pretty severe, then it needs to be estimated and corrected. In this section we propose a novel estimator to estimate the SF offset coefficient β, and either the residual RF oscillator frequency offset γ_e or the phase noise ϑ, but not both [65, 94]. Starting with the d^{th} block, the received sample matrix corresponding to the k^{th} pilot subcarrier position is

$$\mathbf{R}^{d}_{k} = A^{d}_{k} C_k \mathbf{\Lambda}_k \mathbf{S}^{d}_{k} \cdot \mathbf{H}^{d}_{k} + \mathbf{W}^{d}_{k}. \tag{49}$$

For the WLAN and WMAN applications considered in this part of our research, the channel exhibits a very low Doppler. If we proceed under the assumption that the channel remains virtually constant for $2Q$ consecutive OFDM symbols, then the received sample matrix corresponding to the pilot subcarrier positions for the next block of Q OFDM symbols is

$$\mathbf{R}^{d+Q}_{k} = A^{d+Q}_{k} C_k \mathbf{\Lambda}_k \mathbf{S}^{d+Q}_{k} \cdot \mathbf{H}^{d}_{k} + \mathbf{W}^{d+Q}_{k}. \tag{50}$$

Hence, we can correlate $\mathbf{R}^{d}_{k}$ and $\mathbf{R}^{d+Q}_{k}$ at the p^{th} pilot tone position to obtain an initial per sub-carrier estimate of $k_p\beta + \Upsilon$ as, [65]:

$$\begin{aligned} k_p\hat{\beta} + \hat{\Upsilon} &= \frac{\angle \text{Tr}[\mathbf{R}^{d\ \text{H}}_{k_p} \mathbf{R}^{d+Q}_{k_p}] + f\left(P_d, P_{d+Q}\right)}{2\pi Q(N+G)/N} \\ D_p &= \frac{\angle \sum_{d=1}^{Q} \sum_{\ell=1}^{L} |R^{d,\ell}_{k_p}|^2 \text{exp}\left\{j2\pi Q(k_p\beta + \Upsilon)(1+G/N)\right\} + f\left(P_d, P_{d+Q}\right)}{2\pi Q(1+G/N)}, \end{aligned} \tag{51}$$

where $\hat{\Upsilon} = \hat{\gamma_e}$ or $\hat{\Upsilon} = [\hat{\vartheta}^{d+Q} - \hat{\vartheta}^{d}]/[2\pi Q(1+G/N)]$ and $f\left(P_d, P_{d+Q}\right) = \pi$ if $P_d \neq P_{d+Q}$ and 0 if $P_d = P_{d+Q}$. The above measurements may be put in the matrix form

$$\underbrace{\begin{bmatrix} D_1 \\ \vdots \\ D_M \end{bmatrix}}_{\underline{D}} = (2\pi Q(1+G/N)) \underbrace{\begin{bmatrix} k_1 & 1 \\ \vdots & \vdots \\ k_M & 1 \end{bmatrix}}_{\mathbf{J}} \underbrace{\begin{bmatrix} \beta \\ \Upsilon \end{bmatrix}}_{\hat{\underline{\theta}}} + \underbrace{\begin{bmatrix} \epsilon_1 \\ \vdots \\ \epsilon_M \end{bmatrix}}_{\underline{\epsilon}}. \tag{52}$$

The estimate $\hat{\underline{\theta}} = [\hat{\beta}\ \hat{\Upsilon}]^T$ is obtained using a least-square fit as

$$\hat{\underline{\theta}} = \frac{1}{(2\pi Q(1+G/N))} (\mathbf{J}^H \mathbf{J})^{-1} \mathbf{J}^H \underline{D}. \tag{53}$$

The MSE expressions for these estimators are derived in Appendix B and are given by

$$\mathrm{MSE}_{\beta} = \left[\frac{\left[N_0 + \frac{N_0^2}{2\bar{\mathbf{H}}^2} Q^2\right]}{\left(2\pi Q\left(1+\frac{G}{N}\right)\right)^2 \bar{\mathbf{H}}^2} \left(\frac{P}{P\sum_{p=1}^{P} k_p^2 - \left(\sum_{p=1}^{P} k_p\right)^2} \right) \right] \tag{54}$$

$$\mathrm{MSE}_{\gamma_e} = \left[\frac{\left[N_0 + \frac{N_0^2}{2\bar{\mathbf{H}}^2} Q^2\right]}{\left(2\pi Q\left(1+\frac{G}{N}\right)\right)^2 \bar{\mathbf{H}}^2} \left(\frac{\sum_{p=1}^{P} k_p^2}{P\sum_{p=1}^{P} k_p^2 - \left(\sum_{p=1}^{P} k_p\right)^2} \right) \right] \tag{55}$$

$$\mathrm{MSE}_{\vartheta} = \left[\frac{\left[N_0 + \frac{N_0^2}{2\bar{\mathbf{H}}^2} Q^2\right]}{\bar{\mathbf{H}}^2} \left(\frac{\sum_{p=1}^{P} k_p^2}{P\sum_{p=1}^{P} k_p^2 - \left(\sum_{p=1}^{P} k_p\right)^2} \right) \right], \tag{56}$$

where $\bar{\mathbf{H}}^2 = \mathrm{E}\left[\sum_{q=1}^{Q}\sum_{\ell=1}^{L} |H_p^{q,\ell}|^2\right]$.

At this stage, the system designer needs to make a choice whether to estimate the residual frequency offset γ_e or the phase noise difference $[\hat{\vartheta}^{d+Q} - \hat{\vartheta}^{d}]$. If the frame-size is large, then any residual frequency offset causes a linear increase in the phase of the received symbols with time which results in a BER floor. On the other hand, for short frame sizes, large fluctuations in the phase noise can not be ignored. Hence, either,

$$\hat{\gamma_e} = \left[\hat{\underline{\theta}}\right]_2 \tag{57}$$

or, if the residual RF oscillator frequency offsets have been reduced to a small enough value by averaging the time domain estimates over a number of OFDM symbols, then the phase noise difference may be estimated as

$$[\hat{\vartheta}^{d+Q} - \hat{\vartheta}^{d}] = [2\pi Q(1+\frac{G}{N})] \left[\hat{\underline{\theta}}\right]_2. \tag{58}$$

The residual frequency offset estimate is fed back to the time domain RF oscillator frequency offset correction circuit, whereas the estimates of the SF offset and the phase noise difference, are used to construct the terms $\hat{A}_k^d \hat{C}_k \hat{\mathbf{\Lambda}}_k$. The new estimate of the received and demodulated sample matrix sans the effects of $(\Gamma, \gamma, \beta, \vartheta^d)$ is then obtained using

$$\hat{\mathbf{R}}_k = \left(\hat{A}_k^d \hat{C}_k \hat{\mathbf{\Lambda}}_k \right)^{-1} \mathbf{R}_k \tag{59}$$

which is used for decoding the data. Derivation of the MSE performance of this estimator is given in Appendix A.

3.2.3 Step *VIA* - Channel and Noise Variance Estimation

Most contributions on channel estimation do not consider the effects of the residual RF oscillator and SF offset on the preamble while estimating the channel coefficients. The receiver must first estimate the sampling frequency offset using signal transmission matrices at the pilot sub-carriers in the preamble and the next block of Q OFDM data symbols, before estimating the channel, and these effects must be accounted for in the channel estimator. Hence, the channel estimates at sub-carriers excited with known signal transmission matrices may be estimated using

$$\hat{\mathbf{H}}_p = (\mathbf{B}_p^H \mathbf{B}_p)^{-1} \mathbf{B}^H \mathbf{R}_p \ , \tag{60}$$

where $\mathbf{B}_p = A_p^d C_p \mathbf{\Lambda}_p \mathbf{S}_p$. The MSE expression for this estimator is derived in Appendix B and is given by

$$\text{MSE}_{\mathbf{H}} = N_0 \tag{61}$$

When $I \neq 1$, the initial channel coefficients obtained from the preamble must be interpolated/ extrapolated to obtain the channel estimates for all the sub-carriers.

Once all the frequency offsets have been removed the receiver may estimate the noise variance from the unused sub-carriers $[101 \ldots 156]$ of the IEEE 802.16a system or from the additional samples of $\underline{R}$ as a result of over-sampling at the receiver as shown in Figure 18. Noise variance estimates may be utilized in a number of different ways at the receiver; from

implementing an MMSE equalizers to their use in decoding the channel codes such as low density parity check (LDPC) [32]. The estimates of the noise variance are given by

$$N_0 = \frac{1}{N_{\text{unused}}} \sum_{k \in \text{unused}} \left| R_k^{d,l} \right|^2 . \tag{62}$$

This estimator is extremely accurate. The MSE expression for this estimator is derived in Appendix B and is given by

$$\text{MSE}_{\text{noise}} = \frac{N_0^2}{N_{\text{unused}}} \tag{63}$$

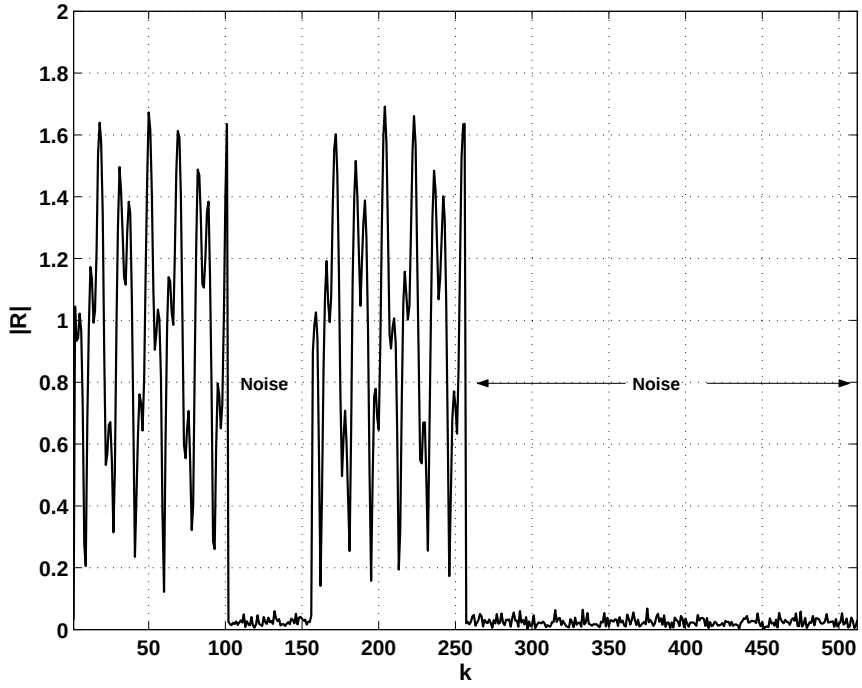

Figure 18: The received over-sampled OFDM-demodulated waveform after removal of the frequency offsets.

3.3 Step B - Parameter Tracking

Since we assume that the RF oscillator frequency offset drifts slowly, in the tracking mode, the receiver needs to track the SF offset, and the channel coefficients.

3.3.1 Step *IB* - Sample Time Tracking

In [65], we presented a technique for open loop sample time tracking based on least-square principles. However, we find that the MSE in the estimation error is high for the suggested estimator. Hence, we suggest the use of (52) to track the SF offset coefficient assuming that it assumes a new value every Q or more OFDM symbols.

The sampling time T' at the receiver suffers from jitters, which are reflected in the changes in the SF offset coefficient β. If we assume that β assumes a new value, every Q OFDM symbols, then the new estimates of β may be obtained using (53). If $\hat{\beta}^{d-Q}$ and $\hat{\beta}^{d}$ are the sampling frequency offset estimates for the MIMO-OFDM blocks at the $(d-Q)^{\text{th}}$ and d^{th} OFDM symbols, respectively, then the final estimate of the sampling frequency offset is computed using a first-order frequency locked loop

$$\hat{\beta}^{d} = \alpha_{\beta}\hat{\beta}^{d-Q} + (1-\alpha_{\beta})\hat{\beta}^{d}. \tag{64}$$

This final estimate is then used to compensate for sampling frequency offset by computing

$$\hat{\mathbf{R}}_k = (\hat{A}_k^d \hat{C}_k \hat{\mathbf{\Lambda}}_k)^{-1}\mathbf{R}_k. \tag{65}$$

3.3.2 Step *IIB* - Channel Tracking

Even though, for WLAN and WMAN applications, the channel changes little from frame to frame, it constantly needs to be updated since the effective channel is constantly changing due to the accumulation in the parameter estimation errors. In this part of our research we use decision directed channel tracking followed by an exponential weighted averaging as shown in the Figure 17. Suppose, $\hat{\mathbf{S}}_k^d$ is the estimated signal transmission matrix at the d^{th} OFDM symbol, then the new estimates of the corresponding channel estimates are given by $\hat{\mathbf{H}}_p^d = (\hat{\mathbf{B}}_p^H \hat{\mathbf{B}}_p)^{-1}\hat{\mathbf{B}}_p^H \mathbf{R}_p$, where, $p = 0, \ldots, N-1$, and $\hat{\mathbf{B}}_p = \hat{A}_p^d \hat{C}_p \hat{\mathbf{\Lambda}}_p \hat{\mathbf{S}}_p^d$. The updated estimates of the channel, used to decode the symbols at the $(d+Q)^{\text{th}}$ OFDM symbol are given by

$$\hat{\mathbf{H}}_p^{d+Q} = \alpha_{\mathbf{H}_p}\hat{\mathbf{H}}_p^{d} + (1-\alpha_{\mathbf{H}_p})\hat{\mathbf{H}}_p^{d-Q}. \tag{66}$$

3.4 Simulation Results

Simulations are conducted for a 4×4 WMAN system very similar to IEEE802.16a [37] at a carrier frequency of 5.8 GHz operating on a Stanford University Interim (SUI)-4 channel [25]. The SUI-4 model is appropriate for intermediate path loss with moderate to heavy tree densities, and has the parameters listed in Table 1. The Doppler power spectrum for the

Table 1: SUI-4 Channel Model [26]

	Tap 1	**Tap 2**	**Tap 3**	**Units**
Delay	0	1.5	4.0	μs
Power (omni ant.)	0	-4	-8	dB
f_m	0.2	0.15	0.25	Hz

channel taps is [26]

$$S(f) = \begin{cases} 1 - bf_0^2 + cf_0^4 & |f_0| \leq 1 \\ 0 & |f_0| > 1 \end{cases} \text{ where } f_0 = \frac{f}{f_m}$$

where $b = 1.72$, $c = 0.784$ and f_m represents the maximum Doppler frequency defined in the Tables **??** and 1. The corresponding autocorrelation function is found as the inverse Fourier transform of the $S(f)$, viz.

$$\phi(f_m\tau) = f_m\rho(f_m\tau), \tag{67}$$

where

$$\begin{aligned} \rho(f_m\tau) \quad = \quad & \frac{2}{4(\pi f_m\tau)^5}\Big\{\Big[-6c\pi f_m\tau - 2b(\pi f_m\tau)^3 + 4c(\pi f_m\tau)^3\Big]\cos(2\pi f_m\tau) + \\ & \Big[b(\pi f_m\tau)^2 + 2(\pi f_m\tau)^4 - 2b(\pi f_m\tau)^4 + c\left(3 - 6(\pi f_m\tau)^2 + 2(\pi f_m\tau)^4\right)\Big] \\ & \sin(2\pi f_m\tau)\Big\}, \end{aligned} \tag{68}$$

and

$$\lim_{\tau\to 0}\rho(f_m\tau) = \int_{-1}^{1} S(f)df = 1.167. \tag{69}$$

The normalized autocorrelation function is shown in Figure 19. Rayleigh faded tap coefficients for the MIMO channel are generated using a filtered Gaussian noise source as described in [93] with spectral shaping in the frequency domain to yield the desired Doppler

power spectrum. The fading tap coefficients are uncorrelated. The sampling rate is assumed to be $1/T = 4.0$ MHz.

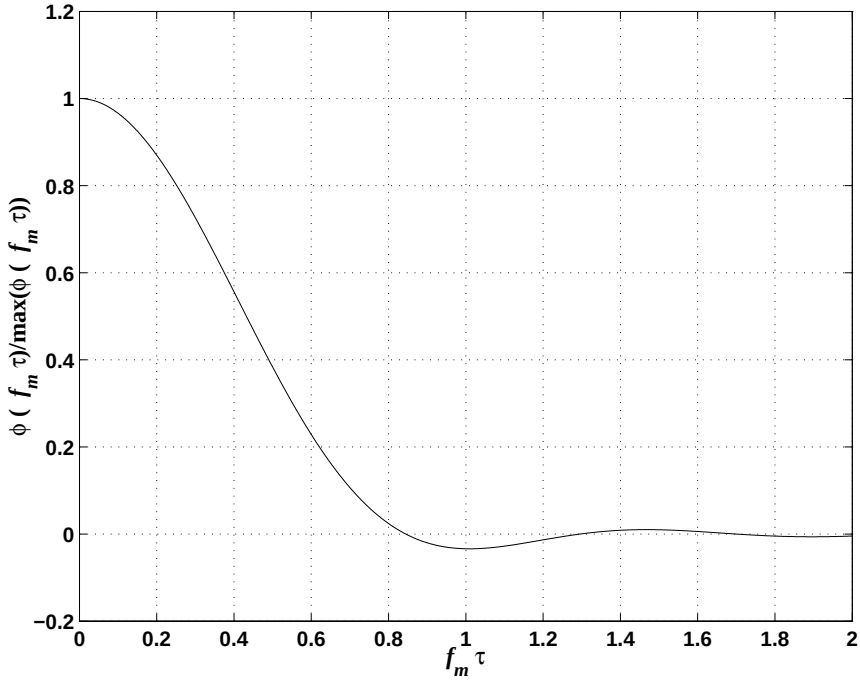

Figure 19: Autocorrelation function for the SUI channel tap.

The preamble signal matrix with 4 transmit antennas is as shown in (38). The preamble sequences are obtained using BPSK modulation in the frequency domain. For various values of I, we use sequences with a lowest peak to average power ratio (PAPR) using computer search. The OFDM blocksize is $N = 256$, and the guard interval length is $G = N/4 = 64$. Of the 256 sub-carrier, the dc sub-carrier and 55 other sub-carriers at the band edges are set to zero [37]. Therefore, $N_u = 200$ sub-carriers, $[1 \ldots 100\ 156 \ldots 255]$, are used. The preamble for a system with $I = 2$, has known symbols at sub-carriers $[2\ 4 \ldots 100\ 156\ 158 \ldots 254]$ and the channel estimates for the remaining sub-carriers are be interpolated/ extrapolated from known ones. In the data mode, 8 pilot tones are inserted for each OFDM block in a manner described earlier. Each frame consists of a preamble followed by F OFDM symbols. The sampling frequency offset coefficient β is initialized at 10 parts per million (ppm) and fluctuates around that value every Q OFDM symbols, as $\beta = 10\text{ppm} + N(0, 10\%\text{ of }\beta\text{ ppm})$, characterizing the timing jitter. The fractional frequency

offset γ is initialized to 0.2 subcarrier spacings, and is made to vary from frame to frame in a random walk as $\gamma = 0.2 + N(0, 10\%$ of γ ppm), symbolizing the relatively slow RF oscillator frequency offset drift. Phase noise is assumed to have a zero-mean Gaussian distribution with variance of 10π and 50π ppm. Phase noise is assumed to change every Q OFDM symbols. The integer frequency offset Γ is assumed to be one sub-carrier spacing. In this research, the transmission is carried out using the rate-3/4 Space-Time Code (STC) suggested by Tarokh [100] with a 16-QAM alphabet; however the suggested algorithms and preamble/ pilot tone structures may be applied to any MIMO-OFDM transmission technique. For the tracking mode, the parameters α_β and $\alpha_{\mathbf{H}_p}$ are set at 0.01 and 0.5 respectively. This part of our research does not apply any channel coding. We have shown elsewhere that the use of channel coding such as low density parity check codes (LDPC) can greatly improve BER performance by sacrificing data rate [34].

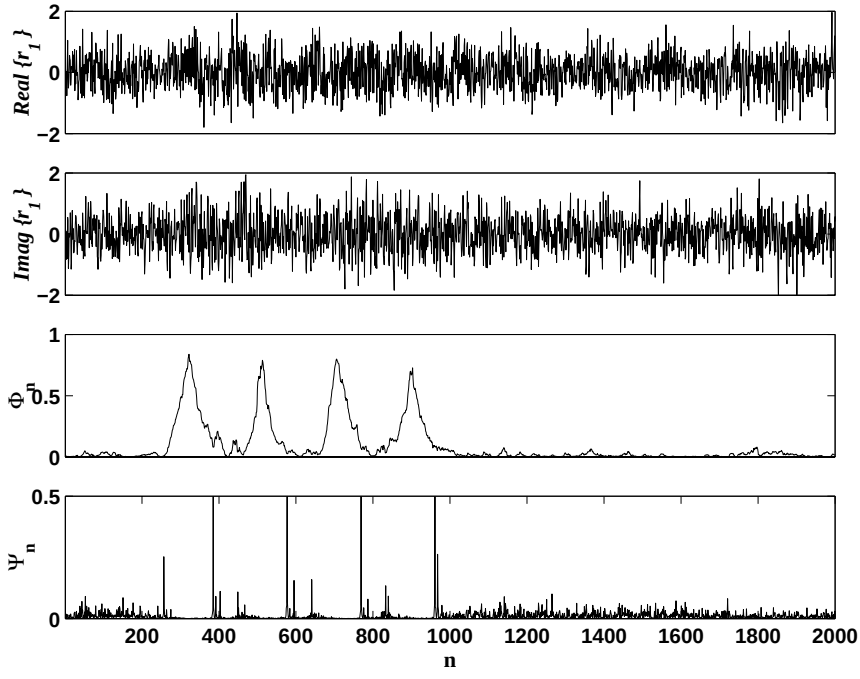

Figure 20: Coarse and fine time synchronization for a 4×4 system with $N_I = 128$ at an E_s/N_0 of 10 dB per receive branch and frequency offset $\Gamma + \gamma$ of 1.2 subcarrier spacings. Steps IA and IVA.

Figure 20 shows the coarse and fine time synchronization performance for a 4×4 system with $N_I = 128, I = 2$, and E_s/N_0=10 dB. Figure 22 shows the theoretical and experimental

MSE performance of the frequency offset estimator used in Step IIA and Step VA as a function of the E_s/N_0 per receive branch, defined earlier. For $I = 2$, the average value of the

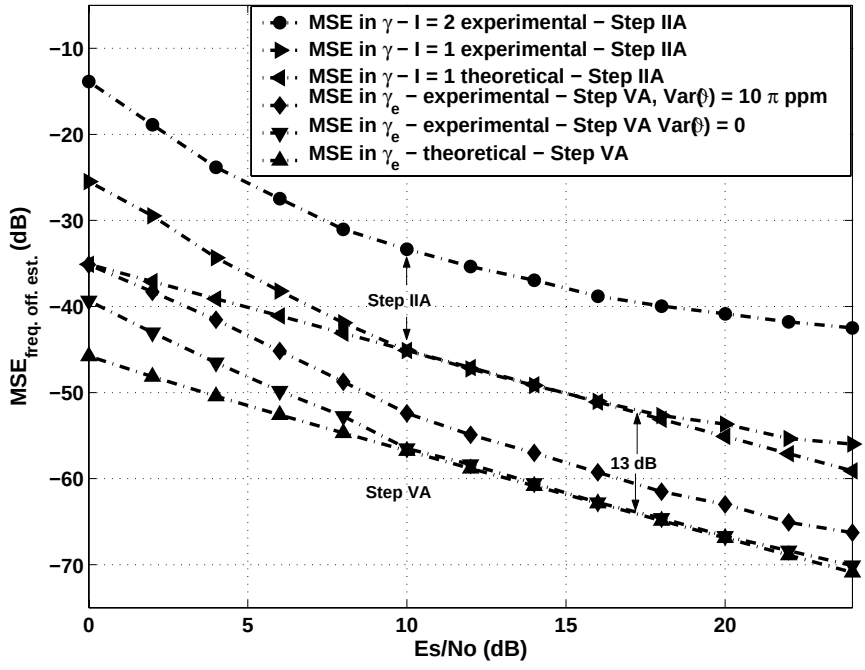

Figure 21: Theoretical and experimental MSE in frequency offset estimates as a function of E_s/N_0 for a 4×4 system - using Step IIA. and the residual RF oscillator frequency offset estimation (52) in the presence and the absence of the phase noise. $\Gamma + \gamma = 1.2$ subcarrier spacings.

frequency offset estimate ($\hat{\gamma}$) using Step IIA is -0.8 subcarrier spacings. This frequency offset estimate is used to correct the received time domain samples. Next the corrected samples are repeated $I = 2$ times and passed through the FFT stage. The demodulated samples are fed back to the integral frequency offset estimator. Figure 22 shows the normalized correlation metric in (44) used to estimate the integer frequency offset at E_s/N_0=10 dB.

The integer frequency offset $\hat{\Gamma}$ is estimated to be 2 subcarrier spacings. The integer frequency offset is removed by either adjusting the local oscillator at RF or by multiplying the samples in baseband with a frequency correction exponent. Finally, fine time synchronization is performed using (46) with the result shown in Fig. 20. Figure 22 also shows the theoretical and experimental MSE of the proposed residual frequency offset estimator (52). This estimator gives a 13 dB performance improvement compared to the one in Step IIA,

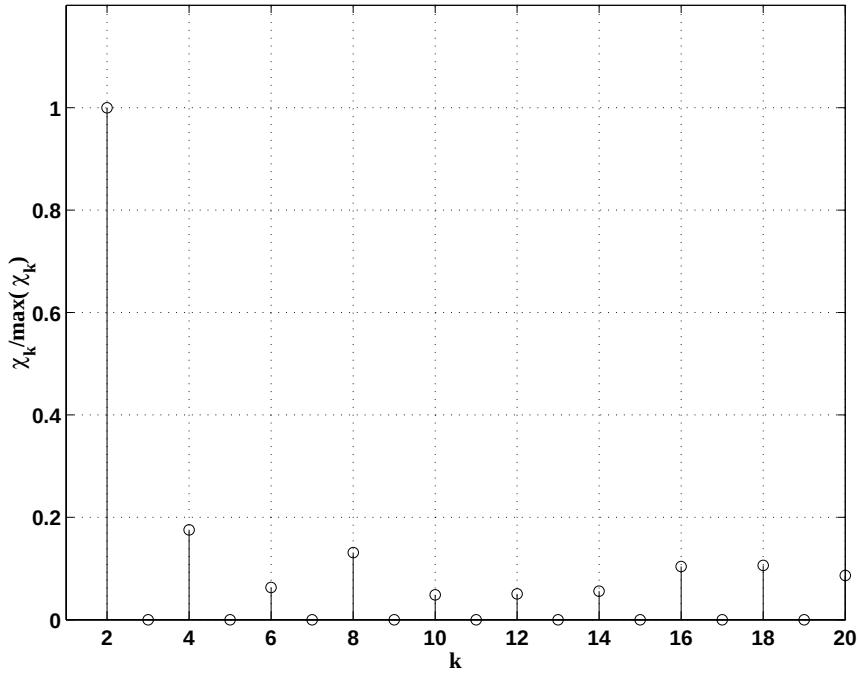

Figure 22: Residual frequency offset estimation in the frequency domain for a 4×4 system, Step IIIA., E_s/N_0=10 dB per receive branch, $\Gamma+\gamma$=1.2, I=2, $\hat{\gamma}=-0.8$, $\hat{\Gamma}=2$.

but its performance degrades in the presence of the phase noise.

Figure 23 shows the performance of the channel estimator for various values of I (or N_I) using (143). No further post-processing is performed on the channel estimates. For $I=2$, we use cubic spline interpolation to obtain the channel coefficients at all the sub-carriers. As I increases, the channel estimates degrade because of imperfect interpolation and extrapolation, especially at the band edges.

Figure 24 shows the theoretical and experimental performance of the sampling frequency offset estimator. The actual performance closely follows the theoretical values, and performs well for the system under consideration.

Figure 25 shows the theoretical and experimental performance of the phase noise estimator for a perfect frequency offset estimation and frequency offset estimation using Step IIA. As can be seen, presence of any residual frequency offset affects the phase noise estimate.

Figure 26 shows the analytical and experimental MSE in the noise variance estimates as a function of E_s/N_0. As can be seen from the graph, the estimator given by (62) performs

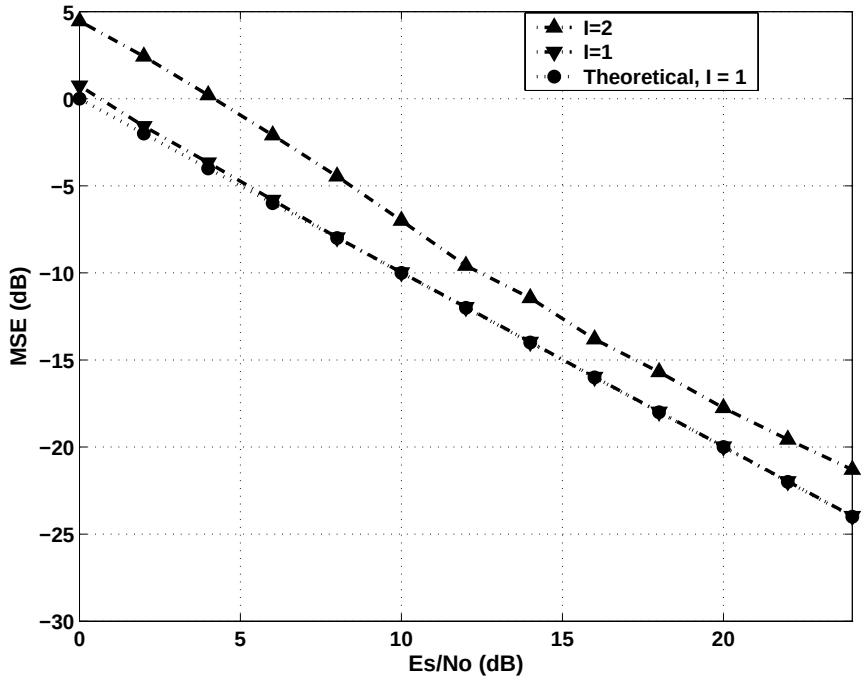

Figure 23: MSE in channel estimates as a function of E_s/N_0, $N = 256$, $N_u = 200$, $\Gamma + \gamma$=1.2, $\mathrm{Var}(\vartheta) = 10\pi$ ppm.

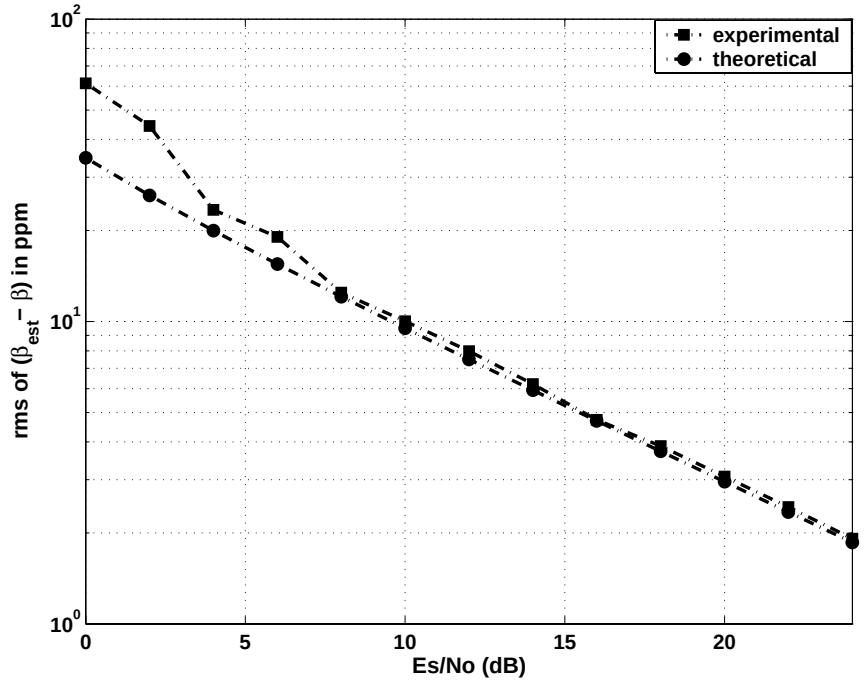

Figure 24: Analytical and experimental root mean square (rms) of the $(\hat{\beta} - \beta)$ in ppm as a function of E_s/N_0.

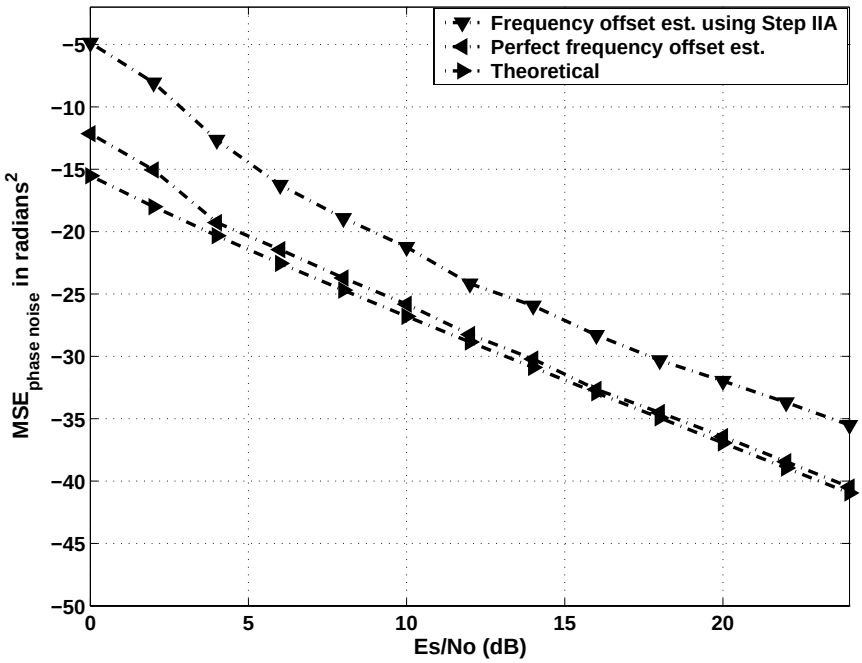

Figure 25: Analytical and experimental MSE in the phase noise estimates in radians^2 as a function of E_s/N_0.

very well and the theoretical and experimental performance curves are very close.

Figure 27 shows the BER performance of the system using the suggested algorithms for signal acquisition in the absence of SF offset phase noise. Hence, the sampling frequency offset stage is bypassed. A system using excitation of all the tones, for example using a chirp sequence in the training sequence gives a BER performance that is about 1 dB from the ideal performance. The curve with $N_u = 200$, and $I = 1$, is about 1.9 dB away from the ideal system performance at a BER of 1×10^{-4}. A system with $I = 2$ requires around 2.75 dB higher E_b/N_0 and, finally, a system with $I = 4$ fails to reach a BER of 1×10^{-4}.

Figures 28 and 29 show the BER performance of the system using the suggested algorithms for signal acquisition and tracking. The BER curves are plotted against the bit energy-to-noise ratio (E_b/N_0) defined as $(E_b/N_0)_{\text{dB}} = (E_s/N_0)_{\text{dB}} - 10\log_{10}(m \cdot R_{\text{st}})$, where $m = 4$ for 16-QAM constellation and the space-time code rate is $R_{\text{st}} = 3/4$. Figure 28 is a simulation of a system with a frame size of $F = 80$ OFDM symbols and a phase noise variance of 10π ppm. For this case, we ignore the phase noise but estimate the residual RF oscillator frequency offset using Step VA. As can be seen, ignoring the phase noise gives

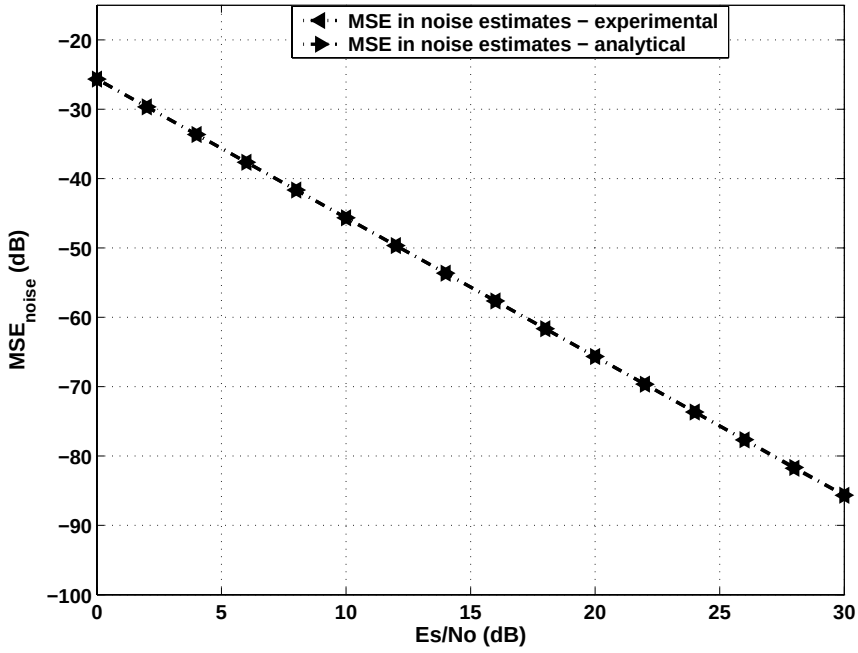

Figure 26: Analytical and experimental MSE in the AWGN estimates as a function of E_s/N_0.

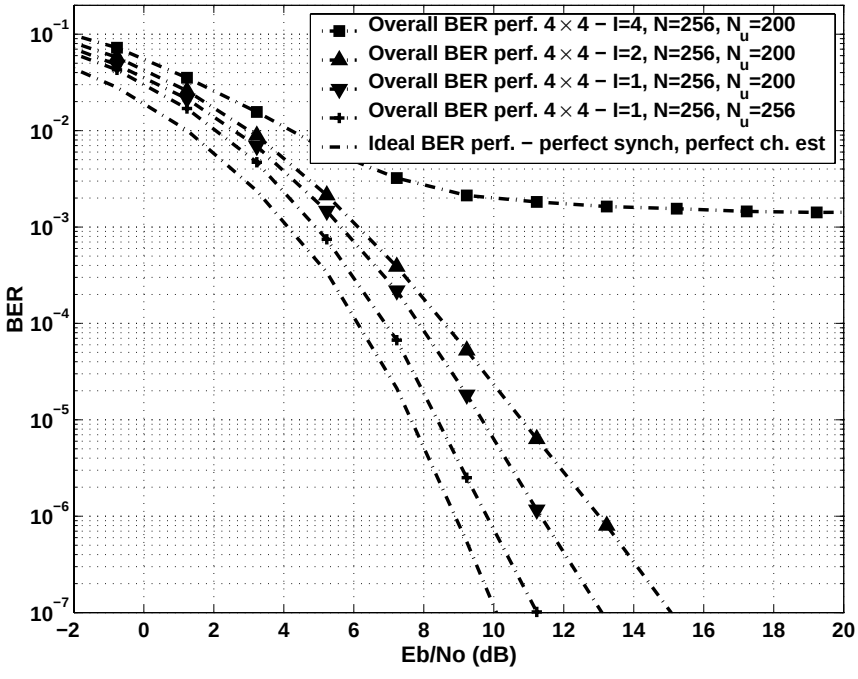

Figure 27: BER performance for a 4×4 system in the acquisition mode with only time synch., frequency synch. and channel estimation algorithms employed, $\beta = 0$, $\vartheta = 0$, frame length = 80 OFDM symbols and frequency offset $\Gamma + \gamma = 1.2$ subcarrier spacings, $N = 256$ and $N_u = 200$.

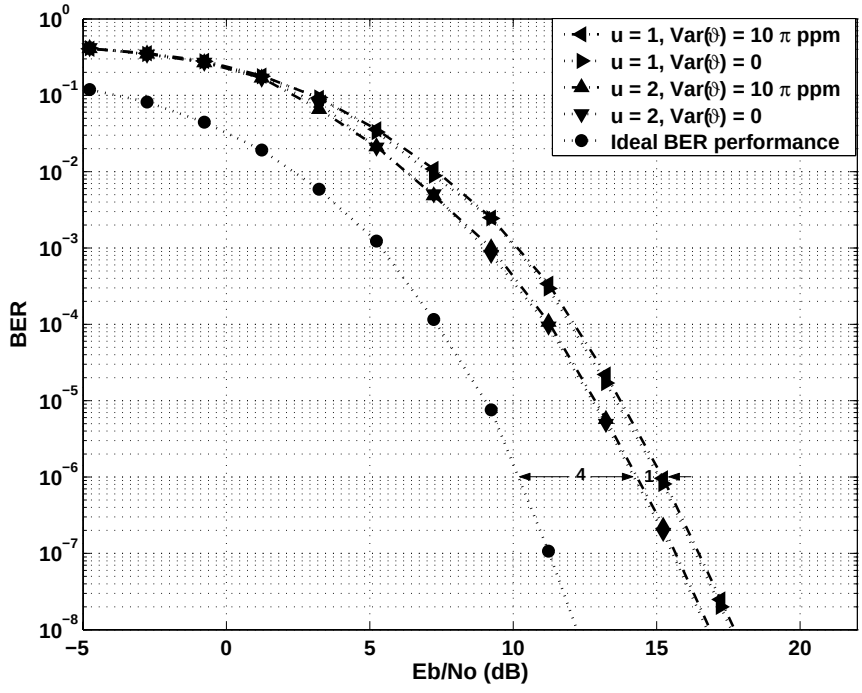

Figure 28: Overall BER performance for a 4×4 system in the presence and absence of the phase noise. $\beta = 10$ ppm, frame length F = 80 OFDM symbols, frequency offset $\Gamma + \gamma$ 1.2 subcarrier spacings, $I = 1$, $N = 256$ and $N_u = 200$.

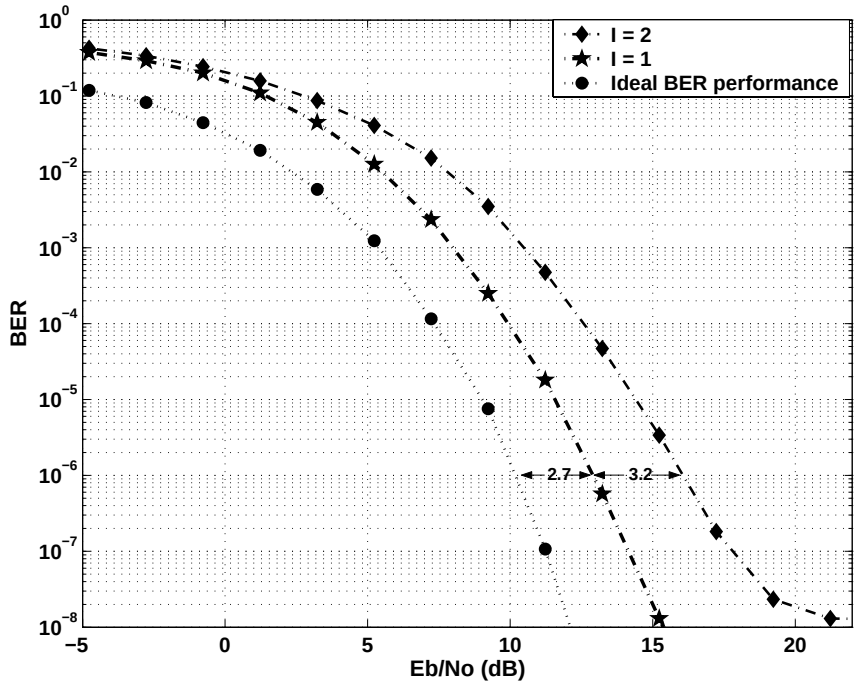

Figure 29: Overall BER performance for a 4×4 system in the presence of the phase noise. $\beta = 10$ ppm, frame length F = 40 OFDM symbols, frequency offset $\Gamma + \gamma = 1.2$ subcarrier spacings, $\mathrm{Var}(\vartheta) = 50\pi$ ppm, $N = 256$ and $N_u = 200$.

almost identical performance to the case when phase noise is non-existent. Over-sampling the received waveform by a factor of 2 provides a gain of 1 dB. The performance of the system for this scenario is around 4 dB away from the ideal system performance. Figures 29 is a simulation of a system with a frame size of $F = 40$ OFDM symbols and phase noise variance of 50π ppm. This time, we ignore the residual RF oscillator frequency offset, but estimate the phase noise using Step VA. The interpolation factor is 2, and simulations are performed for longer and shorter preamble, viz. $I = 1$ and 2. The performance of the system for this scenario is around 2.7 dB away from the ideal system performance. Use of a shorter preamble provides a lower system overhead at a larger penalty in the BER performance.

3.5 Concluding Remarks

This chapter presented a complete suite of signal acquisition and tracking algorithms for a MIMO-OFDM system operating in a fixed wireless access environment. Our algorithms

used a generalized preamble and pilot matrix structure to perform acquisition, consisting of time synchronization, RF and sampling frequency oscillator offset estimation, and channel estimation. This was followed by tracking of the sampling frequency offsets, phase noise jitters and the channel coefficients. Time synchronization is performed in two stages and RF oscillator frequency offset estimation is performed in three stages. Depending upon the intensity of the phase noise, the third RF oscillator frequency offset estimation stage may be used to estimate the phase noise instead. Novel estimators were provided for the sampling and residual RF oscillator frequency/ phase noise offsets that yielded low estimation errors. We also derived the MSE performance for our estimators. Simulation results were performed for a system very similar to IEEE 802.16a. Our algorithms were shown to perform well and our simulation results illustrated the combined effect of all required synchronization processes on the MIMO-OFDM receiver performance. Depending upon the two scenarios considered, our algorithms were found to be 2.7 and 4 dB away from the ideal BER curve. Finally, the proposed algorithms and pilot/training structure were independent of the space-time technology employed to implement the MIMO-OFDM system.

CHAPTER IV

CRAMÉR-RAO BOUNDS FOR THE PARAMETERS ASSOCIATED WITH SISO-OFDM SYSTEMS

4.1 Introduction

Often, it is necessary to establish a lower bound on the variance of an estimator. A lower bound acts as a benchmark against which the performance of any estimator may be compared. In this chapter we derive the Cramér-Rao bound(CRB)s for the parameters associated with a fixed wireless access SISO-OFDM system [60]. It is difficult to derive the CRBs for a MIMO-OFDM system and hence, we leave this as future work. As discussed in the previous chapter, some of the unknowns for a typical OFDM system for wireless applications are the sampling frequency (SF) offset, the radio frequency (RF) oscillator frequency offset, the phase noise, the channel coefficients and, finally, the variance of the additive white Gaussian noise (AWGN). We also saw in Chapter 3 that we can either estimate the RF oscillator frequency offset γ or the phase noise ϑ, but not both. Hence, we ignore the presence of phase noise from our analysis. However, the CRB for the RF oscillator frequency offset and the phase noise are interchangeable and one may be obtained from the other. To simplify the CRB derivation we have changed the frame definitions slightly. However, this will not impact the final result.

4.2 Re-Formulating the System Model

To simplify the CRB derivations, we re-formulate the system model. This however will not affect the final results. Consider a SISO-OFDM system as shown in Figure 30. The individual OFDM modulators and demodulators are implemented using an N-point IFFT and FFT, respectively. A block of N data symbols specifies the frequency domain coefficients input to the IFFT. The block of N time domain coefficients at the IFFT output constitute

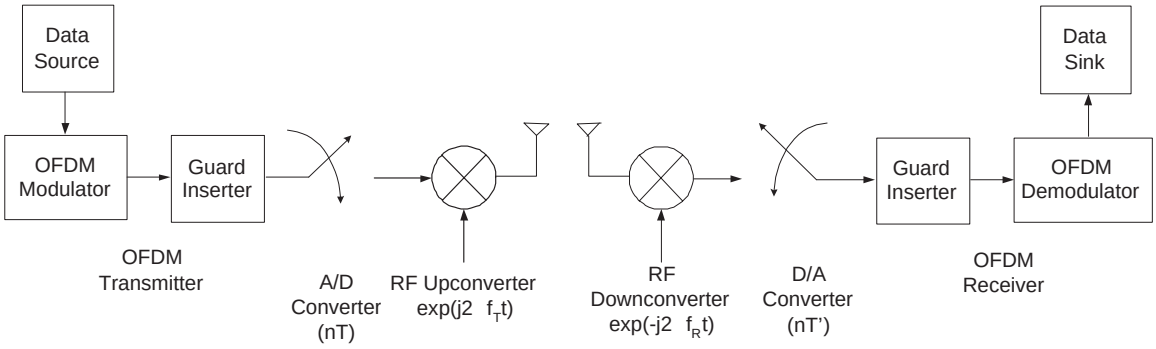

Figure 30: System diagram of a SISO-OFDM system.

an OFDM block. Let $d = 0, 1, \ldots$ be the running OFDM symbol index. Then the time-domain samples are

$$s_n^d = \frac{1}{\sqrt{N}} \sum_{k'=0}^{N-1} S_{k'}^d \exp\left\{ j2\pi n \frac{k'}{N} \right\},\ 0 \le n \le N-1\ , \tag{70}$$

where $S_{k'}^d$ is the data symbol transmitted for the d^{th} OFDM symbol at the k'^{th} sub-carrier. The total average energy transmitted E_s, is normalized to unity such that $E_s = \frac{1}{2}\mathrm{E}\left\{ \left| s_n^d \right|^2 \right\} = 1,\ \forall d,\ n.$

To mitigate the effects of channel delay spread, a cyclic prefix (CP) consisting of the last G coefficients are inserted in front of the OFDM block to form an OFDM symbol. To fully remove ISI the cyclic prefix duration, $T_g = GT$, must equal or exceed the maximum delay of the channel, T_m, where $1/T$ is the sample rate. The time required to transmit one OFDM symbol is the OFDM symbol time, $T_s = GT + NT = GT + T_u$, where $T_u = NT$. Once again, we modify the cyclic prefix insertion slightly, the first $G/2$ samples from the front of the OFDM symbol are inserted at the back of the OFDM symbol as a suffix and the last $G/2$ samples from the back of the OFDM symbols are inserted in the front as a prefix as shown in the Figure 31. The corresponding real and imaginary components of the OFDM symbol samples are applied to a pair of D/A converters operating at a sampling frequency of $1/T$ Hz to generate the set of complex envelopes. The set of complex envelopes on the interval $(dT_s + GT, (d+1)T_s)$ is

$$s^d(t) = \sum_{k'=0}^{N-1} S_{k'}^d \cdot \exp\left\{ j \frac{2\pi k'}{T_u} (t - (d+1)GT - dNT) \right\}. \tag{71}$$

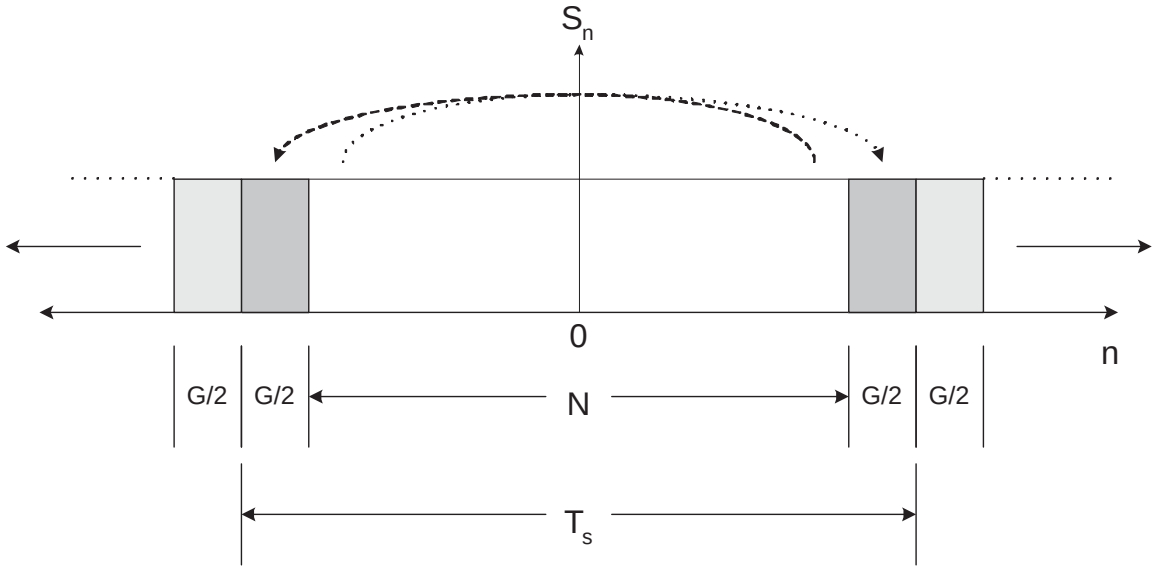

Figure 31: Frame structure for the SISO-OFDM system for the CRB derivation.

The complex envelopes are up-converted to RF with a carrier frequency of f_T Hz.

The waveforms are transmitted over a frequency selective channel characterized by the time-variant impulse responses

$$h(\tau, t) = \sum_{m=0}^{M-1} h_m(t)\delta(\tau - \tau_m), \tag{72}$$

where $\{h_m\}$ are the time varying complex path gains, $\{\tau_m\}$ are the corresponding path time delays, and M is the total number of paths for each channel. Assuming that the channel is static for at least one OFDM symbol duration, the channel transfer functions are given by

$$\tilde{H}_{d,k'} = \sum_{m=0}^{M-1} h_m(dT_s) \exp\left\{-j2\pi\tau_m^{q,l}k'/T_u\right\}, k' = 0, \ldots, N-1. \tag{73}$$

The received bandpass signals are down-converted to complex baseband using a local oscillator with carrier frequency f_R Hz. Since the transmitter and the receiver RF oscillators have different frequencies, the received complex envelope is affected by an RF oscillator frequency offset of $\Gamma + \gamma = (f_R - f_T)T_u$ sub-carrier spacings, where Γ and γ refer to the integer and the fractional components of the radio frequency (RF) oscillator frequency offset in the units of sub-carrier spacings, respectively.

The received complex envelope is also affected by RF oscillator phase noise $\vartheta(t)$. However, since the RF oscillator frequency offset γ and the phase noise $\vartheta(t)$ are dependent

parameters, only one of them can be estimated at a time. Hence in this analysis we ignore the phase noise $\vartheta(t)$. However, we will later show that the CRB result for the RF oscillator frequency offset γ is applicable to the CRB for the phase noise $\vartheta(t)$ and one may be obtained from the other.

Also, since Γ has the net effect of shifting the down-converted OFDM signal by an integer number of sub-carrier spacings, it is ignored for the time being in the system equation. We later show a way to estimate and correct this integer offset. The received complex baseband signal can be expressed as

$$r(t) = \frac{1}{\sqrt{N}} \sum_{k'=0}^{N-1} S_{k'}^{d} \tilde{H}_{d,k'} \exp\left\{\frac{j2\pi k' t}{T_u}\right\} \exp\left\{\frac{j2\pi\gamma t}{T_u}\right\} + w(t). \tag{74}$$

where $w^{\ell}(t)$ represents the complex additive white Gaussian noise (AWGN) with a variance of N_0. The real and imaginary components of the received complex baseband waveform are applied a pair of balanced A/D converters with a sampling frequency of $1/T'$ Hz. To counteract the aliasing introduced by the frequency offsets, and for improved parameter estimation, the waveforms are over-sampled by factor of u followed by a uN-point FFT which acts as an OFDM demodulator. Since the sampling frequencies at the transmitter and receiver differ, the received discrete-time samples are affected by the normalized sampling frequency (SF) offset coefficient $\beta = (T' - T)/T$.

In order to introduce symmetry, let n vary from $-\frac{(N-1)}{2}$ to $\frac{(N-1)}{2}$ in order to collect the time domain samples for the d^{th} OFDM symbol. In essence, this modification will result in the introduction of an additional phase term of the type $\exp\left\{\frac{j2pik'(N+1)/2}{N}\right\}$, which is absorbed in the channel coefficient $\tilde{H}_{k'} = H_{k'}$. Hence, such a modification will have no impact whatsoever on the final results.

Hence, the n^{th} sample for the d^{th} OFDM symbol may be obtained from $r(t)$ by substituting

$$\begin{aligned} t &= (d-1)(N+G)T' + \frac{G}{2}T' + \frac{(N-1)}{2}T' + nT' \\ &= (d-1)(N+G)(\beta+1)T + \frac{G}{2}(\beta+1)T + \frac{(N-1)}{2}(\beta+1)T + n(\beta+1)T \\ &= N\frac{(2d-1)}{2} - G\frac{(2d-1)}{2} - \frac{1}{2} + n(\beta+1)T, \end{aligned} \tag{75}$$

where for this derivation we assume that no up-sampling is carried out. Afterwards, the guard interval is removed and an N-point FFT is applied to the samples $\{r_n\}_{n=0}^{N-1}$ for the d^{th} OFDM symbol. Assuming that the time synchronization window is accurate, the demodulated samples at the k^{th} sub-carrier are [66]

$$\begin{aligned}
R_k^d &= \frac{1}{\sqrt{N}^2}\sum_{k'=0}^{N-1}\sum_{n=-(N-1)/2}^{(N-1)/2} S_{k'}^d \tilde{H}_{k'} \qquad (76)\\
&\quad \exp\left\{\frac{j2\pi k'}{NT}\left[NT\frac{(2d-1)}{2} - GT\frac{(2d-1)}{2} - \frac{1}{2}T + n(\beta+1)T\right]\right\}\\
&\quad \exp\left\{\frac{j2\pi\gamma}{NT}\left[NT\frac{(2d-1)}{2} - GT\frac{(2d-1)}{2} - \frac{1}{2}T + n(\beta+1)T\right]\right\}\exp\left\{\frac{-j2\pi nk}{N}\right\} + W_k^d\\
&= \frac{1}{N}\left(\sum_{k'=0}^{N-1} S_{k'}^d H_{k'} \exp\left\{\frac{j2\pi}{N}(k'+\gamma)(\beta+1)\left[N\frac{(2d-1)}{2} - G\frac{(2d-1)}{2} - \frac{1}{2}\right]\right\}\right)\\
&\quad \sum_{n=-(N-1)/2}^{(N-1)/2} \exp\left\{\frac{j2\pi}{N}(k'+\gamma)(\beta+1)n\right\}\exp\left\{\frac{-j2\pi nk}{N}\right\} + W_k^d\\
&= \sum_{k'=0}^{N-1} S_{k'}^d H_{k'} \underbrace{\exp\left\{\frac{j2\pi(k'+\gamma)(\beta+1)}{N}\left[N\frac{(2d-1)}{2} - G\frac{(2d-1)}{2} - \frac{1}{2}\right]\right\}}_{a^{(d,k')}(\beta,\gamma)}\\
&\quad \underbrace{\frac{1}{N}\frac{\sin\left[\pi\left((k'+\gamma)(\beta+1)-k\right)\right]}{\sin\left[\frac{\pi}{N}\left((k'+\gamma)(\beta+1)-k\right)\right]}}_{\mathbf{F}_{(k,k')}(\beta,\gamma)} + W_k^d
\end{aligned}$$

where W_k^d is the AWGN term in the frequency domain, $a^{(d,k')}(\beta,\gamma)$ is indexed by d and k' and is a function of β and γ, and $\mathbf{F}_{(k,k')}(\beta,\gamma)$ is indexed by k and k' and is a function of β and γ. The above expression for a block of N demodulated OFDM samples may be represented in a matrix form as

$$\underline{R}^d = \mathbf{F}(\beta,\gamma)\text{Diag}\left\{\underline{H}\right\}\underbrace{\left[\underline{S}^d \odot \underline{a}^d(\beta,\gamma)\right]}_{V^d(\beta,\gamma)} + \underline{W}^d, \qquad (77)$$

where

$$\underline{R}^d = [R_0^d, \ldots, R_{N-1}^d]^T \qquad (78)$$

$\mathbf{F}(\beta,\gamma)$ is an $N \times N$ matrix of the form

$$\mathbf{F} = \begin{bmatrix}
\frac{1}{N}\frac{\sin[\pi(\gamma(\beta+1))]}{\sin\left[\frac{\pi}{N}(\gamma(\beta+1))\right]} & \cdots & \frac{1}{N}\frac{\sin[\pi((N-1+\gamma)(\beta+1))]}{\sin\left[\frac{\pi}{N}((N-1+\gamma\ )(\beta+1))\right]}\\
\vdots & \ddots & \vdots\\
\frac{1}{N}\frac{\sin[\pi(\gamma(\beta+1)-(N-1))]}{\sin\left[\frac{\pi}{N}(\gamma(\beta+1)-(N-1))\right]} & \cdots & \frac{1}{N}\frac{\sin[\pi((N-1+\gamma)(\beta+1)-(N-1))]}{\sin\left[\frac{\pi}{N}((N-1+\gamma)(\beta+1)-(N-1))\right]}
\end{bmatrix}, \qquad (79)$$

$$\underline{S}^d = \left[S_0^d, \ldots, S_{N-1}^d\right]^T, \tag{80}$$

$$\underline{H} = [H_0, \ldots, H_{N-1}]^T, \tag{81}$$

$$\begin{aligned} \underline{a}^d &= \left[\exp\left\{\frac{j2\pi\gamma}{N} d(N+G)(\beta+1)\right\}, \ldots, \right. \\ &\quad \left. \exp\left\{\frac{j2\pi(N-1+\gamma)}{N} d(N+G)(\beta+1)\right\}\right]^T, \end{aligned} \tag{82}$$

and $\odot$ refers to an element by element multiplication or the Schur-Hadamard product [33] between the two vectors.

4.3 Problem Formulation

Let

$$\underline{\theta} = [\beta,\ \gamma,\ \underline{H}^T,\ N_0]^T, \tag{83}$$

be a vector of parameters that need to be estimated. Suppose B OFDM blocks are available to estimate the vector $\underline{\theta}$, then we will have B measurement vectors $\underline{R}^d$. These can be stacked as the columns of a matrix $\tilde{\mathbf{R}}$ as

$$\tilde{\mathbf{R}} = \left[\underline{R}^0, \ldots, \underline{R}^{B-1}\right], \tag{84}$$

where,

$$\tilde{\mathbf{R}} = \underbrace{\mathbf{F}(\beta,\gamma)\text{Diag}\left\{\underline{H}\right\}\mathbf{V}(\beta,\gamma)}_{\tilde{\mathbf{Y}}} + \mathbf{W} \tag{85}$$

and where

$$\tilde{\mathbf{V}} = \left[\left[\underline{S}^0 \odot \underline{a}^0(\beta)\right], \ldots, \left[\underline{S}^{B-1} \odot \underline{a}^{B-1}(\beta)\right]\right] \tag{86}$$

Each of the (i,j) elements of these matrices may be expressed as a useful signal plus AWGN as

$$\tilde{\mathbf{R}}_{i,j} = \tilde{\mathbf{Y}}_{i,j} + \mathbf{W}_{i,j} \tag{87}$$

where, the elements $\mathbf{W}_{i,j}$ are independent and identically distributed Gausian random variables with a zero mean and a variance of N_0. Hence the probability density function (pdf) of $\tilde{\mathbf{R}}_{i,j}$ is given by

$$f(\tilde{\mathbf{R}}_{i,j}) = \frac{1}{\pi N_0}\exp\left\{-\frac{|\tilde{\mathbf{R}}_{i,j} - \tilde{\mathbf{Y}}_{i,j}|^2}{N_0}\right\} \tag{88}$$

and assuming that all the elements $\tilde{\mathbf{R}}_{i,j}$ are independent, the joint distribution of $B \times N$ elements is given by

$$\begin{aligned} f(\tilde{\mathbf{R}}) &= \prod_{i,j} f(\tilde{\mathbf{R}}_{i,j}) & (89)\\ &= \prod_{i,j} \frac{1}{\pi N_0}\exp\left\{-\frac{|\tilde{\mathbf{R}}_{i,j} - \tilde{\mathbf{Y}}_{i,j}|^2}{N_0}\right\} & (90)\end{aligned}$$

Taking the natural logarithm on both sides, and negating,

$$-\log\left[f(\tilde{\mathbf{R}})\right] = \left[NB\log[\pi N_0] + \sum_{i,j}\left\{\frac{|\tilde{\mathbf{R}}_{i,j} - \tilde{\mathbf{Y}}_{i,j}|^2}{N_0}\right\}\right]. \tag{91}$$

The CRB for a parameter $\underline{\theta}_i$ is defined as

$$\mathrm{CRB}(\underline{\theta}_i) = (\mathbf{FIM})^{-1}_{i,i} \tag{92}$$

where the individual elements of the Fisher information matrix are given by

$$(\mathbf{FIM})_{i,j} = \mathrm{E}\left[\frac{\partial^2}{\partial\underline{\theta}_i\partial\underline{\theta}_j}\left\{-\log f(\tilde{\mathbf{R}})\right\}\right] \tag{93}$$

Hence, the **FIM** for the vector $\underline{\theta}$ is given by

$$\mathbf{FIM} = \mathrm{E}\begin{array}{c} \begin{matrix} \frac{\partial}{\partial\beta} & \frac{\partial}{\partial\gamma} & \frac{\partial}{\partial\underline{H}} & \frac{\partial}{\partial N_0} \end{matrix} \\ \begin{matrix} \frac{\partial}{\partial\beta} \\ \frac{\partial}{\partial\gamma} \\ \frac{\partial}{\partial\underline{H}} \\ \frac{\partial}{\partial N_0} \end{matrix} \end{array} \left[\begin{array}{c|c} & \\ -\log f(\tilde{\mathbf{R}}) & \\ & \\ \hline & \end{array}\right]. \tag{94}$$

The cross terms of the elements of the **FIM** containing the noise variance N_0 is given by

$$\left[\frac{\partial^2}{\partial N_0\partial\underline{\theta}_j}\left\{-\log f(\tilde{\mathbf{R}})\right\}\right] = 0, \tag{95}$$

when $\underline{\theta}_j \neq N_0$. However, when $\underline{\theta}_j = N_0$,

$$\left[\frac{\partial^2}{\partial N_0 \partial \underline{\theta}_j}\left\{-\log f(\tilde{\mathbf{R}})\right\}\right] = \frac{NB}{N_0^2}. \tag{96}$$

Hence the **FIM** for the vector $\underline{\theta}$ is given by

$$\mathbf{FIM} = \left[\begin{array}{ccc|c} & & & 0 \\ & \widetilde{\mathbf{FIM}} & & \vdots \\ & & & 0 \\ \hline 0 & \dots & 0 & \frac{NB}{N_0^2} \end{array}\right]. \tag{97}$$

The elements of the new matrix $\widetilde{\mathbf{FIM}}$ are given by

$$\left[\widetilde{\mathbf{FIM}}\right]_{i,j} = \frac{\partial^2}{\partial \underline{\theta}_i \partial \underline{\theta}_j} - \log\left[f(\tilde{\mathbf{R}})\right] \tag{98}$$

$$= \frac{1}{N_0}\sum_{i,j} \Re\left\{\frac{\partial \tilde{\mathbf{Y}}^*_{i,j}}{\partial \underline{\theta}_i}\frac{\partial \tilde{\mathbf{Y}}_{i,j}}{\partial \underline{\theta}_j}\right\} \tag{99}$$

$$= \frac{1}{N_0}\Re\left\{\mathrm{Tr}\left[\frac{\partial \tilde{\mathbf{Y}}^H}{\partial \underline{\theta}_i}\frac{\partial \tilde{\mathbf{Y}}}{\partial \underline{\theta}_j}\right]\right\}. \tag{100}$$

4.4 Elements of the Fisher Information Matrix $\widetilde{\mathbf{FIM}}$

In this section we derive the elements of the $\widetilde{\mathbf{FIM}}$.

4.4.1 Partial Derivatives with respect to the Elements Containing $\underline{\mathbf{H}}$

4.4.1.1 $\widetilde{\mathbf{FIM}}_{\underline{H}_p \underline{H}_q}$

Consider,

$$\frac{\partial \tilde{\mathbf{R}}}{\partial \underline{H}_p} = \mathbf{F}\ \mathrm{Diag}\left[0,\dots,1,\dots,0\right]_{p,p}\ \tilde{\mathbf{V}} \tag{101}$$

$$= \mathbf{F}\underline{e}_p\underline{e}_p^T\tilde{\mathbf{V}} \tag{102}$$

$$= \left\{\mathbf{F}\underline{e}_p\right\}\left\{\underline{e}_p^T\tilde{\mathbf{V}}\right\}$$

$$= \mathbf{F}_p\tilde{\mathbf{V}}_p$$

where $\underline{e}_p$ is a vector with a one in its p^{th} element and all the other elements set to zero, $\mathbf{F}_p$ is the p^{th} column of the matrix $\mathbf{F}$ and $\tilde{\mathbf{V}}_p$ is the p^{th} row of the matrix $\tilde{\mathbf{V}}$. Hence,

$$\mathrm{E}\left[\frac{1}{N_0}\Re\left[\mathrm{Tr}\left\{\frac{\partial \tilde{\mathbf{R}}^H}{\partial \underline{H}_p}\frac{\partial \tilde{\mathbf{R}}^H}{\partial \underline{H}_q}\right\}\right]\right] = \mathrm{E}\left[\frac{1}{N_0}\Re\left[\mathrm{Tr}\left\{\tilde{\mathbf{V}}_p^H\mathbf{F}_p^H\mathbf{F}_q\tilde{\mathbf{V}}_q\right\}\right]\right] \tag{103}$$

$$= \begin{cases} \frac{1}{N_0}\frac{1}{N}\sum_{i=0}^{B-1}\left|S_p^i\right|^2 & p=q \\ 0 & p\neq q \end{cases}$$

4.4.1.2 $\widetilde{\mathbf{FIM}}_{\underline{H}_p\beta}$

Initially, we derive the expression for the term $\frac{\partial\tilde{\mathbf{R}}}{\partial\beta}$ which is given by

$$\begin{aligned} \frac{\partial\tilde{\mathbf{R}}}{\partial\beta} &= \frac{\partial}{\partial\beta}\left[\mathbf{F}\text{Diag}\{\underline{H}\}\tilde{\mathbf{V}}\right] \\ &= \frac{\partial\mathbf{F}}{\partial\beta}\text{Diag}\{\underline{H}\}\tilde{\mathbf{V}} + \mathbf{F}\text{Diag}[\underline{H}]\frac{\partial\tilde{\mathbf{V}}}{\partial\beta} \end{aligned} \tag{104}$$

where the $(i,j)^{\text{th}}$ term of the matrix $\frac{\partial\mathbf{F}}{\partial\beta}$ is given by

$$\left[\frac{\partial\mathbf{F}}{\partial\beta}\right]_{i,j} = \frac{\pi(k'+\gamma)}{N}\frac{\left\{\begin{array}{c}\sin\left[\frac{\pi}{N}\left((k'+\gamma)(\beta+1)-k\right)\right]\cos\left[\pi\left((k'+\gamma)(\beta+1)-k\right)\right] \\ -\frac{1}{N}\sin\left[\pi\left((k'+\gamma)(\beta+1)-k\right)\right]\cos\left[\frac{\pi}{N}\left((k'+\gamma)(\beta+1)-k\right)\right]\end{array}\right\}}{\left[\sin\left[\frac{\pi}{N}\left((k'+\gamma)(\beta+1)-k\right)\right]\right]^2}$$

and the $(i,j)^{\text{th}}$ element of the matrix $\frac{\partial\tilde{\mathbf{V}}}{\partial\beta}$ is given by

$$\left[\frac{\partial\tilde{\mathbf{V}}}{\partial\beta}\right]_{i,j} = \left[j2\pi(k'+\gamma)\left[\frac{N(2d-1)}{2}-\frac{G(2d-1)}{2}-\frac{1}{2}\right]\right][\tilde{\mathbf{V}}]_{i,j} \tag{105}$$

Hence, the term $\text{E}\left[\frac{1}{N_0}\Re\left[\text{Tr}\left\{\frac{\partial\tilde{\mathbf{R}}^H}{\partial\underline{H}_p}\frac{\partial\tilde{\mathbf{R}}^H}{\partial\beta}\right\}\right]\right]$ is given by

$$\begin{aligned} \text{E}\left[\frac{1}{N_0}\Re\left[\text{Tr}\left\{\frac{\partial\tilde{\mathbf{R}}^H}{\partial\underline{H}_p}\frac{\partial\tilde{\mathbf{R}}}{\partial\beta}\right\}\right]\right] &= \text{E}\left[\frac{1}{N_0}\Re\left[\text{Tr}\left\{\tilde{\mathbf{V}}_p^H\mathbf{F}_p^H\left[\frac{\partial\mathbf{F}}{\partial\beta}\text{Diag}\{\underline{H}\}\tilde{\mathbf{V}}\right.\right.\right.\right. \\ &\quad \left.\left.\left.\left.+\mathbf{F}\text{Diag}[\underline{H}]\frac{\partial\tilde{\mathbf{V}}}{\partial\beta}\right]\right\}\right]\right] \end{aligned} \tag{106}$$

Similarly, the terms

$$\begin{aligned} \text{E}\left[\frac{1}{N_0}\Re\left[\text{Tr}\left\{\frac{\partial\tilde{\mathbf{R}}^H}{\partial\beta}\frac{\partial\tilde{\mathbf{R}}}{\partial\underline{H}_p}\right\}\right]\right] &= \text{E}\left[\frac{1}{N_0}\Re\left[\text{Tr}\left\{\left[\frac{\partial\mathbf{F}}{\partial\beta}\text{Diag}\{\underline{H}\}\tilde{\mathbf{V}}\right.\right.\right.\right. \\ &\quad \left.\left.\left.\left.+\mathbf{F}\text{Diag}[\underline{H}]\frac{\partial\tilde{\mathbf{V}}}{\partial\beta}\right]^H\mathbf{F}_p\tilde{\mathbf{V}}_p\right\}\right]\right] \end{aligned} \tag{107}$$

4.4.1.3 $\widetilde{\mathbf{FIM}}_{\underline{H}_p\gamma}$

The expression for the term $\frac{\partial\tilde{\mathbf{R}}}{\partial\gamma}$ is given by

$$\begin{aligned} \frac{\partial\tilde{\mathbf{R}}}{\partial\gamma} &= \frac{\partial}{\partial\gamma}\left[\mathbf{F}\text{Diag}\{\underline{H}\}\tilde{\mathbf{V}}\right] \\ &= \frac{\partial\mathbf{F}}{\partial\gamma}\text{Diag}\{\underline{H}\}\tilde{\mathbf{V}} + \mathbf{F}\text{Diag}[\underline{H}]\frac{\partial\tilde{\mathbf{V}}}{\partial\gamma} \end{aligned} \tag{108}$$

where the $(i,j)^{\text{th}}$ term of the matrix $\frac{\partial \mathbf{F}}{\partial \gamma}$ is given by

$$\left[\frac{\partial \mathbf{F}}{\partial \gamma}\right]_{i,j} = \frac{\pi(\beta+1)}{N} \frac{\left\{ \begin{array}{c} \sin\left[\frac{\pi}{N}\left((k'+\gamma)(\beta+1)-k\right)\right]\cos\left[\pi\left((k'+\gamma)(\beta+1)-k\right)\right] \\ -\frac{1}{N}\sin\left[\pi\left((k'+\gamma)(\beta+1)-k\right)\right]\cos\left[\frac{\pi}{N}\left((k'+\gamma)(\beta+1)-k\right)\right] \end{array} \right\}}{\left[\sin\left[\frac{\pi}{N}\left((k'+\gamma)(\beta+1)-k\right)\right]\right]^2}$$

and the $(i,j)^{\text{th}}$ element of the matrix $\frac{\partial \tilde{\mathbf{V}}}{\partial \gamma}$ is given by

$$\left[\frac{\partial \tilde{\mathbf{V}}}{\partial \gamma}\right]_{i,j} = \left[\frac{j2\pi(\beta+1)}{N}\left[\frac{N(2d-1)}{2} - \frac{G(2d-1)}{2} - \frac{1}{2}\right]\right][\tilde{\mathbf{V}}]_{i,j} \tag{109}$$

Hence the term $\mathrm{E}\left[\frac{1}{N_0}\Re\left[\mathrm{Tr}\left\{\frac{\partial \tilde{\mathbf{R}}^H}{\partial \underline{H}_p}\frac{\partial \tilde{\mathbf{R}}^H}{\partial \gamma}\right\}\right]\right]$ is given by

$$\begin{aligned} \mathrm{E}\left[\frac{1}{N_0}\Re\left[\mathrm{Tr}\left\{\frac{\partial \tilde{\mathbf{R}}^H}{\partial \underline{H}_p}\frac{\partial \tilde{\mathbf{R}}}{\partial \gamma}\right\}\right]\right] &= \mathrm{E}\left[\frac{1}{N_0}\Re\left[\mathrm{Tr}\left\{\tilde{\mathbf{V}}_p^H \mathbf{F}_p^H\left[\frac{\partial \mathbf{F}}{\partial \gamma}\mathrm{Diag}\{\underline{H}\}\tilde{\mathbf{V}}\right.\right.\right.\right. \\ &\quad \left.\left.\left.\left. +\mathbf{F}\mathrm{Diag}[\underline{H}]\frac{\partial \tilde{\mathbf{V}}}{\partial \gamma}\right]\right\}\right]\right] \end{aligned} \tag{110}$$

Similarly, the term

$$\begin{aligned} \mathrm{E}\left[\frac{1}{N_0}\Re\left[\mathrm{Tr}\left\{\frac{\partial \tilde{\mathbf{R}}^H}{\partial \gamma}\frac{\partial \tilde{\mathbf{R}}}{\partial \underline{H}_p}\right\}\right]\right] &= \mathrm{E}\left[\frac{1}{N_0}\Re\left[\mathrm{Tr}\left\{\left[\frac{\partial \mathbf{F}}{\partial \gamma}\mathrm{Diag}\{\underline{H}\}\tilde{\mathbf{V}}\right.\right.\right.\right. \\ &\quad \left.\left.\left.\left. +\mathbf{F}\mathrm{Diag}[\underline{H}]\frac{\partial \tilde{\mathbf{V}}}{\partial \gamma}\right]^H \mathbf{F}_p \tilde{\mathbf{V}}_p\right\}\right]\right] \end{aligned} \tag{111}$$

4.4.2 Partial derivatives with respect to Elements Containing β

4.4.2.1 $\widetilde{\mathbf{FIM}}_{\beta\beta}$

From (104),

$$\frac{\partial \tilde{\mathbf{R}}}{\partial \beta} = \frac{\partial \mathbf{F}}{\partial \beta}\mathrm{Diag}\{\underline{H}\}\tilde{\mathbf{V}} + \mathbf{F}\mathrm{Diag}[\underline{H}]\frac{\partial \tilde{\mathbf{V}}}{\partial \beta} \tag{112}$$

Hence, $\mathrm{E}\left[\frac{1}{N_0}\Re\left[\mathrm{Tr}\left\{\frac{\partial \tilde{\mathbf{R}}^H}{\partial \beta}\frac{\partial \tilde{\mathbf{R}}}{\partial \beta}\right\}\right]\right]$ is given by

$$\begin{aligned} \mathrm{E}\left[\frac{1}{N_0}\Re\left[\mathrm{Tr}\left\{\frac{\partial \tilde{\mathbf{R}}^H}{\partial \beta}\frac{\partial \tilde{\mathbf{R}}}{\partial \beta}\right\}\right]\right] &= \mathrm{E}\left[\frac{1}{N_0}\Re\left[\mathrm{Tr}\left\{\left[\frac{\partial \mathbf{F}}{\partial \beta}\mathrm{Diag}\{\underline{H}\}\tilde{\mathbf{V}} + \mathbf{F}\mathrm{Diag}[\underline{H}]\frac{\partial \tilde{\mathbf{V}}}{\partial \beta}\right]^H\right.\right.\right. \\ &\quad \left.\left.\left.\left[\frac{\partial \mathbf{F}}{\partial \beta}\mathrm{Diag}\{\underline{H}\}\tilde{\mathbf{V}} + \mathbf{F}\mathrm{Diag}[\underline{H}]\frac{\partial \tilde{\mathbf{V}}}{\partial \beta}\right]\right\}\right]\right] \end{aligned} \tag{113}$$

4.4.2.2 $\widetilde{\mathbf{FIM}}_{\beta\gamma}$

From (104),

$$\frac{\partial \tilde{\mathbf{R}}}{\partial \beta} = \frac{\partial \mathbf{F}}{\partial \beta}\mathrm{Diag}\{\underline{H}\}\tilde{\mathbf{V}} + \mathbf{F}\mathrm{Diag}[\underline{H}]\frac{\partial \tilde{\mathbf{V}}}{\partial \beta} \tag{114}$$

Also, from (108)

$$\frac{\partial \tilde{\mathbf{R}}}{\partial \gamma} = \frac{\partial \mathbf{F}}{\partial \gamma}\mathrm{Diag}\{\underline{H}\}\tilde{\mathbf{V}} + \mathbf{F}\mathrm{Diag}[\underline{H}]\frac{\partial \tilde{\mathbf{V}}}{\partial \gamma} \tag{115}$$

Hence, $\mathrm{E}\left[\frac{2}{N_0}\Re\left[\mathrm{Tr}\left\{\frac{\partial \tilde{\mathbf{R}}^H}{\partial \beta}\frac{\partial \tilde{\mathbf{R}}}{\partial \gamma}\right\}\right]\right]$ is given by

$$\begin{aligned}\mathrm{E}\left[\frac{1}{N_0}\Re\left[\mathrm{Tr}\left\{\frac{\partial \tilde{\mathbf{R}}^H}{\partial \beta}\frac{\partial \tilde{\mathbf{R}}}{\partial \gamma}\right\}\right]\right] &= \mathrm{E}\left[\frac{1}{N_0}\Re\left[\mathrm{Tr}\left\{\left[\frac{\partial \mathbf{F}}{\partial \beta}\mathrm{Diag}\{\underline{H}\}\tilde{\mathbf{V}} + \mathbf{F}\mathrm{Diag}[\underline{H}]\frac{\partial \tilde{\mathbf{V}}}{\partial \beta}\right]^H\right.\right.\right. \\ &\quad \left.\left.\left.\left[\frac{\partial \mathbf{F}}{\partial \gamma}\mathrm{Diag}\{\underline{H}\}\tilde{\mathbf{V}} + \mathbf{F}\mathrm{Diag}[\underline{H}]\frac{\partial \tilde{\mathbf{V}}}{\partial \gamma}\right]\right\}\right]\right]\end{aligned} \tag{116}$$

Similarly,

$$\begin{aligned}\mathrm{E}\left[\frac{1}{N_0}\Re\left[\mathrm{Tr}\left\{\frac{\partial \tilde{\mathbf{R}}^H}{\partial \gamma}\frac{\partial \tilde{\mathbf{R}}}{\partial \beta}\right\}\right]\right] &= \mathrm{E}\left[\frac{1}{N_0}\Re\left[\mathrm{Tr}\left\{\left[\frac{\partial \mathbf{F}}{\partial \gamma}\mathrm{Diag}\{\underline{H}\}\tilde{\mathbf{V}} + \mathbf{F}\mathrm{Diag}[\underline{H}]\frac{\partial \tilde{\mathbf{V}}}{\partial \gamma}\right]\right.\right.\right. \\ &\quad \left.\left.\left.\left[\frac{\partial \mathbf{F}}{\partial \beta}\mathrm{Diag}\{\underline{H}\}\tilde{\mathbf{V}} + \mathbf{F}\mathrm{Diag}[\underline{H}]\frac{\partial \tilde{\mathbf{V}}}{\partial \beta}\right]^H\right\}\right]\right]\end{aligned} \tag{117}$$

4.4.3 Partial derivatives with respect to Elements Containing γ

4.4.3.1 $\widetilde{\mathbf{FIM}}_{\gamma\gamma}$

From (108),

$$\frac{\partial \tilde{\mathbf{R}}}{\partial \gamma} = \frac{\partial \mathbf{F}}{\partial \gamma}\mathrm{Diag}\{\underline{H}\}\tilde{\mathbf{V}} + \mathbf{F}\mathrm{Diag}[\underline{H}]\frac{\partial \tilde{\mathbf{V}}}{\partial \gamma}. \tag{118}$$

Hence,$\mathrm{E}\left[\frac{1}{N_0}\Re\left[\mathrm{Tr}\left\{\frac{\partial \tilde{\mathbf{R}}^H}{\partial \gamma}\frac{\partial \tilde{\mathbf{R}}}{\partial \gamma}\right\}\right]\right]$ is given by

$$\begin{aligned}\mathrm{E}\left[\frac{1}{N_0}\Re\left[\mathrm{Tr}\left\{\frac{\partial \tilde{\mathbf{R}}^H}{\partial \gamma}\frac{\partial \tilde{\mathbf{R}}}{\partial \gamma}\right\}\right]\right] &= \mathrm{E}\left[\frac{1}{N_0}\Re\left[\mathrm{Tr}\left\{\left[\frac{\partial \mathbf{F}}{\partial \gamma}\mathrm{Diag}\{\underline{H}\}\tilde{\mathbf{V}} + \mathbf{F}\mathrm{Diag}[\underline{H}]\frac{\partial \tilde{\mathbf{V}}}{\partial \gamma}\right]^H\right.\right.\right. \\ &\quad \left.\left.\left.\left[\frac{\partial \mathbf{F}}{\partial \gamma}\mathrm{Diag}\{\underline{H}\}\tilde{\mathbf{V}} + \mathbf{F}\mathrm{Diag}[\underline{H}]\frac{\partial \tilde{\mathbf{V}}}{\partial \gamma}\right]\right\}\right]\right]\end{aligned} \tag{119}$$

4.5 Maximum-Likelihood Estimation of the Parameters Associated with SISO-OFDM Systems

The Maximum Likelihood (ML) estimates of $\underline{H}$ may be obtained by minimizing the cost function

$$\min_{\beta,\gamma,\underline{H}} \mathrm{Tr}\left[\left(\tilde{\mathbf{R}}-\tilde{\mathbf{Y}}\right)^H\left(\tilde{\mathbf{R}}-\tilde{\mathbf{Y}}\right)\right] \tag{120}$$

Since it is difficult to get a closed form expression for this function, we try to minimize it one parameter at a time as follows

$$\Re\left\{\mathrm{Tr}\left[\left(\tilde{\mathbf{R}}-\tilde{\mathbf{Y}}\right)^H\frac{\partial\tilde{\mathbf{Y}}}{\partial\theta_i}\right]\right\} = 0 \tag{121}$$

4.5.1 Maximum Likelihood Channel Estimates

From (101),

$$\frac{\partial\tilde{\mathbf{R}}}{\partial\underline{H}_p} = \mathbf{F}_p\tilde{\mathbf{V}}_p, \tag{122}$$

Hence, minimizing with respect to a channel coefficient H_p by taking the partial derivative and equating it to zero,

$$\begin{aligned}\Re\left\{\mathrm{Tr}\left[\left(\tilde{\mathbf{R}}-\tilde{\mathbf{Y}}\right)^H\frac{\partial\tilde{\mathbf{R}}}{\partial\underline{H}_p}\right]\right\} &= \Re\left\{\mathrm{Tr}\left[\left(\tilde{\mathbf{R}}-\tilde{\mathbf{Y}}\right)^H\mathbf{F}_p\tilde{\mathbf{V}}_p\right]\right\} \\ &= \Re\left\{\mathrm{Tr}\left[\tilde{\mathbf{V}}_p\left(\tilde{\mathbf{R}}-\tilde{\mathbf{Y}}\right)^H\mathbf{F}_p\right]\right\} \\ &= \Re\left\{\mathrm{Tr}\left[\tilde{\mathbf{V}}_p\tilde{\mathbf{R}}^H\mathbf{F}_p-\tilde{\mathbf{V}}_p\tilde{\mathbf{Y}}^H\mathbf{F}_p\right]\right\} \\ &= \Re\left\{\mathrm{Tr}\left[\tilde{\mathbf{V}}_p\tilde{\mathbf{R}}^H\mathbf{F}_p-\tilde{\mathbf{V}}_p\{\mathbf{F}\mathrm{Diag}\left\{\underline{H}\right\}\mathbf{V}\}^H\mathbf{F}_p\right]\right\}\end{aligned} \tag{123}$$

Hence the ML estimate of of $\underline{H}_p$ may be obtained from (121) as

$$\Re\left\{\mathrm{Tr}\left[\tilde{\mathbf{V}}_p\tilde{\mathbf{R}}^H\mathbf{F}_p-\tilde{\mathbf{V}}_p\{\mathbf{F}\mathrm{Diag}\left\{\underline{H}\right\}\tilde{\mathbf{V}}\}^H\mathbf{F}_p\right]\right\} = 0 \tag{124}$$

which gives

$$\begin{aligned}\Re\left\{\mathrm{Tr}\left[\tilde{\mathbf{V}}_p\tilde{\mathbf{R}}^H\mathbf{F}_p\right]\right\} &= \Re\left\{\mathrm{Tr}\left[\tilde{\mathbf{V}}_p\{\mathbf{F}\mathrm{Diag}\left\{\underline{H}\right\}\tilde{\mathbf{V}}\}^H\mathbf{F}_p\right]\right\} \\ &= \Re\left\{\mathrm{Tr}\left[\tilde{\mathbf{V}}_p\tilde{\mathbf{V}}^H\mathrm{Diag}\left\{\underline{H}\right\}^H\mathbf{F}^H\mathbf{F}_p\right]\right\} \\ &= \Re\left\{\mathrm{Tr}\left[\tilde{\mathbf{V}}_p\tilde{\mathbf{V}}^H\mathrm{Diag}\left\{\mathbf{F}^H\mathbf{F}_p\right\}^H\underline{H}\right]\right\}\end{aligned} \tag{125}$$

Hence,

$$\left[\tilde{\mathbf{V}}_p\tilde{\mathbf{V}}^H\text{Diag}\left\{\mathbf{F}_p^H\mathbf{F}\right\}\right]\underline{H} \;=\; \tilde{\mathbf{V}}_p\tilde{\mathbf{R}}^H\mathbf{F}_p \tag{126}$$

where $\left[\tilde{\mathbf{V}}_p\tilde{\mathbf{V}}^H\text{Diag}\left\{\mathbf{F}_p^H\mathbf{F}\right\}\right]$ is a matrix of dimensions $1\times N$ and $\tilde{\mathbf{V}}_p\tilde{\mathbf{R}}^H\mathbf{F}_p$ is a scalar. The above equations may be put in a matrix form as

$$\begin{bmatrix} \left[\tilde{\mathbf{V}}_1\tilde{\mathbf{V}}^H\text{Diag}\left\{\mathbf{F}_1^H\mathbf{F}\right\}\right] \\ \vdots \\ \left[\tilde{\mathbf{V}}_N\tilde{\mathbf{V}}^H\text{Diag}\left\{\mathbf{F}_N^H\mathbf{F}\right\}\right] \end{bmatrix}\underline{H} \;=\; \begin{bmatrix} \tilde{\mathbf{V}}_1\tilde{\mathbf{R}}^H\mathbf{F}_1 \\ \vdots \\ \tilde{\mathbf{V}}_N\tilde{\mathbf{R}}^H\mathbf{F}_N \end{bmatrix} \tag{127}$$

which may be put in a more compact form as

$$\left[\tilde{\mathbf{V}}\tilde{\mathbf{V}}^H\odot\mathbf{F}^H\mathbf{F}\right]\underline{H} \;=\; \begin{bmatrix} \tilde{\mathbf{V}}_1\tilde{\mathbf{R}}^H\mathbf{F}_1 \\ \vdots \\ \tilde{\mathbf{V}}_N\tilde{\mathbf{R}}^H\mathbf{F}_N \end{bmatrix} \tag{128}$$

Hence, the ML estimate of $\underline{H}$ is given by

$$\underline{\hat{H}} \;=\; \left[\tilde{\mathbf{V}}\tilde{\mathbf{V}}^H\odot\mathbf{F}^H\mathbf{F}\right]^{-1}\begin{bmatrix} \tilde{\mathbf{V}}_1\tilde{\mathbf{R}}^H\mathbf{F}_1 \\ \vdots \\ \tilde{\mathbf{V}}_N\tilde{\mathbf{R}}^H\mathbf{F}_N \end{bmatrix} \tag{129}$$

4.5.2 Maximum Likelihood Estimates of the RF Oscillator Frequency Offset (γ) and the Sampling Frequency Offset Coefficient (β)

The ML estimates of β and γ may be obtained by minimizing the expression

$$\min_{\beta,\gamma,\underline{H}}\text{Tr}\left[\left(\tilde{\mathbf{R}}-\tilde{\mathbf{Y}}\right)^H\left(\tilde{\mathbf{R}}-\tilde{\mathbf{Y}}\right)\right] \tag{130}$$

where, from (85), and (129), the ML estimates of β and γ may be obtained by minimizing the expression

$$\min_{\beta,\gamma}\text{Tr}\left[\left(\tilde{\mathbf{R}}-\mathbf{F}\text{Diag}\left\{\left[\tilde{\mathbf{V}}\tilde{\mathbf{V}}^H\odot\mathbf{F}^H\mathbf{F}\right]^{-1}\begin{bmatrix} \tilde{\mathbf{V}}_1\tilde{\mathbf{R}}^H\mathbf{F}_1 \\ \vdots \\ \tilde{\mathbf{V}}_N\tilde{\mathbf{R}}^H\mathbf{F}_N \end{bmatrix}\right\}\tilde{\mathbf{V}}\right)^H \left(\tilde{\mathbf{R}}-\mathbf{F}\text{Diag}\left\{\left[\tilde{\mathbf{V}}\tilde{\mathbf{V}}^H\odot\mathbf{F}^H\mathbf{F}\right]^{-1}\begin{bmatrix} \tilde{\mathbf{V}}_1\tilde{\mathbf{R}}^H\mathbf{F}_1 \\ \vdots \\ \tilde{\mathbf{V}}_N\tilde{\mathbf{R}}^H\mathbf{F}_N \end{bmatrix}\right\}\tilde{\mathbf{V}}\right)\right] \tag{131}$$

As can be seen from (131), the estimates of β and γ may be obtained in spite of not knowing the channel estimates $\underline{\hat{H}}$. Hence, it is possible to estimate the parameters related to the SISO-OFDM system, viz. $\underline{\theta} = [\beta,\ \gamma,\ \underline{H}^T]^T$, from a single OFDM symbol.

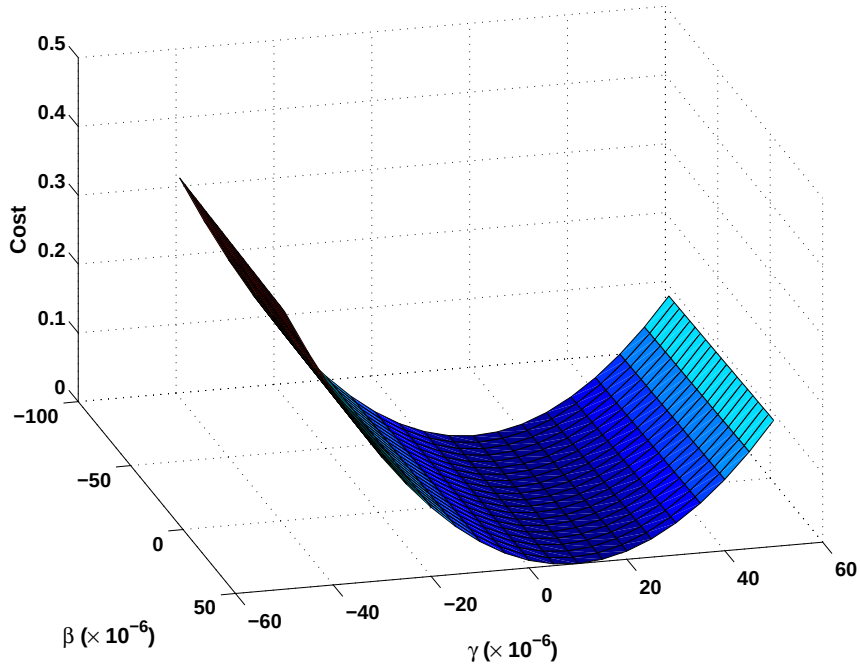

Figure 32: Variation of the cost as a function of β and γ for a high value of E_s/N_0. $\beta = 10 \times 10^{-6}$, $\gamma = 10 \times 10^{-6}$.

4.6 Simulation Results

Simulations are conducted for a 1×1 (SISO) WMAN system operating at a carrier frequency of 5.8 GHz operating on a Stanford University Interim (SUI)-4 channel [25]. The SUI-4 model is appropriate for intermediate path loss with moderate to heavy tree densities, and has the parameters listed in Table 1 of the Chapter 3. Rayleigh faded tap coefficients for the SISO channel are generated using a filtered Gaussian noise source as described in [93] with spectral shaping in the frequency domain to yield the desired Doppler power spectrum. The fading tap coefficients are uncorrelated. The sampling rate is assumed to be $1/T = 4.0$ MHz.

The OFDM blocksize is $N = 256$, and the guard interval length is $G = N/4 = 64$. The CRBs are calculated based on the transmission of B OFDM blocks with all its sub-carriers excited using known symbols obtained from a BPSK alphabet. The sampling

frequency offset coefficient β is initialized at 10 parts per million (ppm) and is assumed to remain constant for the duration of B OFDM symbols constituting the training phase. The fractional frequency offset γ is initialized to 0.2 subcarrier spacings and that also remains constant for the duration of B OFDM symbols. For simplicity, we assume the phase noise to be zero. As explained before, this is due to the dependency between the RF oscillator frequency offset γ and the phase noise. No knowledge of the statistics of the channel or any other parameters are assumed to be known.

Figure 33 shows the CRB for the estimates of the sampling frequency offset coefficient β as a function of E_s/N_0 for different number of training symbols B. Figure 34 shows

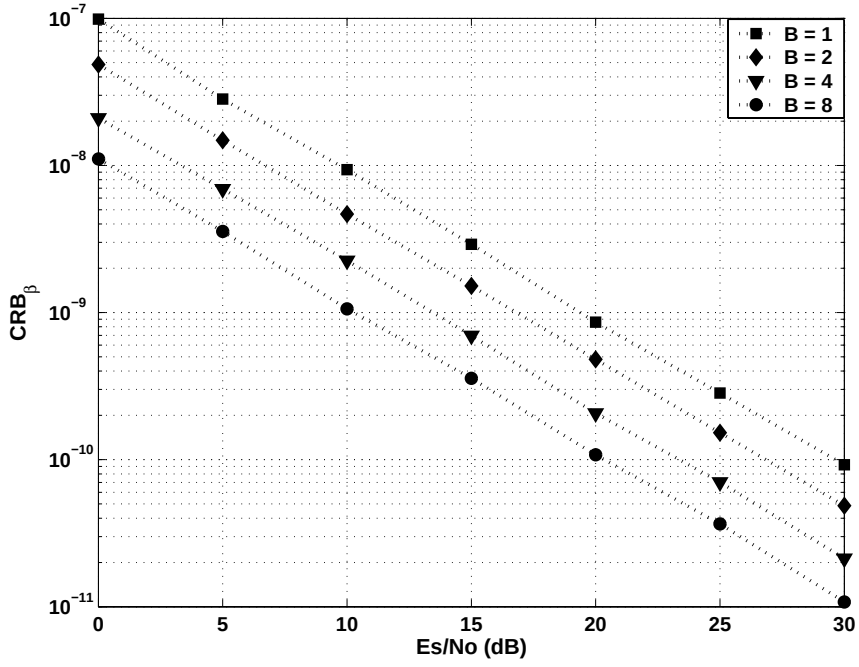

Figure 33: CRB for the estimates of the sampling frequency offset coefficient β as a function of E_s/N_0 for different number of training symbols B.

the CRB for the estimates of the RF oscillator frequency offset γ as a function of E_s/N_0 for different number of training symbols B. Figure 35 shows the CRB for the estimates of a frequency domain channel channel coefficient H_p as a function of E_s/N_0 for different number of training symbols B.

Figure 36 shows theCRB for the estimates of the noise variance as a function of E_s/N_0

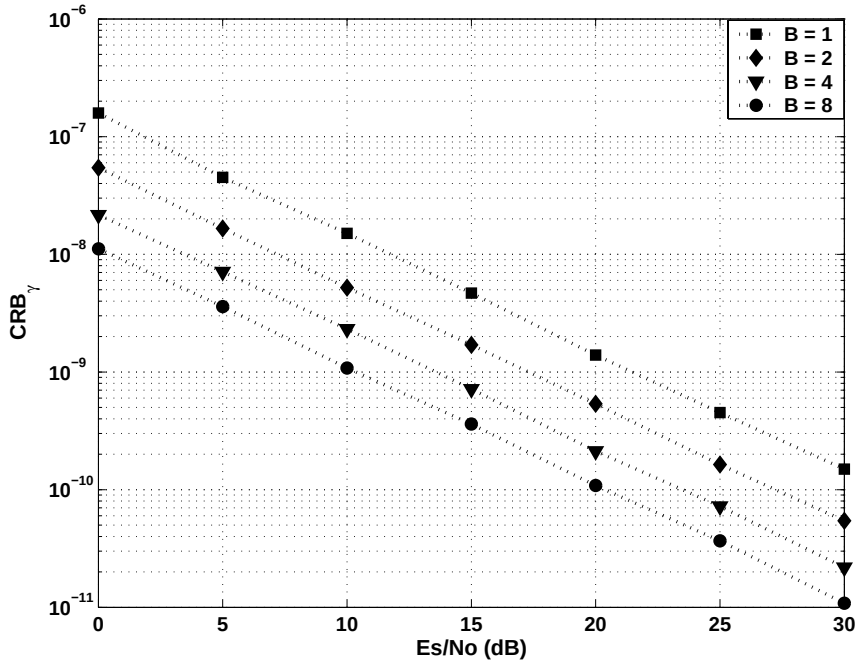

Figure 34: CRB for the estimates of the RF oscillator frequency offset γ as a function of E_s/N_0 for different number of training symbols B.

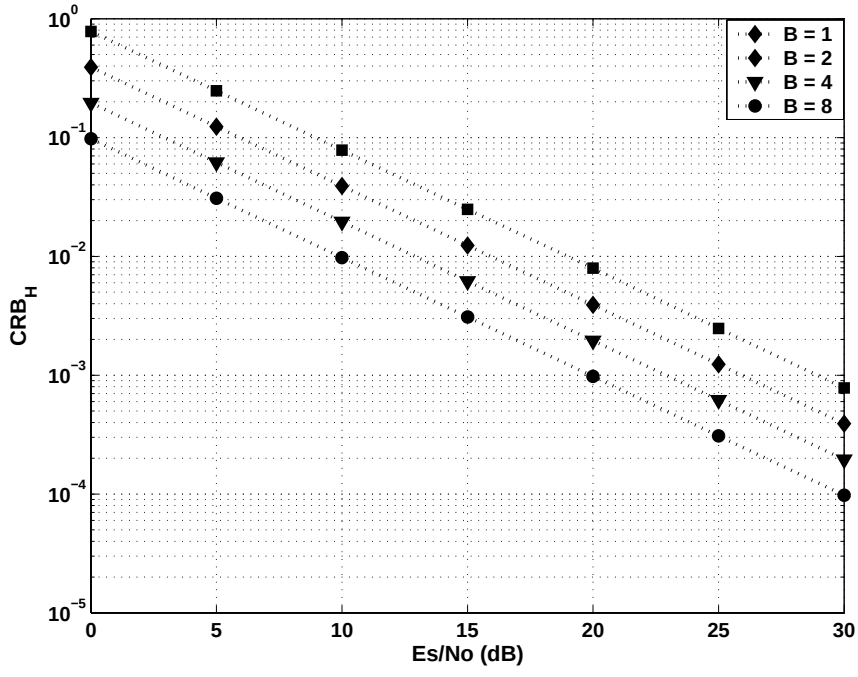

Figure 35: CRB for the estimates of a frequency domain channel channel coefficient H_p as a function of E_s/N_0 for different number of training symbols B.

for different number of training symbols B.

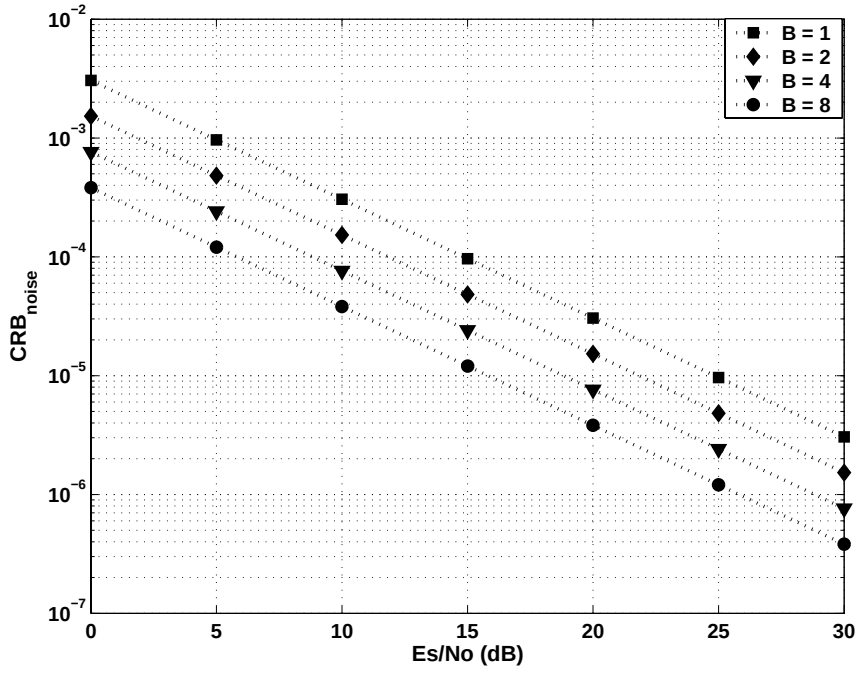

Figure 36: CRB for the estimates of the noise variance as a function of E_s/N_0 for different number of training symbols B.

4.7 Concluding Remarks

In this chapter we derived the CRBs for the parameters associated with a fixed wireless access SISO-OFDM system. The parameters for which the bounds were developed were the SF offset, the RF oscillator frequency offset, the channel coefficients and finally the variance of the AWGN. Since RF oscillator frequency offset and the RF oscillator phase noise are dependent parameters, only one can be estimated in the frequency domain. However, the CRBs for both of them are related. We presented a few results which showed these CRBs as a function of E_s/N_0 and the number of training symbols available.

CHAPTER V

USE OF CODING ALONG WITH OFDM AND ALAMOUTI/SVD DIVERSITY TECHNIQUE

5.1 Introduction

In a joint research work [34] we evaluate how channel coding can improve the performance of a MIMO-OFDM system. The channel codes are the low density parity check codes (LDPC) and the bit interleaved convolutional codes (BICC). In this chapter we do not consider the effects of SF offset, RF oscillator frequency offset and the phase noise.

We also look into the availability of the channel estimates at the transmitter and how they can be utilized to improve the system performance. Since this is a joint work, the system terminologies and equations for this chapter are different from the rest of this thesis and have been re-defined.

Two transmit two receive space-time processing with LDPC coding is evaluated for OFDM transmission. The two methods for space-time processing are Alamouti's combining and the SVD technique. The channel estimates are calculated and provided to the diversity combiner, the SVD filters and LDPC decoder. Noise variance estimates are provided to the LDPC decoder. Using the proposed scheme we can obtain a BER of 10^{-5} at an E_s/N_0 of 2.6 dB with spectral efficiency of 0.4 bits/sec/Hz and 14.5 dB with a spectral efficiency of 4.2 bits/sec/Hz.

Recently, many space-time techniques have been proposed for array-to-array communication systems when channel information is available at the receiver but not at the transmitter. Such techniques provide transmit diversity in a flat-fading channel. Alamouti suggested a space-time code for two transmit antennas, which provides a diversity gain and has a very simple decoder [6]. If the transmitter knows the channel, this knowledge can be exploited to further improve the performance [97]. In this case, it is known that a procedure based

on singular-value decomposition (SVD) is optimal in information-theoretical sense [9]. The SVD scheme employs a transmit pre-filter and a receive filter to diagonalize the array-to-array channel into a bank of independent scalar channels, where some of scalar channels have much larger channel gains than the fading channel. This advantage in channel gain can be interpreted as a diversity gain.

Space-time techniques can be integrated with orthogonal frequency division multiplexing (OFDM) for frequency-selective channels by applying either Alamouti's scheme (Alamouti-OFDM) [62] or SVD scheme (SVD-OFDM) [97] to each OFDM subcarrier.

In order to provide the channel coding gain, low-density parity-check (LDPC) codes are used for both Alamouti-OFDM and SVD-OFDM schemes. LDPC coding was first introduced by Gallager in the 1960's [32]. Several recent research results show that turbo codes can be expressed as LDPC codes, and well-structured irregular LDPC codes outperform turbo codes at high code rates. Aside from the superior performance, message-passing decoders of LDPC codes have a fully parallelized structure which can be realized with parallel connections of simple basic elements. Thus, we can achieve a good coding gain with relatively small complexity. LDPC codes inherently have random inter-leavers which can mitigate performance degradation due to deep attenuation of a data symbol on a subcarrier.

Parameter estimation for such a scheme is important. The Alamouti and SVD schemes require accurate channel estimates for their functioning whereas the LDPC codes require accurate noise variance estimates to calculate the log-likelihood ratios (LLR).

5.2 Two Space-Time Strategies

First, consider a single-carrier 2×2 communication system in a flat-fading environment. The notations for this chapter are slightly different from the previous chapters. Let $h^{q,\ell}$ denote the channel response at the ℓ^{th} receive antenna from the q^{th} transmit antenna. At the receiver, the sampled base-band signal $r^{d,\ell}$ at the ℓ^{th} receive antenna during the d^{th} symbol interval is represented in discrete time by

$$\begin{bmatrix} r^{d,1} \\ r_{d,2} \end{bmatrix} = \breve{\mathbf{H}} \begin{bmatrix} s^{d,1} \\ s^{d,2} \end{bmatrix} + \begin{bmatrix} w^{d,1} \\ w_{d,2} \end{bmatrix}, \tag{132}$$

where $s^{d,q}$ is the transmitted sequence from the q^{th} transmit antenna, and $w^{d,\ell}$ is the complex additive white Gaussian noise. The 2×2 matrix $\breve{\mathbf{H}}$ is called matrix channel, which is given by

$$\breve{\mathbf{H}} = \begin{bmatrix} h^{1,1} & h^{2,1} \\ h^{1,2} & h^{2,2} \end{bmatrix}.$$

Note that the channel matrix in this chapter is a transpose of the channel matrix in previous chapters.

5.2.1 Alamouti's Transmit Diversity Technique

In Alamouti's scheme, the transmitted sequences $s^{d,1}$ and $s^{d,2}$ are generated from the two incoming symbols as x^1 and x^2 during two symbol intervals according to $\underline{s}^{2d} = [x^1, x^2]^T$ and $\underline{s}^{2d+1} = [-x^{2*}, x^{1*}]^T$, where the asterisk denotes complex conjugate. At the receiver, assuming that $\breve{\mathbf{H}}$ does not change during the $(2d)^{\text{th}}$ and $(2d+1)^{\text{st}}$ symbol intervals, the received signals

$$\begin{aligned} \underline{r}^{2d} &= \breve{\mathbf{H}}\underline{s}^{2d} + \underline{w}^{2d} \\ \underline{r}^{2d+1} &= \breve{\mathbf{H}}\underline{s}^{2d+1} + \underline{w}^{2d+1} \end{aligned} \tag{133}$$

are combined by a matched filter:

$$\begin{aligned} &\left[h^{1,1}, h^{1,2}\right]^* \underline{r}^{2d} + [h^{2,1}, h^{2,2}]\underline{r}^{2d+1*} \quad \text{for } x^1 \\ &\left[h^{2,1}, h^{2,2}\right]^* \underline{r}^{2d} + [h^{1,1}, h^{1,2}]\underline{r}^{2d+1*} \quad \text{for } x^2. \end{aligned} \tag{134}$$

This combining results in a separable decoding of x^1 and x^2 owing to the orthogonality of $\underline{s}^{2d}$ and $\underline{s}^{2d+1}$.

5.2.2 Space-Time Processing Based on SVD

A transmitter with knowledge of $\breve{\mathbf{H}}$ can exploit this knowledge in order to approach the Shannon capacity [88]. In particular, it is known that a capacity-achieving transmitter bases its space-time processing on a channel SVD, $\breve{\mathbf{H}} = \mathbf{U}\mathbf{D}\mathbf{V}^H$, where H denotes the Hermitian transpose. A capacity-achieving transmitter will then pre-process the transmitted symbols with a unitary pre-filter $\mathbf{V}$, and the receiver will post-process with a unitary filter $\mathbf{U}^H$

such that the overall system is diagonal: $\mathbf{D} = \text{diag}[D^1, D^2] = \mathbf{U}^H\mathbf{HV}$, as shown in Figure 37-a. The problem has thus been reduced to one of communication across two independent parallel scalar subchannels in Figure 37-b, where the channel gains are singular values D^1 and D^2 ($D^1 \geq D^2$).

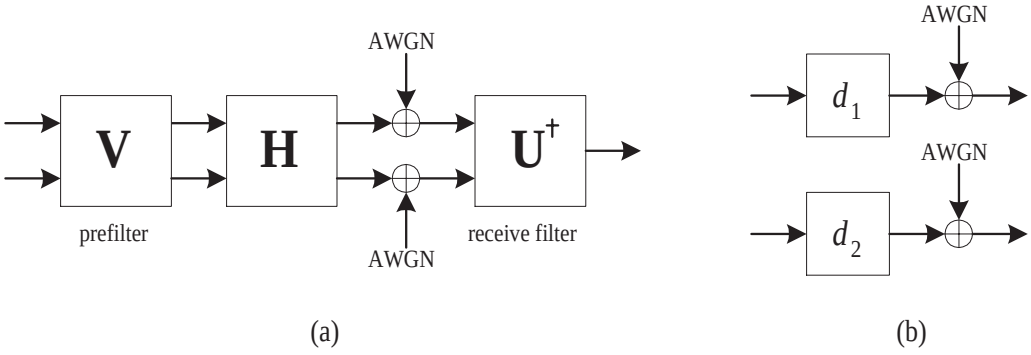

Figure 37: SVD scheme for a 2×2 matrix channel.

Once the matrix channel is diagonalized, there remains the problem of allocating bits and power to each of the scalar sub-channels. In this research, we use a fixed allocation instead of dynamic allocation to reduce the complexity with a marginal performance loss [97]. In this fixed allocation, we avoid using the second sub-channel (D^2), since E[D^2] is too small and the errors from this sub-channel dominate.

Although the SVD scheme requires the channel information at the transmitter, it will significantly outperform Alamouti's scheme. The complexity of both the schemes increases linearly with the number of transmit antennas however SVD requires slightly more computation due to SVD calculation. For a 2×2 system, the SVD scheme has an advantage of approximately 2.43 dB in SNR over Alamouti's scheme [97]. This SNR gap increases up to approximately 3.6 dB when the second sub-channel is also used by dynamic allocation.

5.3 Integration with OFDM

An example of 2×2 OFDM system is illustrated in Figure 38. Let $\{S_k^{d,q}\}_{k=0}^{N-1}$ be the input symbols to the N-point IFFT for q^{th} transmit antenna. *Capital* letter in $S_k^{d,q}$ is used to emphasize that input symbols are in the frequency domain. The output sequence of the

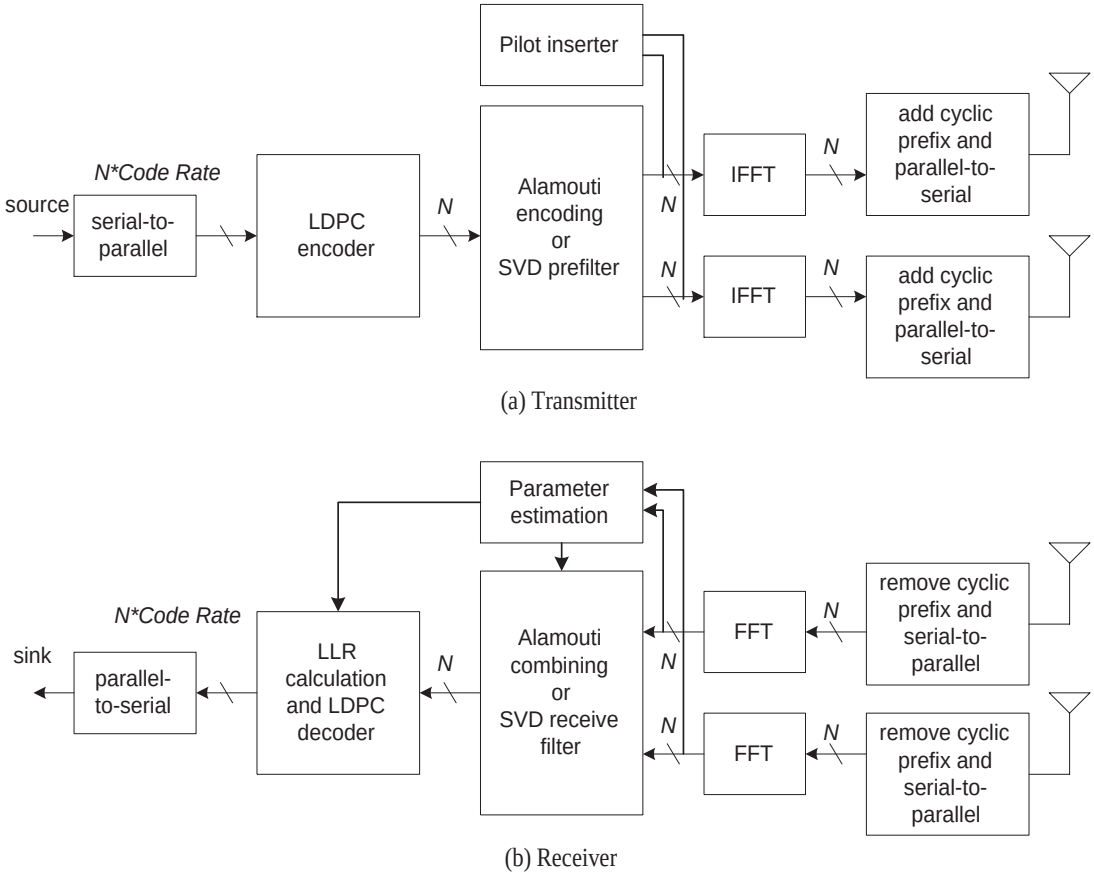

Figure 38: Block diagram of the proposed system.

IFFT is

$$s_n^{d,q} = \frac{1}{\sqrt{N}} \sum_{k=0}^{N-1} S_k^{d,q} \exp\left(j\frac{2\pi nk}{N}\right) \quad 0 \le n \le N-1. \tag{135}$$

A cyclic prefix is inserted in front of the IFFT output sequence. The time length of the cyclic prefix should be greater than the maximum delay spread of the channel. The main function of the cyclic prefix is to guard the OFDM symbol against inter-symbol interference. Hence, this cyclic prefix is called the guard interval of the OFDM symbol and has a time duration $T_g = GT$, where G is the number of samples in the cyclic prefix and $1/T$ is the sampling frequency at the output of the cyclic prefix inserter. The guard-inserted sequence is applied to a pair of balanced D/A converters, up-converted to radio frequency, and transmitted over the channel. The received sequence for the $(dT_s)^{\text{th}}$ time instant after the removal of the guard interval is given by

$$r_n^{d,\ell} = \sum_{q=1}^{2} \sum_{m=0}^{M-1} h_{d(N+G)+n}^{q,\ell}(m) s_{(n-m)_N}^{d,q} + w_n^{d,\ell}, \tag{136}$$

where $h_{d(N+G)+n}^{q,\ell}(m)$ is the channel impulse response for the m^{th} tap at the $(d(N+G)+n)^{\text{th}}$ instant, from the q^{th} transmit antenna to the ℓ^{th} receive antenna and T_s is the OFDM symbol period including the guard interval. The $w_n^{d,\ell}$ are complex additive white Gaussian noise samples with $\mathrm{E}[|w_n^{d,\ell}|^2] = N_0$. The received sample sequence $\{r_n^{d,\ell}\}_{n=0}^{N-1}$ is demodulated as

$$\begin{aligned} R_k^{d,\ell} &= \mathrm{FFT}\{r^\ell\}(k) \\ &= \sum_{q=1}^{2} H_k^{q,\ell} S_k^{d,q} + W_k^{d,\ell} \end{aligned} \tag{137}$$

where [62]

$$H_k^{q,\ell} = \sum_{m=0}^{M-1} H_m^{q,\ell(d)}(0) \exp\left(\frac{-j2\pi km}{N}\right) \tag{138}$$

and where

$$H_m^{q,\ell(d)}(0) = \frac{1}{N} \sum_{n=0}^{N-1} h_{(N+G)+k}^{q,\ell}(m). \tag{139}$$

The 2×2 OFDM system is equivalently described by a bank of matrix channels, as shown in Fig. 39. The received samples at the k-th subcarrier in (137) can be rewritten as

$$\begin{bmatrix} R_k^{d,1} \\ R_k^{d,2} \end{bmatrix} = \breve{\mathbf{H}}_k \begin{bmatrix} S_k^{d,1} \\ S_k^{d,2} \end{bmatrix} + \begin{bmatrix} W_k^{d,1} \\ W_k^{d,2} \end{bmatrix}, \tag{140}$$

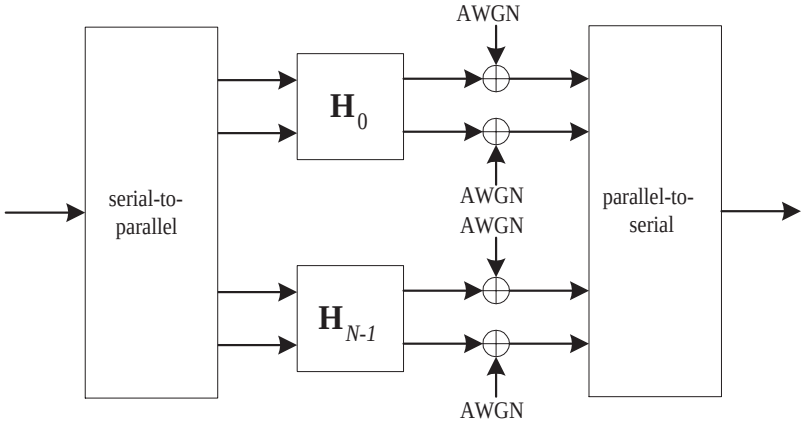

Figure 39: An equivalent matrix-channel model of 2×2 OFDM.

where the matrix channel is

$$\breve{\mathbf{H}}_k = \begin{bmatrix} H_k^{1,1} & H_k^{2,1} \\ H_k^{1,2} & H_k^{2,2} \end{bmatrix}. \tag{141}$$

Consequently, we can use either Alamouti's scheme or the SVD scheme to provide the diversity of $\breve{\mathbf{H}}_k$.

By the same argument for a channel that is flat over each subcarrier, in SVD-OFDM, each matrix channel is diagonalized by SVD: $\mathbf{D}_k = \text{diag}[d_k^1, d_k^2] = \mathbf{U}_k^H \breve{\mathbf{H}}_k \mathbf{V}_k$, with $d_k^1 \geq d_k^2$. Then, the matrix-channel model in Figure 39 further reduces to a bank of $2N$ parallel scalar channels.

We have the same problem of bit and power allocation as a single-carrier SVD scheme. In SVD-OFDM, however, the dynamic allocation requires much more complexity than the single-carrier system, since the number of scalar channels increases to $2N$. Thus, a fixed allocation algorithm is more attractive for SVD-OFDM. In this research, we allocate the same number of bits to each $\mathbf{D}_k$. Then, the fixed allocation for single-carrier system is used for the allocation for $\mathbf{D}_k$. Power is distributed equally to all used channels, which is called on-off power allocation.

5.3.1 Parameter Estimation for the Proposed Scheme

Parameter estimation for the proposed scheme is carried out using the method described in [62]. Two consecutive blocks of a known sequence of samples $\{S_k^{d,q}\}_{k=0}^{N-1}$ which form the

pilot/ training symbols are transmitted. Any sequence having good correlation properties, flat amplitude spectrum and low peak to average power ratio (PAPR) can be used as a training sequence. Here we use N-point FFT coefficients of a chirp sequence for parameter estimation. Chirp sequences are directly modulatable and are optimal for channel estimation (Chapter 2). The preamble structure is as shown in (37). We now briefly describe the channel and the noise variance algorithms used that we used in this part of our research [62].

5.3.2 Channel Estimation and MSE reduction

For the parameter estimation, we revert back to our original MIMO model of the earlier chapters which was

$$\mathbf{R}_k^d = \mathbf{S}_k^d \cdot \mathbf{H}_k^d + \mathbf{W}_k, \tag{142}$$

in absence of SF offset, RF oscillator frequency offset and the phase noise and where $\mathbf{S}_k^d$ is as defined in (37) and $\mathbf{H}_k^d$ is the original channel matrix as defined in (34). The LS estimates of the channel are first obtained in the frequency domain using

$$\hat{\mathbf{H}}_k^d = (\mathbf{S}_k^{dH}\mathbf{S}_k^d)^{-1}\mathbf{S}_k^{dH}\mathbf{R}_k \ , \tag{143}$$

5.3.2.1 MSE reduction

The Mean Squared Error (MSE) of the channel estimates for the LS estimator is high. In case the preamble consists of a sequence with pilot sub-carriers placed at an equal and symmetric distance from each other, then the method suggested in [62], may be applied for MSE reduction. The method consists of windowing the channel estimates in the time domain. The method assumes that the length of the channel impulse response (CIR) in the time domain does not exceed the guard interval of G samples. Hence channel estimates can be further improved by first taking N-point IFFT of the $Q \times L$ coarse channel estimate vectors to convert them to the time domain as

$$\begin{aligned} \underline{g}^{q,\ell} &= \text{IFFT}_N\{\underline{\hat{\mathbf{H}}}^{q,\ell}\} \\ &= \begin{cases} \sqrt{N}H_m^{q,\ell}(0) + w_m^{q,\ell} & 0 \le m \le G-1 \\ w_m^{q,\ell} & G \le m \le N-1. \end{cases} \end{aligned} \tag{144}$$

where $1 \leq q \leq Q$ and $1 \leq \ell \leq L$. The $Q \times L$ length-N vectors $\{g_m^{q,\ell}\}_{m=0}^{N-1}$ are then passed through a rectangular window [57] such that

$$\hat{h}_m^{q,\ell} = \begin{cases} g_m^{q,\ell} & 0 \leq m \leq (G-1) \\ 0 & m \geq G. \end{cases} \tag{145}$$

The time domain fine channel estimates $\hat{h}_m^{q,\ell}$ are then converted using FFT to fine channel estimates $\{\hat{\mathbf{H}}_k^{q,\ell}\}_{k=0}^{N-1}$ in the frequency domain as

$$\begin{aligned} \underline{\hat{\mathbf{H}}}_{\text{fine}}^{q,\ell} &= \text{FFT}_N\{\underline{\hat{h}}^{q,\ell}\} \quad 1 \leq q \leq Q,\ 1 \leq \ell \leq L \\ &= \underline{\mathbf{H}}^{q,\ell} + \underline{\hat{W}}^{q,\ell}. \end{aligned} \tag{146}$$

Because of the windowing operation, the variance in channel estimates due to AWGN and ICI is reduced by the factor of $\frac{G}{N}$. Hence the MSE in this estimator is given by

$$\text{MSE}_{\mathbf{H}} = N_0 \frac{G}{N} \tag{147}$$

Note that time domain windowing results in frequency domain averaging or smoothing. The performance analysis of the channel estimator is derived in Appendix C.

5.3.3 Noise Variance Estimation

If the channel estimates are obtained using the method in [62] and if the signal transmission matrices $\mathbf{S}_k$s are unitary, then the noise variance estimates can be obtained for each of the receiver antennas from the coarse channel estimates $\underline{g}^{q,\ell}$ in the time domain. Since we have *a priori* information on the length of the channel in the time domain, all the samples in the sequences $\{g^{q,\ell}\}_{n=0}^{N-1}$ for $n > (G-1)$ are contributed by noise. Hence, the variance of the noise at each of the receive antennas can be estimated as

$$N_0 = \frac{1}{Q}\left[\frac{1}{(N-G)}\sum_{q=1}^{Q}\sum_{n=G}^{N-1}\left|g_n^{q,\ell}\right|^2\right] \tag{148}$$

The derivation of the MSE expression for this noise variance estimator is very similar to the one derived in Appendix B. The MSE in noise variance estimates is given by

$$\text{MSE}_{\text{noise}} = \frac{N_0^2}{Q(N-G)}. \tag{149}$$

The channel estimates are utilized by the combiner in Alamouti's scheme, by the transmit and receive filters in the SVD scheme and for the log-likelihood ratio computation in the LDPC decoder. Noise variance estimates are provided to the LDPC decoder. The proposed technique gives sufficiently accurate channel estimates and almost perfect noise variance estimates.

5.3.4 Low-Density Parity-Check Codes

LDPC codes are specified by a sparse parity-check matrix and can be categorized into regular and irregular LDPC codes. The regular LDPC codes have parity-check matrices whose columns have the same number of ones. In this research, we only consider regular LDPC codes.

A parity-check matrix, $\mathbf{P}$ of a (c, t, r) LDPC code has c columns, t ones in each column and r ones in a row. A (c, t, r) LDPC code has a code rate of $1 - t/r$. Gallager [32] showed that there is at least one LPDC code whose minimum distance, d_{min} grows linearly with block length c when $t > 2$. Therefore, we can expect a better coding gain with a longer code length, although the coding length is limited by practical considerations like decoding latency, decoder complexity etc. The rate of growth of $d_{\min}$ is bounded by a nonzero number, which is determined by the selection of t and r.

The belief propagation algorithm has been widely adopted for decoding LDPC codes. MacKay [54] gives a good description of the iterative message passing decoder based on the belief propagation algorithm which can be implemented in either probability or log-probability domain. The decoder in this research works in the log-probability domain. For the message-passing decoder, we need LLR of each bit. A general form of LLR computing formula is given by

$$\mathrm{LLR}(b_j) = \log \left[\frac{\sum_{i=1}^{2^{k-1}} \mathrm{P}(\mathbf{R}|b_j = 1, \mathbf{m}_j = m_i)}{\sum_{i=1}^{2^{k-1}} \mathrm{P}(\mathbf{R}|b_j = 0, \mathbf{m}_j = m_i)} \right] \tag{150}$$

where $\mathbf{R}$ is a received signal vector, b_j is j^{th} bit of a transmitted message, $\mathbf{m}_j$ is a message less the j^{th} bit, m_i is one of 2^{k-1} possible symbols of $\mathbf{m}_j$ and each symbol carries k bits .

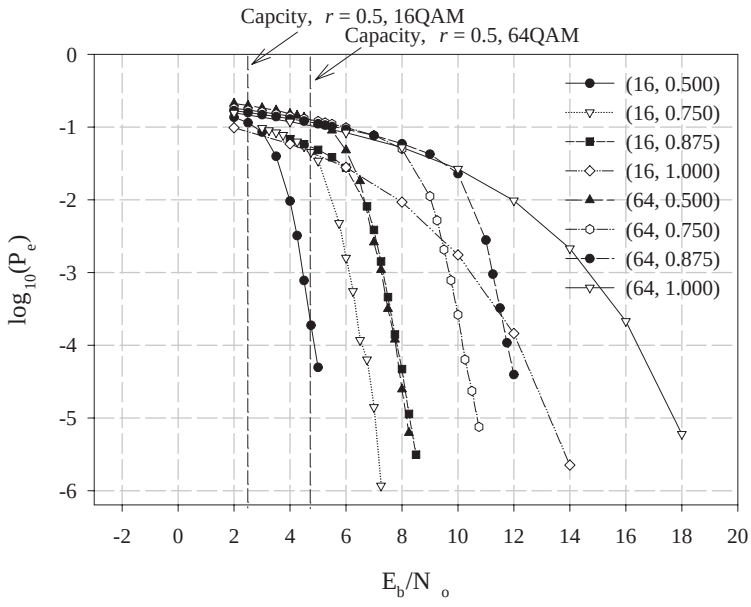

Figure 40: BER perf. of LDPC codes having code length, $c = 1024$ and code rates of 0.5, 0.75, 0.875 and 1.0 (uncoded) with 16 and 64-QAM on an AWGN channel.

On an AWGN channel and flat fading, (150) can be expressed as

$$\mathrm{LLR}(b_j) = \log \left[\frac{\sum_{i=1}^{2^{k-1}} e^{-\frac{d(\mathbf{R}, \mathbf{c}_i^{b_j=1})^2}{2\sigma^2}}}{\sum_{i=1}^{2^{k-1}} e^{-\frac{d(\mathbf{R}, \mathbf{c}_i^{b_j=0})^2}{2\sigma^2}}} \right] \tag{151}$$

where $\mathbf{c}_i^{b_j=b}$ is a signal constellation for a message defined by m_i and b_j and $d(\mathbf{R}, \mathbf{c}_i^{b_j=b})$ is a distance between a received signal vector $\mathbf{R}$ and $\mathbf{c}_i^{b_j=b}$.

To prevent possible underflow or overflow, the equation can be modified to a more applicable form as

$$\begin{aligned} \mathrm{LLR}(b_j) &= \frac{\left(d^0_{\min}(j)\right)^2 - \left(d^1_{\min}(j)\right)^2}{2\sigma^2} \\ &+ \log \left[1 + \sum_{\substack{i=1, \\ i \neq l_1}}^{2^{k-1}} e^{-\frac{d(\mathbf{R}, \mathbf{c}_i^{b_j=1})^2 - \left(d^1_{\min}(j)\right)^2}{2\sigma^2}} \right] \\ &- \log \left[1 + \sum_{\substack{i=1, \\ i \neq l_0}}^{2^{k-1}} e^{-\frac{d(\mathbf{R}, \mathbf{c}_i^{b_j=0})^2 - \left(d^0_{\min}(j)\right)^2}{2\sigma^2}} \right] \end{aligned} \tag{152}$$

where $d^b_{\min}(j) = d(\mathbf{R}, \mathbf{c}_{l_b}^{b_j=b}) = \min_{1 \le i \le 2^{k-1}} d(\mathbf{R}, \mathbf{c}_i^{b_j=b})$ and b is in $\{0, 1\}$.

Fig. 40 shows the BER performance of LDPC codes having code length, $c = 1024$ and code rates of 0.5, 0.75, 0.875 and 1.0 (uncoded) with 16 and 64-QAM modulation on an AWGN channel.

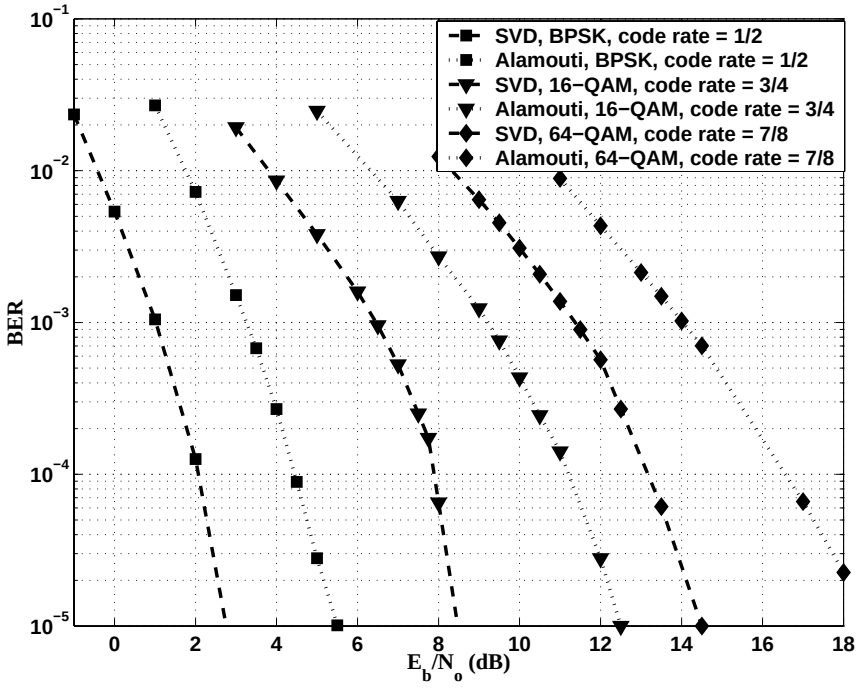

Figure 41: Perf. of rate 1/2, 3/4 and 7/8 coded LDPC with BPSK, 16 and 64-QAM Alamouti/SVD diversity techniques over a frequency selective fading channel.

5.4 Simulation Results

Simulations are carried out for a 2×2 system in a frequency-selective faded quasi-static indoor environment. Each channel is assumed to be composed of 6 uncorrelated Rayleigh faded taps with the tap coefficients obtained from the modified Jakes simulator [23]. All the channels are uncorrelated and length of each channel impulse response is less than 100 ns. The Jakes simulator assumes uniformly distributed angle of arrival for the incoming incident waves. The complex low-pass channels are modeled as transversal filters with the sample-spaced taps. Quasi-static assumption implies that the time of arrival of rays remains constant for a frame but may change from frame to frame. The symbol rate at the input

of the OFDM modulator is 64 Mbaud. The performance is evaluated by sending $200,000$ OFDM symbols of block size $N = 1024$ and guard length $G = 64$. It is assumed that the maximum delay spread of the indoor channel (T_m) is less than the guard time (T_g). The carrier frequency is chosen to be 5.8 GHz. Simulations are carried out for LDPC code rates of 1/2, 3/4 and 7/8 using BPSK, 16-QAM and 64-QAM constellations. The SNR per bit is defined as $E_b/N_o = 1/(N_0 R\gamma)$, where R is the transmission per symbol interval in bits/sec/Hz, and where γ denotes the code rate. We set $\mathrm{E}[|S_k^{d,1}|^2 + |S_k^{d,2}|^2] = 1$ and $\mathrm{E}[|\mathbf{H}_k^{q,\ell}|^2] = 1$.

The simulations are carried out for a Doppler frequency of 48.33 Hz corresponding to a velocity of 2.5 m/s. Two training symbols are sent for every 10 OFDM symbols for channel estimation. We have assumed perfect time and frequency synchronization. The BER degradation due to imperfect channel estimation in the following simulations is around 1.1 dB. Once channel parameters are estimated, the same parameters are used for the entire frame until the transmission of the new training symbols.

Figure 41 illustrates the BER performance of Alamouti-OFDM and SVD-OFDM using BPSK. Use of LDPC code along with the Alamouti's scheme provides a gain of around 5.8 dB as compared to the uncoded case at a BER of 10^{-3} and a 1/2 rate code. Using the SVD scheme instead of Alamouti's scheme along with LDPC coding gives a further improvement of 2.3 dB.

Figure 41 also shows the performance of the system using higher rate codes and higher order constellations. The SVD technique outperforms Alamouti' s scheme almost always by around 3 dB. The simulation results show that the proposed system can provide low BER at a high spectral efficiency and low SNR.

5.5 Concluding Remarks

Performance of a 2×2 space-time processing with LDPC coding is evaluated for OFDM transmission. The two methods for space-time processing are Alamouti' s scheme and the SVD technique. The channel estimates are calculated and provided to Alamouti' s combiner, the SVD filters and LDPC decoder. Noise variance estimates are provided to the

LDPC decoder. By using the proposed scheme we can obtain a BER of 10^{-5} at an SNR of 2.6 dB with spectral efficiency of 0.4 bits/sec/Hz and 14.5 dB with a spectral efficiency of 4.2 bits/sec/Hz. Hence, the proposed system can provide low BER at a high spectral efficiency and low SNR.

CHAPTER VI

CONCLUDING REMARKS

6.1 Introduction

The main objective of the proposed research was to provide a holistic solution to the receiver implementation for the broadband fixed wireless access (BFWA) multiple-input multiple-output (MIMO) orthogonal frequency division multiplexing (OFDM) systems. Along with the algorithm development, we also derived the Cramér-Rao lower bound(CRB)s for the parameters associated with typical single-input single-output (SISO)-OFDM systems. In a joint research we showed how coding and the knowledge of the channel estimates at the transmitter may be used to improve the bit error rate (BER) performance.

The main contributions of this research were as follows:

1. We developed a comprehensive system model for a MIMO-OFDM system suffering from the system impairments such as the sampling frequency (SF) offset, radio frequency (RF) oscillator offset, RF oscillator phase noise, frequency selective channel impairments and the additive white Gaussian noise(AWGN).

2. We suggested a generalized frame structure and pilot patterns compliant with the future extensions of the standards such as the IEEE 802.16a [37] and the IEEE 802.11n [36] to aide our signal acquisition and tracking algorithms. The suggested preamble and the pilot patterns were independent of the space-time coding technology.

3. We divided the receiver functionality in to the time domain and the frequency domain components. A part of signal acquisition was performed in the time domain and a part was performed in the frequency domain. Majority of tracking was performed in the frequency domain.

4. We performed time synchronization and the RF oscillator frequency offset in two stages.

5. We introduced a novel third stage in the frequency domain to estimate and track the SF offset and the residual RF oscillator frequency offset or the phase noise.

6. We suggested a novel method of estimating the variance of the noise in the MIMO-OFDM system.

7. We performed a mean squared error (MSE) analysis for all the estimators presented in our research.

8. We derived CRBs for the parameters associated with a typical single-input single-output (SISO)-OFDM system.

9. In a joint research we showed how channel coding along with the presence of the channel estimates at the receiver may be used to greatly enhance the system performance.

10. Finally we suggested the directions in which this proposed research may be taken.

Some more light is thrown on our contributions in the following section.

6.2 Signal Acquisition and Tracking for Fixed Wireless Access MIMO-OFDM

In this part of our research, we presented a complete suite of signal acquisition and tracking algorithms for a MIMO-OFDM system operating in a fixed wireless access environment. Our algorithms used a generalized preamble and pilot matrix structure to perform acquisition, consisting of time synchronization, RF and sampling frequency oscillator offset estimation, and channel estimation. This was followed by tracking of the sampling frequency offsets, phase noise jitters and the channel coefficients. Time synchronization is performed in two stages and RF oscillator frequency offset estimation is performed in three stages. Depending upon the intensity of the phase noise, the third RF oscillator frequency offset estimation stage was used to estimate the phase noise instead. Novel estimators were provided for the sampling and residual RF oscillator frequency/ phase noise offsets that yielded low

estimation errors. We also derived the MSE performance for our estimators. Simulation results were performed for a system very similar to IEEE 802.16a. Our algorithms were shown to perform well and our simulation results illustrated the combined effect of all required synchronization processes on the MIMO-OFDM receiver performance. Depending upon the two scenarios considered, our algorithms were found to be 2.7 and 4 dB away from the ideal BER curve. Finally, the proposed algorithms and pilot/training structure were independent of the space-time technology employed to implement the MIMO-OFDM system.

6.3 Cramér-Rao Bounds for the Parameters Associated with SISO-OFDM Systems

Often, it is necessary to establish a lower bound on the variance of an estimator. A lower bound acts as a benchmark against which the performance of any estimator may be compared. In this part of our research, we derived the Cramér-Rao bound(CRB)s for the parameters associated with a fixed wireless access SISO-OFDM system. It was difficult to derive the CRBs for a MIMO-OFDM system and hence we left this as a future work for the on-going research. In order to simplify the derivation process, we altered the frame related parameters slightly. Also, since we could either estimate the RF oscillator frequency offset γ or the phase noise ϑ, but not both [66], we ignored the presence of phase noise from our analysis. However, the CRB for the RF oscillator frequency offset and the phase noise were found to be interchangeable and one could be obtained from the other.

6.4 Use of Coding along with OFDM and Alamouti/SVD Diversity Technique

As a joint research, we studied the performance of a 2×2 space-time processing with LDPC coding for OFDM transmission. The two methods for space-time processing were Alamouti' s scheme and the SVD technique. The channel estimates were calculated and provided to Alamouti' s combiner, the SVD filters and LDPC decoder. Noise variance estimates were provided to the LDPC decoder. By using the proposed scheme we could obtain a BER of 10^{-5} at an SNR of 2.6 dB with spectral efficiency of 0.4 bits/sec/Hz and 14.5 dB with a

spectral efficiency of 4.2 bits/sec/Hz. Hence, the proposed system could provide low BER at a high spectral efficiency and low SNR.

6.5 Conclusions

Some of the major conclusions of this research were as follows:

1. As the length of the frame increases, any residual RF oscillator frequency offset and the SF offset severely degrade the MIMO-OFDM system performance.

2. If the variance of the RF oscillator phase noise is low, it may be ignored but the phase noise must be estimated and corrected for higher values of variance.

3. It is not possible to estimate both, the residual RF oscillator frequency offset and the RF oscillator phase noise in the frequency domain since both of them are dependent parameters. Hence one of them needs to be estimated in the time domain.

4. For shorter frame sizes, RF oscillator phase noise must be estimated while the residual RF oscillator frequency offset may be ignored whereas for longer frame lengths, the estimation and the removal of the residual RF oscillator frequency offset is critical.

5. Up-sampling the received waveform by a factor of two provides 1 dB gain in the BER performance of the system under consideration.

6. Even in low mobility WLAN and WMAN systems, variations in the effective channel occur due to the presence of the residual RF oscillator frequency offset, fluctuations in the RF oscillator phase noise and jitters in the oscillators used at baseband to clock the digital-to-analog (D/A) and analog-to-digital (A/D) converters in the transmitter and receiver, respectively. Hence the effective channel must be tracked continuously using schemes such as a decision directed channel estimation.

7. Presence of the channel estimates at the transmitter and use of powerful channel coding techniques may be used to significantly improve the system' s BER performance.

CHAPTER VII

FUTURE RESEARCH

7.1 Introduction

In this section we point out the directions in which this research might be taken in the future. The possible directions for the future research include verifying the performance of our signal acquisition and tracking algorithms for different space-time techniques such as the Bell labs layered space-time (BLAST) [29], use of powerful coding schemes such as the low density parity check (LDPC) and the turbo codes [13], extending the algorithms to the mobile environments also referred to as mobile broadband wireless access (MBWA), analyzing the effects and finding the solutions for the presence of insufficient guard interval on the performance of MIMO-OFDM systems, and finally, extending the Cramér-Rao bound analysis to MIMO OFDM systems. Each of these future research topics are explained in brief as follows:

7.2 Performance Evaluation of the Algorithms Using Alternate Space-Time Technologies

So far we have considered the use of space-time block codes (STBC) for our system implementation. However, it is well known that STBCs do not give a throughput advantage. In fact, optimal code-rate STBCs for systems with the number of transmitter antennas greater than two are difficult to find. An alternative solution is to use vertical Bell labs layered space-time (V-BLAST) type of architecture, where different information symbols are transmitted from each transmit antenna for every new OFDM symbol. Consider a MIMO-OFDM system as shown in Figure 42. If $\underline{R}_k^d = [R_k^{d,1}, \ldots, R_k^{d,1}]^T$ is the vector of received demodulated samples at the k^{th} sub-carrier and the d^{th} OFDM symbol, $\breve{\mathbf{H}}_k$ is a matrix of channel coefficients as defined in Chapter 5, $\underline{S}_k^d = [S_k^{d,1}, \ldots, S_k^{d,1}]^T$ is the vector of transmitted symbols at sub-carrier k and the d^{th} OFDM symbol, and $\underline{W}_k^d$ represents a

vector of uncorrelated AWGN samples, then,

$$\underline{R}_k^d = \breve{\mathbf{H}}_k \underline{S}_k^d + \underline{W}_k^d, \tag{153}$$

where, length of the vectors is equal to the number of received antennas and $\breve{\mathbf{H}}_k$ is a transpose of the matrix $\mathbf{H}$ used in Chapter 1.

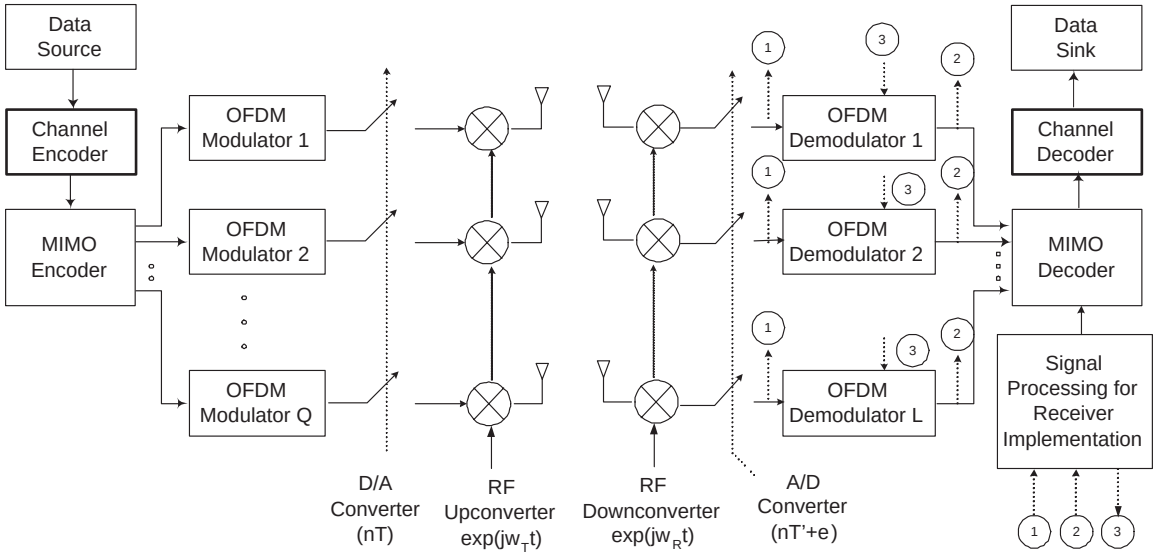

Figure 42: Q-Transmit L-Receive MIMO OFDM system.

In a V-BLAST type of a scheme, a new set of information symbols is transmitted for every new OFDM symbol. This results in a net capacity increase in the system by a factor of Q. At the same time the symbols transmitted from different antennas suffer from mutual interference at the receiver. This makes the decoding for BLAST more complex. The maximum likelihood (ML) detector for BLAST is optimal, however, its complexity increases exponentially with the number of transmit antennas. Hence, simpler decoders in the form of zero forcing (ZF) and minimum mean squared error (MMSE) are available and are given by

$$\underline{\hat{S}}_k^d = \mathbf{F}_k^{\dagger} \underline{R}, \tag{154}$$

where, for a zero forcing case,

$$\mathbf{F}^{\dagger} = (\breve{\mathbf{H}}^H \breve{\mathbf{H}})^{-1} \breve{\mathbf{H}}^H, \tag{155}$$

and for the MMSE case, the decoder is given by

$$\mathbf{F}^{\dagger} = (\breve{\mathbf{H}}^{H}\breve{\mathbf{H}} + N_0\mathbf{I})^{-1}\breve{\mathbf{H}}^{H}. \tag{156}$$

The system model for the above scenario is very similar to the system model used in this thesis. Hence the algorithms developed in Chapter **??** may be easily extended to a system using a different space-time technology.

7.3 Use of Channel Coding

In a joint paper [34] and the Chapter 5, we showed how channel coding may be used along with space-time techniques to improve the system performance. In that research, we used low density parity check codes (LDPC) [32] along with Alamouti [6] and singular value decomposition (SVD) schemes to obtain very good BER performance. Channel codes such as the LDPC and Turbo codes [13] are shown to perform close to the Shannon' s capacity [88]. In addition to improved BER performance, estimates of the decoded information symbols may be fed back to the estimators, to further improve the estimation performance and to track various system parameters. This scheme is also referred to as iterative decoding and decision feedback and is shown in Figure 43.

In our paper [66], we used a decision feedback mechanism to track the effective channel, however in that scenario, the STBC itself performed the task of a channel code. No other channel coding was used explicitly. Hence as a future research, it would be worth investigating the performance of the MIMO-OFDM systems using powerful channel coding techniques.

7.4 MIMO-OFDM for Mobile Broadband Wireless Access

As the demand multi-media applications and high speed wireless access increases new methods will be needed to boost capacity and performance of the existing systems. The standards for wireless local area network (WLAN) IEEE 802.11a and wireless metropolitan area network (WMAN) IEEE 802.16a are in place and now there is interest in adding mobility to these existing standards. Two task groups have been created to look into the mobility

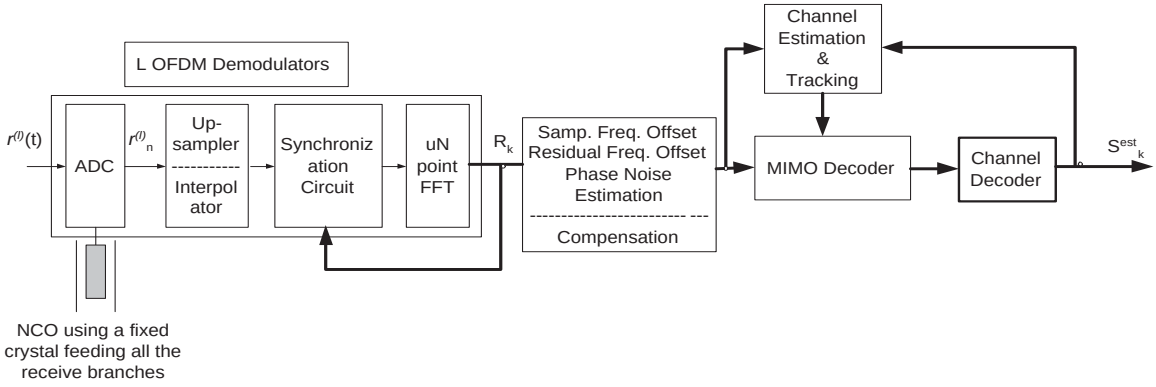

Figure 43: Receiver Implementation for the MIMO OFDM System.

issues. The task group IEEE 802.16e and the task group IEEE 802.20 also known as the mobile broadband wireless access (MBWA).

Orthogonal frequency division multiplexing (OFDM) exists in two modes in the IEEE 802.16a Standard. One by it self and the other known as the orthogonal frequency division multiple access (OFDMA). Multiple-input multiple-output (MIMO) systems on the other hand may be used to increase the diversity gain or increase the data throughput of the system. Diversity gain at the receiver can be used to offset the degradations caused due to the inter-symbol interference (ISI), inter-carrier interference (ICI) and channel estimation.

In [66] we proposed a complete receiver implementation for a MIMO-OFDM system working in a broadband fixed wireless access (BFWA) environment such as the IEEE 802.16a. The receiver implementation included all the signal acquisition and tracking tasks. As a future research, we need to investigate if the current physical (PHY) layer specifications for the IEEE 802.16a Standard in the OFDM and the OFDMA modes can support mobility. Along with the possibilities and limitations of the currently designed PHY we need to figure out the modifications that are necessary for adaptation of the standard and our algorithms to mobile environments.

We find that in order to extend the IEEE 802.16a to mobile environments, we need to add variable location pilot tones to the existing PHY as shown in the Figure 44. M_t and M_f in the figure correspond to the maximum tolerable distances between the pilot tones in the time and the frequency directions, respectively. Table 2 shows the M_t and the M_f

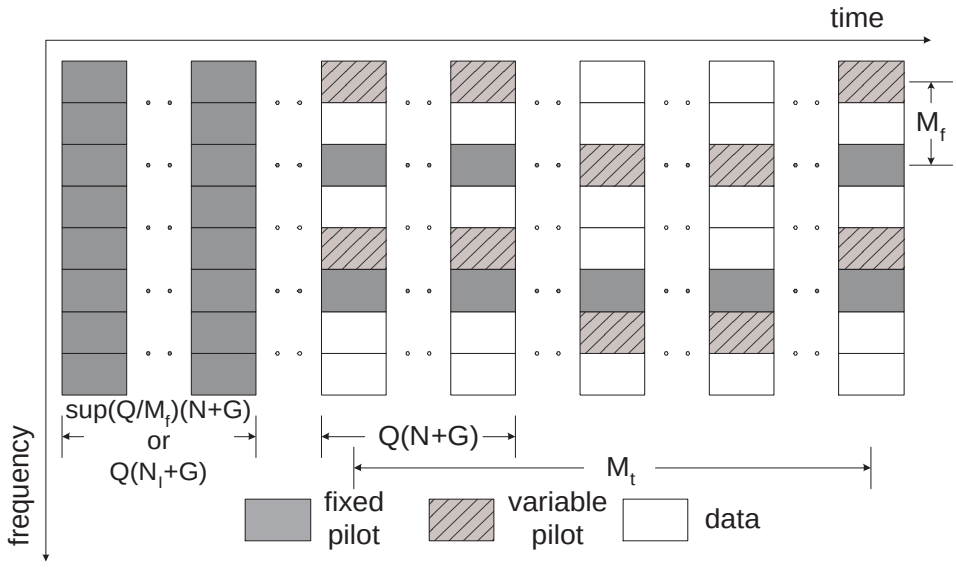

Figure 44: Frame structure for the $Q \times L$ OFDM system in an MBWA environment.

values required for an IEEE 802.16a PHY to be extended to the mobile environment using its typical channelization parameters. Figure 45 shows the preliminary bit error rate (BER)

Table 2: Maximum Tolerable Distance Between Pilot Tones in Time and Frequency Domains, IEEE 802.16a MMDS Band, $f_c = 2.4GHz$, v=80 miles/hour

BW (MHz)	M_t N=256	M_f N=256	M_t N=2048	M_f N=2048
1.5	7	18	0	146
3.0	15	9	1	73
6.0	30	4	3	36
12.0	61	2	7	18
24.0	123	1	15	9

performance curves for a 4×4 MIMO-OFDM system using the IEEE 802.16a PHY but with additional variable pilot tones inserted for channel tracking. The algorithms perform all the time and frequency synchronization tasks as suggested in [66], however for the results in these simulations, no sampling frequency offset estimation is carried out. M_f is fixed to a value of one and the effect of M_t on the BER is examined.

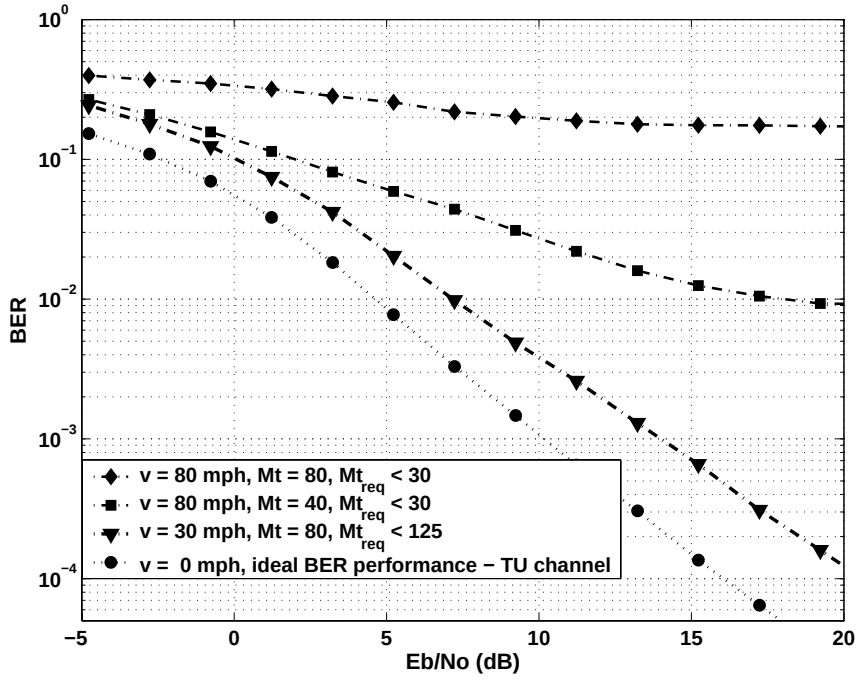

Figure 45: BER performance plots for a 4×4 MIMO-OFDM system using 16-QAM alphabet and a bandwidth of 6 MHz, with IEEE 802.16a modified PHY designed for the MBWA environment.

7.5 Effects of Insufficient Guard Interval on OFDM Systems

One of the main advantages of OFDM is its resilience to the ISI due to the presence of a guard interval. Ideally, the guard interval should be greater than the maximum delay spread of the channel. However, on many occasions due to a number of constraints such as processing power, data throughput, maximum end-to-end transmission delay, packet size and system impairments such as the SF offset, etc., [5, 16, 17, 35] the length of the guard interval is not sufficiently long. In such cases, the maximum length of the channel impulse response exceeds the guard interval duration and results in ISI, *intra*block inter-carrier interference (ICI_1) and *inter*block inter-carrier interference (ICI_2) [75, 76, 91] as shown in Figure 46.

In [76] and [91] the effect of insufficient guard interval on the performance of an OFDM system is presented . Pollet *et al.* [76] have presented an analysis for the useful (U), the ISI, the ICI_1 and the ICI_2 components of the received signal in terms of the FFT' s of the head,

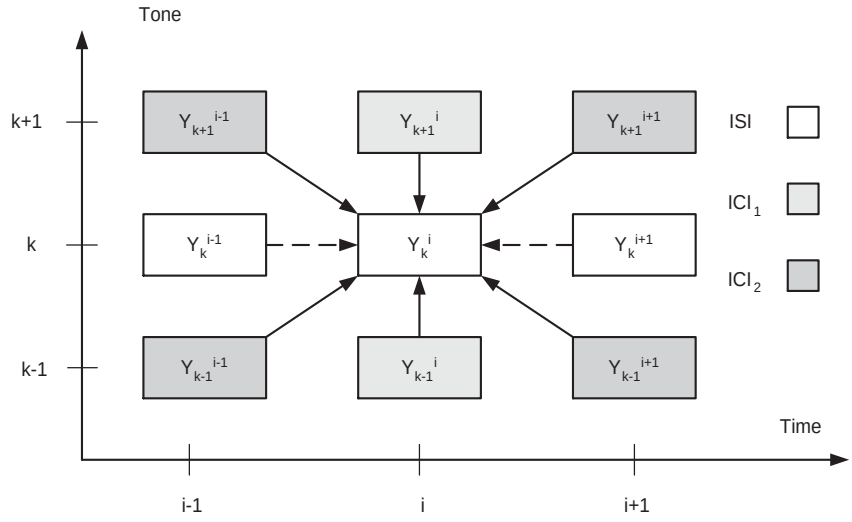

Figure 46: Interference types [75].

body and the tail of the channel impulse response. The analysis is carried out for a discrete multi-tone (DMT) system which is a type of MCM [19]. From the analytical expressions, optimum synchronization instant is obtained. *Head* is equivalent to the precursor portion of the channel impulse response. The *body* consists of ν consecutive samples of the channel impulse response containing the maximum energy and *tail* consists of the post-cursor channel impulse response. A typical channel impulse response with head, body and tail portions is shown in the Fig. 47.

The principles of OFDM apply to a DMT system. DMT systems are deployed in general for wire-line applications whereas OFDM systems are generally deployed for wireless systems. Hence in this section we explain the suggested future research from a DMT stand point.

A typical DMT transmitted signal can be expressed as follows

$$s(t) = \frac{1}{2N} \sum_{d=-\infty}^{\infty} \sum_{k=0}^{2N-1} S_k^d \sum_{n=-\nu}^{2N-1} e^{j2\pi \frac{kn}{2N}} p(t - nT - d(2N+G)T) \tag{157}$$

where pulse $p(t)$ is the pulse shape of the transmit filter, d is the running index of a DMT symbol and k is the sub-carrier index. The symmetry $S_k^d = (S_{2N-k}^d)^*$ is imposed in order obtain a real signal.

At the receiver, the signal is down converted and sampled at instants $t = d^{'}(2N+G)T +$

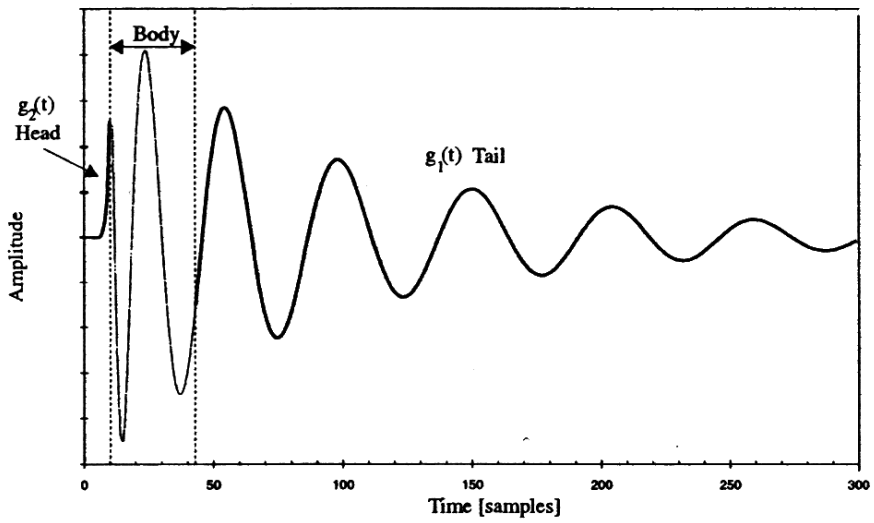

Figure 47: An example of a typical composite channel impulse response [76].

$n^{'}T + \Delta T$ where ΔT is an offset between the receiver and the transmitter symbol frame and $n^{'} \in [-G, 2N-1]$. The received down-converted sampled signal can then be expressed as

$$y_{n'+d'(2N+G)+\Delta} = \frac{1}{2N} \sum_{d=-\infty}^{\infty} \sum_{k=0}^{2N-1} \sum_{n=-G}^{2N-1} S_k^d e^{j2\pi \frac{kn}{2N}} h((n^{'}-n)T + (d^{'}-d)(2N+\nu)T + \Delta T) + N_{n'}^{d'} \quad (158)$$

where $h(t)$ denotes the composite channel impulse response (CIR) consisting of the cascade of the channel, the transmit filter and the receive filter. The terms $N_{n'}^{d'}$ are the contributions from the noise added to the DMT signal. After removal of the guard interval, the samples are demodulated using a $2N$ point FFT stage.

Assuming that the CIR is restricted to $-(2N-1-\Delta)T \leq t \leq (2N-1+G+\Delta)T$, the demodulated samples contain contributions from the transmitted symbols $\{S_{k'}^{d'-1}, S_{k'}^{d'}, S_{k'}^{d'+1}\}$, $k^{'} \in [0, \ldots, 2N-1]$ only. The useful portion of the received demodulated samples, neglecting the noise terms can then be represented as

$$U(d^{'}, k^{'}) = S_{k'}^{d'} \sum_{n=-(2N-1)}^{2N-1+G} w(n) h((n+\Delta)T) e^{-j\frac{2\pi}{2N}k^{'}n} \quad (159)$$

where the window function $w(n)$ is as shown in the Figure 48.

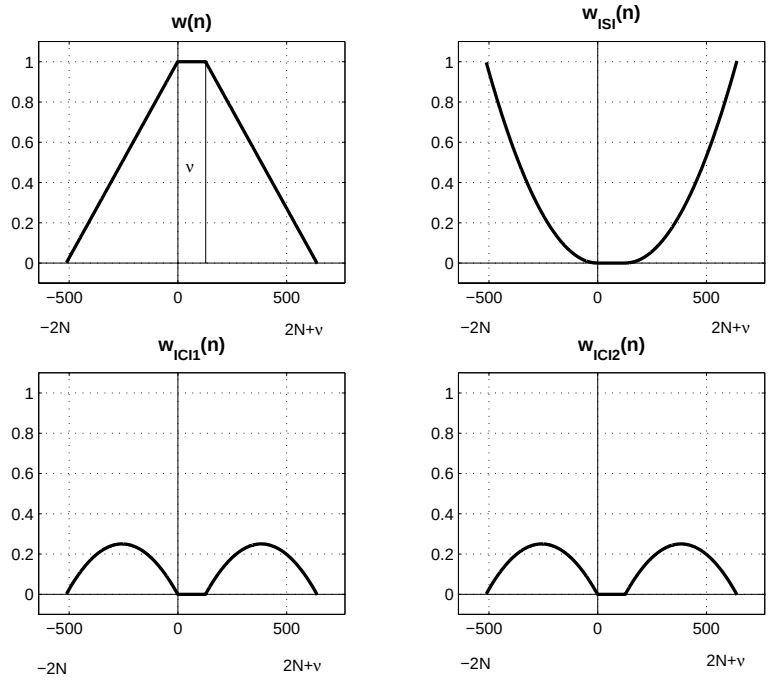

Figure 48: The weight functions $w(n)$, $w_{ISI}(n)$, $w_{ICI_1}(n)$ and $w_{ICI_2}(n)$ [76].

The ISI, ICI_1 and ICI_2 components can be represented as

$$\begin{aligned} ISI(d^{'},k^{'}) &= S_{k^{'}}^{d^{'}-1}e^{-j\frac{2\pi}{2N}k^{'}}\frac{1}{2N}\left[\mathrm{FFT}_1(k^{'})+\mathrm{FFT}_3(k^{'})\right]+ \\ &\quad S_{k^{'}}^{d^{'}+1}e^{-j\frac{2\pi}{2N}k^{'}G}\frac{1}{2N}\left[2N\mathrm{FFT}_2(k^{'})-\mathrm{FFT}_4(k^{'})\right] \qquad (160) \\ ICI_1(d^{'},k^{'},k) &= A(k-k^{'})\frac{S_k^{d^{'}}}{2N}\left[e^{-j\frac{2\pi}{2N}k\nu}\left[e^{-j\frac{2\pi}{2N}k^{'}}\mathrm{FFT}_1(k^{'})\right.\right. \\ &\quad \left.\left.-e^{-j\frac{2\pi}{2N}k}\mathrm{FFT}_1(k)\right]+\left[\mathrm{FFT}_2(k)-\mathrm{FFT}_2(k^{'})\right]\right] \qquad (161) \\ ICI_2(d^{'},k^{'},k) &= A(k-k^{'})\frac{1}{2N} \\ &\quad \left[S_k^{d^{'}-1}\left[e^{-j\frac{2\pi}{2N}k}\mathrm{FFT}_1(k)-e^{-j\frac{2\pi}{2N}k^{'}}\mathrm{FFT}_1(k^{'})\right]\right. \\ &\quad \left.+S_k^{d^{'}+1}e^{-j\frac{2\pi}{2N}kG}\left[\mathrm{FFT}_2(k^{'})-\mathrm{FFT}_2(k)\right]\right] \qquad (162) \end{aligned}$$

where

$$A(k-k^{'})=[1-e^{-j\frac{2\pi}{2N}(k-k^{'})}]^{-1}, \qquad (163)$$

and

$$\mathrm{FFT}_1(k) = \sum_{n=0}^{2N-1}h((n+\nu+1+\Delta)T)e^{-j\frac{2\pi}{2N}kn} \qquad (164)$$

$$\mathrm{FFT}_2(k) = \sum_{n=0}^{2N-1} h((n-2N+\Delta)T)e^{-j\frac{2\pi}{2N}kn} \quad (165)$$

$$\mathrm{FFT}_3(k) = \sum_{n=0}^{2N-1} nh((n+\nu+1+\Delta)T)e^{-j\frac{2\pi}{2N}kn} \quad (166)$$

$$\mathrm{FFT}_4(k) = \sum_{n=0}^{2N-1} nh((n-2N+\Delta)T)e^{-j\frac{2\pi}{2N}kn} \quad (167)$$

Note that FFT_1 and FFT_2 for $k \in [0, \ldots, 2N-1]$, are the FFTs of the sampled tail and the head of the CIR.

Presence of ISI, ICI_1 and ICI_2 degrades the performance of a DMT/ OFDM system. The net SNR per carrier avaiable at the receiver is expressed as a ratio of the power in the useful component to the power in the remaining contributions

$$\mathrm{SNR}(k^{'})(\Delta) = \frac{E[|U(d^{'},k^{'})|^2](\Delta)}{E[|ISI(d^{'},k^{'})|^2](\Delta)+E[|ICI_1(d^{'},k^{'},k)|^2](\Delta)+E[|ICI_2(d^{'},k^{'},k)|^2](\Delta)+E[|N_{k^{'}}^{d^{'}}|^2]}, \quad (168)$$

where

$$E[|U(d^{'},k^{'})|^2](\Delta) = 2NE_s \sum_{n=-\infty}^{\infty} w^2(n)h^2((n+\Delta)T) \quad (169)$$

$$E[|ISI(d^{'},k^{'})|^2](\Delta) = 2NE_s \sum_{n=-\infty}^{\infty} w_{ISI}(n)h^2((n+\Delta)T) \quad (170)$$

$$E[|ICI_1(d^{'},k^{'},k)|^2](\Delta) = 2NE_s \sum_{n=-\infty}^{\infty} w_{ICI_1}(n)h^2((n+\Delta)T) \quad (171)$$

$$E[|ICI_2(d^{'},k^{'},k)|^2](\Delta) = 2NE_s \sum_{n=-\infty}^{\infty} w_{ICI_2}(n)h^2((n+\Delta)T), \quad (172)$$

and $E_s = \mathrm{E}[|S_k^d|^2]$ is the symbol energy which is different from the *OFDM symbol energy* equal to NE_s. The various weight functions are as shown in the Fig. 48 and can be expressed as

$$w_{ISI}(n) = (1-w(n))^2 \quad (173)$$

$$w_{ICI_1}(n) = w_{ICI_2}(n) = w(n) - w^2(n) \quad (174)$$

The reduction in SNR effectively translates into reduction in the size of the constellation per subcarrier. Size of the constellation can be expressed in terms of bits/symbol and

represented as

$$b_{k'} = \left\lfloor \log_2 \left(1 + \frac{\mathrm{SNR}(k')G}{\delta J} \right) \right\rfloor \tag{175}$$

where δ is the SNR gap and it depends on the required BER, J denotes the system SNR margin and G denotes the coding gain. This results in reduction in the capacity/ throughput (bits/sec) which is given by

$$C = \frac{2N}{2N+G} \frac{1}{2NT} \sum_{k'=0}^{N} b_{k'} \tag{176}$$

An illustration of the degradation in capacity as a function of distance in meters, for a DMT system is given in Figure 49. The simulation was carried out for no interference, using a time domain equalizer (TDE/TEQ) to shorten and restrict the guard and finally with no equalization. It can be seen that the capacity reduces drastically when the guard interval is not sufficient.

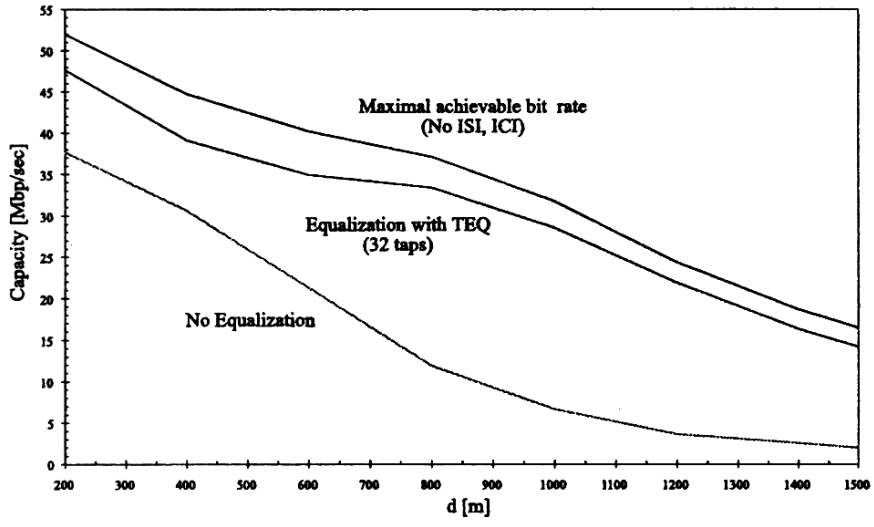

Figure 49: Throughput degradation as a function of distance [meters] caused due to the insufficient guard interval [76].

From the above equations it can be concluded that ISI, ICI_1 and ICI_2 depend on the characteristics of the head and the tail of the CIR. If most of the energy of the CIR is constrained to its body, then the effect of these interfering components can be minimized and the system capacity may be improved. Several solutions have been suggested in literature

to counter-act the effects of an insufficient guard interval in DMT systems. These include the time domain solutions in the form of inserting a TDE/TEQ at the receiver [4, 5], or inserting frequency domain equalizer (FDE/FEQ) [1–3, 109]. Such a DMT/ MCM/ OFDM system with a TEQ/FEQ is shown in the Figure 50.

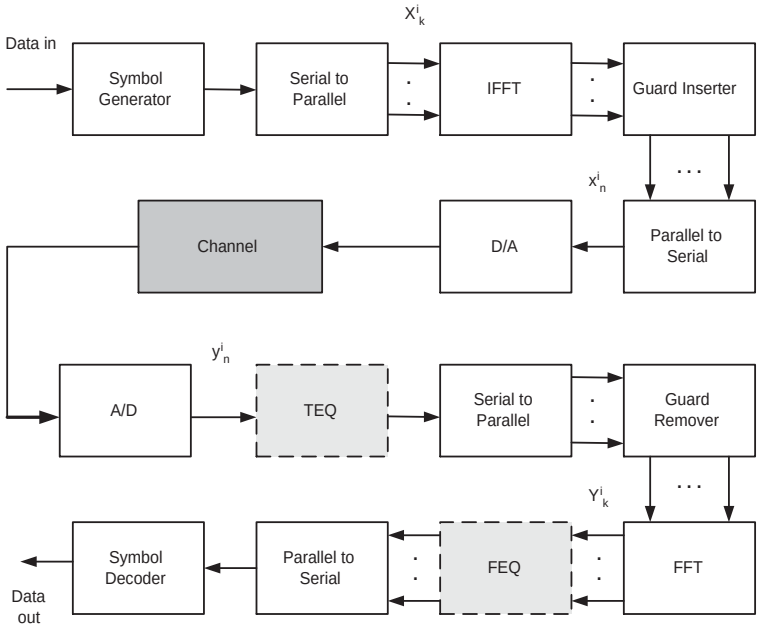

Figure 50: Commercial implementation of an OFDM system.

From the above discussion, it can be seen that an insufficient guard interval causes ISI, ICI_1 and ICI_2 which results in a reduction in the system capacity. The effects of an insufficient guard interval in MIMO-OFDM systems are expected to be pretty severe and a similar system analysis and solutions to counteract the problems are left as a future research.

7.6 Extension of the Cramér-Rao Bound Analysis to MIMO-OFDM Systems

In chapter 4 we developed the Cramér-Rao bound (CRB) for the parameters associated with SISO-OFDM systems. The extension of the bounds to MIMO-OFDM systems was not done and needs to be carried out as a future research.

APPENDIX A

GRAM-SCHMIDT ORTHOGONALIZATION TO MAKE S_K 'S UNITARY

Given a matrix $\mathbf{Sin}_k$ whose rows are not orthonormal we can use the Gram-Schmidt procedure [92] to orthonormalize the rows. The matrix $\mathbf{Sout}_k$ that is formed using this procedure is unitary provided that $\mathbf{Sin}_k$ has full rank. The first row of $\mathbf{Sin}_k$ remains unchanged and based on the first, row Gram-Schmidt procedure is performed to make the remaining rows orthonormal. The following example shows the conversion of a 3×3 matrix $\mathbf{Sin}_k$ to $\mathbf{Sout}_k$. Given $\mathbf{Sin}_k$ whose elements are chosen from a 16-PSK alphabet,

$$\mathbf{Sin}_k = \begin{bmatrix} .5774e^{0j} & .5774e^{1.5708j} & .5774e^{0j} \\ .5774e^{2.3562j} & .5774e^{0j} & .5774e^{0j} \\ .5774e^{0j} & .5774e^{-0.3926j} & .5774e^{0j} \end{bmatrix}, \tag{A 1}$$

after the Gram-Schmidt orthogonalization, we obtain a unitary $\mathbf{Sout}_k$ as follows:

$$\mathbf{Sout}_k = \begin{bmatrix} .5774e^{0j} & .5774e^{1.5708j} & .5774e^{0j} \\ .6634e^{2.3562j} & .5291e^{-0.1078j} & .5291e^{0.1078j} \\ .4760e^{-0.5890j} & .6219e^{-0.9818j} & .6219e^{1.3745j} \end{bmatrix}. \tag{A 2}$$

The conversion of $\mathbf{Sin}_k$ to $\mathbf{Sout}_k$ is as shown in Figure 51.

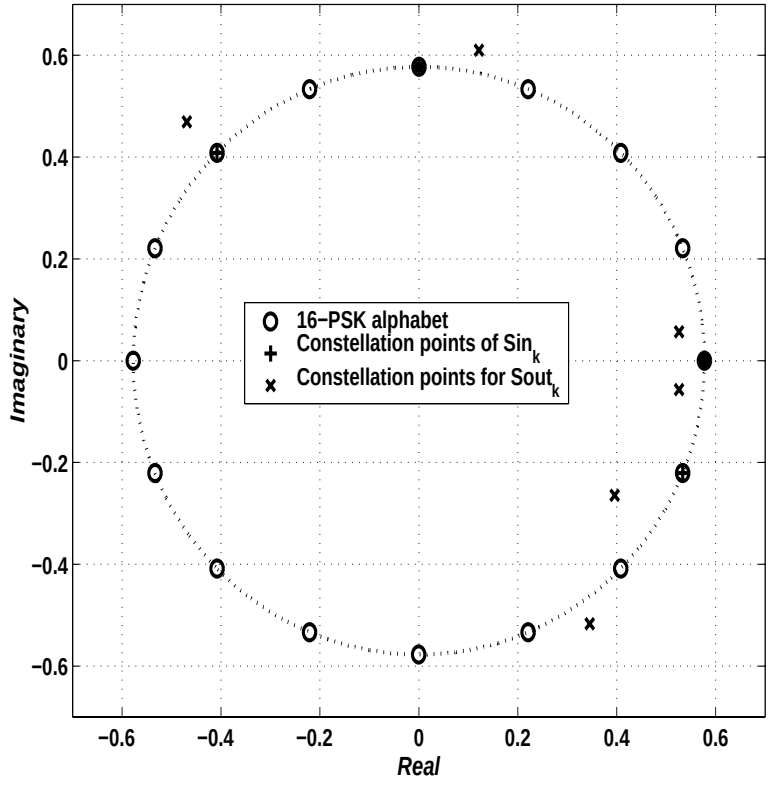

Figure 51: Graphical illustration of the Gram-Schmidt orthogonalization procedure to obtain unitary $\mathbf{S}_k$.

APPENDIX B

DERIVATION OF THE MEAN SQUARED ERROR EXPRESSIONS FOR THE ESTIMATORS

In this section we derive the MSE expressions for the SF offset, residual RF oscillator frequency offset/ phase noise, channel and the noise variance estimators.

B.1 Mean Squared Error Analysis for the Sampling Frequency/ Residual RF Oscillator Frequency Offset Estimator

For the MSE analysis of the sampling frequency offset estimator, we assume without loss of generality that $P_d = P_{d+Q}$, which implies that $f(P_d, P_{d+Q}) = 0$. The received OFDM-demodulated sample matrix at the pilot tone p is $\mathbf{R}_p^d = \underbrace{A_p^d C_p \mathbf{\Lambda}_k \mathbf{S}_p^d \cdot \mathbf{H}_p^d}_{\mathbf{X_p}} + \mathbf{W}_p$. The term $\angle\mathrm{Tr}[\mathbf{R}_p^{d\ \mathrm{H}} \mathbf{R}_p^{d+Q}]$ in the sampling and the residual frequency offset estimator can be expanded as

$$\begin{aligned} \angle\mathrm{Tr}[\mathbf{R}_p^{d\ \mathrm{H}} \mathbf{R}_p^{d+Q}] &= \angle\mathrm{Tr}[(\mathbf{X}_p^{d\ H} + \mathbf{W}_\mathbf{p}^{\mathbf{d}\ \mathbf{H}})((\mathbf{X}_p^{d+Q} + \mathbf{W}_p^{d+Q})] \\ &= \angle\Big\{\mathrm{Tr}[\mathbf{X}_p^{d\ H} \mathbf{X}_p^{d+Q}] + \mathrm{Tr}[\mathbf{X}_p^{d\ H} \mathbf{W}_p^{d+Q}] + \mathrm{Tr}[\mathbf{W}_p^{d\ H} \mathbf{X}_p^{d+Q}] \\ &\quad \mathrm{Tr}[\mathbf{W}_p^{d\ H} \mathbf{W}_p^{d+Q}]\Big\} \\ &= \angle\Big(A \cdot \exp\{j\chi\} + \epsilon_p^{'}\Big), \end{aligned} \tag{B 1}$$

where $A = \Big|\mathrm{Tr}[\mathbf{X}_p^{d\ H} \mathbf{X}_p^{d+Q}]\Big| = \sum_{q=1}^{Q} \sum_{\ell=1}^{L} |H_p^{q,\ell}|^2$, χ is the desired phase, and $\epsilon_p^{'}$ represent the contribution from the error terms. Assuming a small error analysis [40, 67], the angle of the error terms may be expressed as

$$\epsilon_p \approx \frac{\mathrm{imag}\{\epsilon_p^{'} \exp\{-j\chi\}\}}{A}. \tag{B 2}$$

Let $\underline{\theta} = [\beta\ \Upsilon]^T$ and $\underline{\hat{\theta}} = [\hat{\beta}\ \hat{\Upsilon}]^T$. From (53),

$$\underline{\hat{\theta}} = \frac{1}{(2\pi Q(1 + G/N))} (\mathbf{J}^H \mathbf{J})^{-1} \mathbf{J}^H \underline{D}. \tag{B 3}$$

Substituting the value of $\underline{D}$ yields

$$\underline{\hat{\theta}} = \frac{1}{(2\pi Q(1+G/N))}(\mathbf{J}^H\mathbf{J})^{-1}\mathbf{J}^H((2\pi Q(1+G/N))\mathbf{J}\underline{\theta} + \underline{\epsilon}). \quad \text{(B 4)}$$

Hence, $\underline{\hat{\theta}} = \underline{\theta} + \frac{1}{(2\pi Q(1+G/N))}(\mathbf{J}^H\mathbf{J})^{-1}\mathbf{J}^H\underline{\epsilon}$. The MSE in the estimates of $\underline{\theta}$ may be expressed as

$$\begin{aligned} \text{MSE}_{\underline{\hat{\theta}}} &= \text{E}\left[(\underline{\hat{\theta}} - \underline{\theta})(\underline{\hat{\theta}} - \underline{\theta})^H\right] \quad \text{(B 5)} \\ &= \text{E}\left[\left(\frac{1}{(2\pi Q(1+G/N))}(\mathbf{J}^H\mathbf{J})^{-1}\mathbf{J}^H\underline{\epsilon}\right)\left(\frac{1}{(2\pi Q(1+G/N))}(\mathbf{J}^H\mathbf{J})^{-1}\mathbf{J}^H\underline{\epsilon}\right)^H\right] \\ &= \frac{1}{(2\pi Q(1+G/N))^2}(\mathbf{J}^H\mathbf{J})^{-1}\mathbf{J}^H\text{E}\left[\underline{\epsilon}\underline{\epsilon}^H\right]\left((\mathbf{J}^H\mathbf{J})^{-1}\mathbf{J}^H\right)^H. \end{aligned}$$

The term $\text{E}\left[\underline{\epsilon}\ \underline{\epsilon}^H\right]$ is a diagonal matrix since the transmitted symbols and noise at different sub-carriers are uncorrelated. Assuming that the $\epsilon_p^{'}$ are Gaussian distributed, the $(p,p)^{\text{th}}$ element is given by

$$\text{E}[\underline{\epsilon}\underline{\epsilon}^H]_{(p,p)} = \text{E}\left[\text{Im}(\epsilon_p^{'})\text{Im}(\epsilon_p^{'})/(A)^2\right] = [N_0\bar{\mathbf{H}}^2 + N_0^2/2Q^2]/(\bar{\mathbf{H}}^2)^2. \quad \text{(B 6)}$$

where $\bar{\mathbf{H}}^2 = \text{E}\left[\sum_{q=1}^{Q}\sum_{\ell=1}^{L}|H_p^{q,\ell}|^2\right]$. Hence,

$$\left[\text{MSE}_{\underline{\hat{\theta}}_{(i)}}\right] = \left[\frac{\left[N_0 + \frac{N_0^2}{2\bar{\mathbf{H}}^2}Q^2\right]}{\left(2\pi Q\left(1+\frac{G}{N}\right)\right)^2\bar{\mathbf{H}}^2}(\mathbf{J}^H\mathbf{J})^{-1}\right]_{(i,i)} \quad \text{(B 7)}$$

and, therefore,

$$\text{MSE}_{\beta} = \left[\frac{\left[N_0 + \frac{N_0^2}{2\bar{\mathbf{H}}^2}Q^2\right]}{\left(2\pi Q\left(1+\frac{G}{N}\right)\right)^2\bar{\mathbf{H}}^2}\left(\frac{P}{P\sum_{p=1}^{P}k_p^2 - \left(\sum_{p=1}^{P}k_p\right)^2}\right)\right] \quad \text{(B 8)}$$

$$\text{MSE}_{\gamma_e} = \left[\frac{\left[N_0 + \frac{N_0^2}{2\bar{\mathbf{H}}^2}Q^2\right]}{\left(2\pi Q\left(1+\frac{G}{N}\right)\right)^2\bar{\mathbf{H}}^2}\left(\frac{\sum_{p=1}^{P}k_p^2}{P\sum_{p=1}^{P}k_p^2 - \left(\sum_{p=1}^{P}k_p\right)^2}\right)\right] \quad \text{(B 9)}$$

$$\text{MSE}_{\vartheta} = \left[\frac{\left[N_0 + \frac{N_0^2}{2\bar{\mathbf{H}}^2}Q^2\right]}{\bar{\mathbf{H}}^2}\left(\frac{\sum_{p=1}^{P}k_p^2}{P\sum_{p=1}^{P}k_p^2 - \left(\sum_{p=1}^{P}k_p\right)^2}\right)\right] \quad \text{(B 10)}$$

B.2 Mean Squared Error Analysis of the Channel Estimator

The least-square channel estimator is given by (143)

$$\hat{\mathbf{H}}_k = (\mathbf{B}_k^H\mathbf{B}_k)^{-1}\mathbf{B}_k^H\mathbf{R}_k \quad \text{(B 11)}$$

$$
\begin{aligned}
&= (\mathbf{B}_k^H \mathbf{B}_k)^{-1} \mathbf{B}_k^H (\mathbf{B}_k \mathbf{H}_k + \mathbf{W}_k) \\
&= \mathbf{H}_k + (\mathbf{B}_k^H \mathbf{B}_k)^{-1} \mathbf{B}_k^H \mathbf{W}_k
\end{aligned}
$$

Hence, the error in the channel estimates is

$$
\hat{\mathbf{H}}_k - \mathbf{H}_k = (\mathbf{B}_k^H \mathbf{B}_k)^{-1} \mathbf{B}_k^H \mathbf{W}_k, \tag{B 12}
$$

and the MSE of channel estimate is

$$
\begin{aligned}
\frac{1}{QL} \mathrm{E}\left[||\hat{\mathbf{H}}_k - \mathbf{H}_k||^2 \right] &= \frac{1}{QL} \mathrm{E}\left[\mathrm{Tr}\left[((\mathbf{B}_{\mathrm{k}}^{\mathrm{H}} \mathbf{B}_{\mathrm{k}})^{-1} \mathbf{B}_{\mathrm{k}}^{\mathrm{H}} \mathbf{W}_{\mathrm{k}}) ((\mathbf{B}_{\mathrm{k}}^{\mathrm{H}} \mathbf{B}_{\mathrm{k}})^{-1} \mathbf{B}_{\mathrm{k}}^{\mathrm{H}} \mathbf{W}_{\mathrm{k}})^{\mathrm{H}} \right] \right] \quad \text{(B 13)} \\
&= \frac{1}{QL} \mathrm{Tr}\left[((\mathbf{B}_k^H \mathbf{B}_k)^{-1} \mathbf{B}_k^H) \mathrm{E}\left[\mathbf{W}_k \mathbf{W}_k^H \right] ((\mathbf{B}_k^H \mathbf{B}_k)^{-1} \mathbf{B}_k^H)^H \right] \\
&= \frac{1}{QL} \mathrm{Tr}\left[((\mathbf{B}_k^H \mathbf{B}_k)^{-1} \mathbf{B}_k^H) (L N_0 \mathbf{I}_{Q \times Q}) ((\mathbf{B}_k^H \mathbf{B}_k)^{-1} \mathbf{B}_k^H)^H \right] \\
&= N_0.
\end{aligned}
$$

B.3 MSE is Noise Variance Estimates

The noise variance estimator is also asymptotically unbiased since

$$
\begin{aligned}
\lim_{N_{\mathrm{unused}} \to \infty} \mathrm{E}\{\{N_0^\ell\}\} &= \lim_{N_{\mathrm{unused}} \to \infty} \mathrm{E}\left\{ \frac{1}{N_{\mathrm{unused}}} \sum_{k \in \mathrm{unused}} \left| R_k^{d,l} \right|^2 \right\} \quad \text{(B 14)} \\
&= \lim_{N_{\mathrm{unused}} \to \infty} \frac{1}{N_{\mathrm{unused}}} \sum_{k \in \mathrm{unused}} \mathrm{E}\left\{ \left| R_k^{d,l} \right|^2 \right\} \\
&= \frac{1}{N_{\mathrm{unused}}} \left[N_{\mathrm{unused}} \{N_0^\ell\} \right] \\
&= N_0^\ell
\end{aligned}
$$

Mean Squared Error in noise variance estimates is given by

$$
\begin{aligned}
\mathrm{MSE}_{\mathrm{noise}} &= \mathrm{E}\{|N_0^\ell - \hat{N}_0^\ell|^2\} \\
&= \mathrm{E}\left\{ \left(N_0^\ell - \frac{1}{N_{\mathrm{unused}}} \sum_{p \in \mathrm{unused}} \left| R_p^{d,l} \right|^2 \right)^* \right. \quad \text{(B 15)} \\
&\qquad \left. \left(N_0^\ell - \frac{1}{N_{\mathrm{unused}}} \sum_{g \in \mathrm{unused}} \left| R_g^{d,l} \right|^2 \right) \right\} \\
&= \mathrm{E}\left\{ N_0^{\ell 2} - N_0^\ell \frac{1}{N_{\mathrm{unused}}} \sum_{p \in \mathrm{unused}} \left| R_p^{d,l} \right|^2 \right. \\
&\qquad \left. - -N_0^\ell \frac{1}{N_{\mathrm{unused}}} \sum_{g \in \mathrm{unused}} \left| R_g^{d,l} \right|^2 + C \right\} \\
&= \{\{N_0^\ell\}^2 - \{N_0^\ell\}^2 - \{N_0^\ell\}^2 + \mathrm{E}\{C\}
\end{aligned}
$$

where $(\ )^*$ denotes complex conjugation and $\mathrm{E}\{C\}$ is given by

$$\mathrm{E}\{C\} = \mathrm{E}\left\{ \frac{1}{N_{\text{unused}}} \sum_{p \in \text{unused}} \left| R_p^{d,l} \right|^2 \frac{1}{N_{\text{unused}}} \sum_{g \in \text{unused}} \left| R_g^{d,l} \right|^2 \right\} \tag{B 16}$$

The noise terms for $p \neq g$ are uncorrelated. Hence

$$\begin{aligned} \mathrm{E}\left\{ \left| R_p^{d,l} \right|^2 \left| R_g^{d,l} \right|^2 \right\} &= (N_0^\ell) \cdot (N_0^\ell) \text{ for } p \neq g \\ &= 1 \cdot 3 \cdot (N_0^\ell)^2 \text{ for } p = g, \end{aligned} \tag{B 17}$$

so that

$$\begin{aligned} \mathrm{E}\{C\} = \frac{1}{N_{\text{unused}}^2} \Big[& N_{\text{unused}} \cdot 3 (N_0^\ell)^2 \\ & + \left(N_{\text{unused}}^2 - N_{\text{unused}} \right) (N_0^\ell)^2 \Big] \end{aligned} \tag{B 18}$$

Hence, MSE in the noise variance estimates can be expressed as

$$\begin{aligned} \mathrm{MSE}_{\text{noise}} &= \mathrm{E}\{ |N_0^\ell - \{\hat{N}_0^\ell\}|^2 \} \\ &= \frac{2\{N_0^\ell\}^2}{N_{\text{unused}}} \end{aligned} \tag{B 19}$$

APPENDIX C

MSE PERFORMANCE FOR THE CHANNEL ESTIMATOR IN [34]

The MSE in channel estimates for the scheme described in Chapter 5 are derived as follows. We assume that the channel is not static and changes with a maximum Doppler frequency of f_m Hz which results in an ICI term in the equations [80]

$$\begin{aligned}
\mathrm{E}\{|\underline{H}^{q,\ell} - \underline{\hat{H}}^{q,\ell}|^2\} &= \frac{1}{QL}\sum_{q=1}^{Q}\sum_{\ell=1}^{L} E\left\{|\underline{H}^{q,\ell} - \underline{\hat{H}}^{q,\ell}|^2\right\} && \text{(C 1)}\\
&= \frac{1}{QL}\sum_{q=1}^{Q}\sum_{\ell=1}^{L} \mathrm{E}\left\{(\underline{H}^{q,\ell} - \underline{\hat{H}}^{q,\ell})^H(\underline{H}^{q,\ell} - \underline{\hat{H}}^{q,\ell})\right\}\\
&= \frac{1}{QL}\sum_{q=1}^{Q}\sum_{\ell=1}^{L} \mathrm{E}\left\{(\underline{W}^{q,\ell,\mathrm{AWGN}} + \underline{W}^{q,\ell,\mathrm{ICI}})^H(\underline{W}^{q,\ell,\mathrm{AWGN}} + \underline{W}^{q,\ell,\mathrm{ICI}})\right\}\\
&= \frac{1}{QL}\sum_{q=1}^{Q}\sum_{\ell=1}^{L} \left\{\mathrm{E}\{|\underline{W}^{q,\ell,\mathrm{AWGN}}|^2\} + \mathrm{E}\{|\underline{W}^{q,\ell,\mathrm{ICI}}|^2\}\right\}\\
&= \frac{1}{QL}\sum_{q=1}^{Q}\sum_{\ell=1}^{L} \left\{N_0\frac{G}{N} \right. && \text{(C 2)}\\
&\quad \left. + \frac{G}{N_I}\left[1 - \frac{1}{N_I^2}\left(N_I + 2\sum_{p=1}^{N_I-1}(N_I - p)\frac{1}{1.167}\rho(f_m T p)\right)\right]\right\}\\
&= \left\{N_0\frac{G}{N} + \frac{G}{N_I}\left[1 - \frac{1}{N_I^2}\left(N_I + 2\sum_{p=1}^{N_I-1}(N_I - p)\frac{1}{1.167}\rho(f_m T p)\right)\right]\right\}
\end{aligned}$$

Hence, the lower bound for the MSE is attained in the absence of any ICI and is given by

$$\mathrm{MSE}_{\mathrm{LB}} = N_0\frac{G}{N} \qquad \text{(C 3)}$$

APPENDIX D

USEFUL MATHEMATICAL FUNCTIONS AND FORMULAE

In this section we give some useful mathematical functions and formulae that we have used in the derivation of system model, MSE expressions and the algorithms.

D.1 Harmonic Series

$$\sum_{n=0}^{M} a^n = \frac{1-a^{M+1}}{1-a} \quad |a| \leq 1 \tag{D 1}$$

$$\sum_{n=-M}^{M} a^n = a^{-M}\frac{1-a^{2M+1}}{1-a} \quad |a| \leq 1 \tag{D 2}$$

D.2 Matrix Operations

$$\mathrm{Tr}[\mathbf{ABC}] = \mathrm{Tr}[\mathbf{CAB}] = \mathrm{Tr}[\mathbf{BCA}] \tag{D 3}$$

REFERENCES

[1] Acker, K. V., Leus, G., Moonen, M., and Pollet, T., "RLS-based initialization for per-tone equalizers in DMT receivers," *IEEE Trans. Commun.*, vol. 51, pp. 885–889, June 2003.

[2] Acker, K. V., Leus, G., Moonen, M., Wiel, O. v. d., and Pollet, T., "Per tone equalization for DMT-based systems," *IEEE Trans. Commun.*, vol. 49, pp. 109–119, Jan. 2001.

[3] Acker, K. V., Moonen, M., and Pollet, T., "Per-tone echo cancellation for DMT-based systems," *IEEE Trans. Commun.*, vol. 51, pp. 1582–1590, Sept. 2003.

[4] Al-Dhahir, N. and Cioffi, J. M., "Efficiently Computed Reduced-Parameter Input-Aided MMSE Equalizers for ML Detection: A Unified Approach," *IEEE Trans. Inform. Theory*, vol. 42, pp. 903–915, May 1996.

[5] Al-Dhahir, N. and Cioffi, J. M., "Optimum Finite-Length Equalization for Multicarrier Transcievers," *IEEE Trans. Commun.*, vol. 44, pp. 56–64, Jan. 1996.

[6] Alamouti, S., "A Simple Transmit Diversity Technique for Wireless Communications," *IEEE J. Select. Areas Commun.*, pp. 1451–1458, Oct. 1998.

[7] Alard, M. and Lassalle, R., "Principles of Modulation Channel Coding for Digital Broadcasting for Mobile Receivers," *EBU Review*, vol. 224, pp. 3–25, Aug. 1987.

[8] ANSI, "Network and Customer Installation Interfaces - Asymmetrical Digital Subscriber Line Standard (ADSL) Metallic Interface," Tech. Rep. T1.413-1995, Americal National Standards Institute, New York, 1995.

[9] A.Reial and Wilson, S. G., "Capacity Maximizing Transmitter Processing for Fading Matrix Channels," in *IEEE Comm. Theory Mini Conference*, 1999.

[10] Armada, A. G., Jiménez, V. P. G., and Darriba, J., "Phase Noise and Sub-Carrier Spacing Effects on the Performance of an OFDM Communication System," *IEEE Commun. Lett.*, vol. 2, pp. 11–13, Jan. 1998.

[11] Barhumi, I., Leus, G., and Moonen, M., "Optimal Training Design for MIMO OFDM Systems in Mobile Wireless Channels," *IEEE Trans. Signal Processing*, vol. 51, pp. 1615–1624, June 2003.

[12] Barry, J. R., Lee, E. A., and Messerschmitt, D. G., *Digital Comuunication.* Norwell, Massachusetts: Kluwer Academic Publishers, 3 ed., 2004.

[13] Berrou, C. and Glavieux, A., "Near Optimum Error Correcting Coding and Decoding:Turbo Codes," *IEEE Trans. Commun.*, vol. 44, pp. 1261–1271, Oct. 1996.

[14] Bingham, J. A. C., "Multicarrier Modulation for Data Transmission: An Idea whose Time has Come," *IEEE Commun. Mag.*, pp. 5–14, May 1990.

[15] Chen, W. and Mitra, U., "Training Sequence Optimization: Comparisons and Alternative Criterion," *IEEE Trans. Commun.*, vol. 48, Dec. 2000.

[16] Chow, J. S., Cioffi, J. M., and Bingham, J. A., "Equalizer Training Algorithms for Multicarrier Modulation Systems," *Proceedings of International Conference on Communications*, 1993.

[17] Chow, J. S., Tu, J. C., and Cioffi, J. M., "A Discrete Multitone Transciever System for HDSL Applications," *IEEE J. Select. Areas Commun.*, vol. 13, pp. 895–908, Aug. 1991.

[18] Chu, D. C., "Polyphase Codes with Good Periodic Correlation Properties," *IEEE Trans. Inform. Theory*, pp. 531–532, July 1972.

[19] Cioffi, J. M., "A Multicarrier Primer," *Tutorial presented to the Bellcore personnel,*, http://cafe.stanford.edu/people/cioffi/papers.html 1992.

[20] Classen, F. and Meyr, H., "Synchronization Algorithms for an OFDM System for Mobile Communication," in *Proceedings of ITG-Fachtagung*, pp. 105–113, Oct. 1994.

[21] Costa, E. and Pupolin, S., "M-QAM-OFDM System Performance in Presence of Non-Linear Amplifier and Phase Noise," *IEEE Trans. Commun.*, vol. 50, pp. 462–472, Mar. 2002.

[22] Coulson, A. J., "Maximum Likelihood Synchronization for OFDM Using a Pilot Symbol: Algorithms," *IEEE J. Select. Areas Commun.*, vol. 19, pp. 2486–2494, Dec. 2001.

[23] Dent, P., Bottomley, G. E., and Croft, T., "Jakes Fading Model Revisited," *Electronics Letters*, vol. 7, pp. 1162–1163, June 1993.

[24] Edfors, O., Sandell, M., van de Beek, J.-J., Wilson, S. K., and Börjesson, P. O., "OFDM Channel Estimation by Singular Value Decomposition," *IEEE Trans. Commun.*, vol. 46, pp. 931–939, July 1998.

[25] Erceg, V. and others, "An Empirically Based Path Loss Model for Wireless Channels in Suburban Environments," *IEEE J. Select. Areas Commun.*, vol. 17, pp. 1205–1211, July 1999.

[26] Erceg, V. and others, "Contribution to the IEEE 802.16a Working Group," tech. rep., IEEE, June 2003.

[27] ETSI, "Digital video broadcasting (DVB); framing structure, channel coding and modulation for digital terrestrial television (DVB-T).," Tech. Rep. ETS 300 744, European Telecommunications Standards Institute (ETSI), Nov. 1996.

[28] ETSI, "Radio broadcasting systems; digital audio broadcasting (DAB) to mobile, portable and fixed receivers.," Tech. Rep. ETS 300 401, European Telecommunications Standards Institute (ETSI), May 1997.

[29] Foschini, G. J., "Layered Space-Time Architecture for Wireless Communication in a Fading Environment When Using Multi-Element Antennas," *Bell Labs Technical Journal*, pp. 41–59, Autumn 1996.

[30] Foschini, G. J. and Gans, M. J., "On Limits of Wireless Communications in a Fading Environment When Using Multiple Antennas," *Kluwer Journal on Wireless Personal Communications*, pp. 311–335, June 1998.

[31] Frank, R. L. and Zadoff, S. A., "Phase Shift Pulse Codes with Good Periodic Correlation Properties," *IRE Transactions on Infomation Theory*, pp. 381–382, Oct. 1962.

[32] Gallager, R. G., *Low Density Parity Check Codes*. Cambridge, Massachusetts: MIT Press, 1 ed., 1963.

[33] Golub, G. H. and Loan, C. F. v., *Matrix Computations*. Baltimore, Maryland: Johns Hopkins University Press, 3 ed., 1996.

[34] Ha, J., Mody, A. N., Sung, J. H., Barry, J. R., McLaughlin, S. W., and Stüber, G. L., "LDPC Coded OFDM with Alamouti-SVD Diversity Technique," *Kluwer Journal on Wireless Personal Communications*, vol. 23(1), pp. 183–194, Oct. 2002.

[35] IEEE802.11a, "Ieee standard 802.11a-1999, part 11: Wireless lan medium access control (MAC) and physical layer (PHY) specifications: High-speed physical layer in the 5 ghz band.," Tech. Rep. 802.11, IEEE Standards Association, Piscataway, NJ, 1999.

[36] IEEE802.11n, "IEEE Wireless LAN High Throughput Task Group," tech. rep., IEEE Standards Association, http://grouper.ieee.org/groups/802/11, 2004.

[37] IEEE802.16, "Ieee standard 802.16a, for local and metropolitan area networks - part 16, air interface for fixed broadband wireless access systems - medium access control and additional physical layer specifications for 2-11 ghz.," Tech. Rep. 802.16a, IEEE Standards Association, Piscataway, NJ, 2003.

[38] IEEE802.20, "IEEE, Mobile Broaband Wireless Access (MBWA) Working Group," tech. rep., IEEE Standards Association, http://grouper.ieee.org/groups/802/20, 2004.

[39] Jianhua, Z., Rohling, H., and Ping, Z., "Analysis of ICI Cancellation Scheme in OFDM Systems with Phase Noise," *IEEE Trans. Broadcast.*, vol. 50, pp. 97–106, June 2004.

[40] Kay, S. M., *Fundamentals of Statistical Signal Processing: Estimation Theory*, vol. I. New Jersey: Prentice Hall, 1993.

[41] Kay, S. M., *Fundamentals of Statistical Signal Processing: Detection Theory*, vol. II. New Jersey: Prentice Hall, 1998.

[42] Kotecha, J. H. and Sayeed, A. M., "Optimal Signal Design for Estimation of Correlated MIMO Channels," in *Proceedings of The IEEE Int. Comm. Conf., ICC 2003*, vol. 5, pp. 3170–3174, May 2003.

[43] L. J. Cimini, J., "Analysis and Simulation of a Digital Mobile Channel Using Orthogonal Frequency Division Multiplexing," *IEEE Trans. Commun.*, vol. COM-33, pp. 665–675, July 1985.

[44] Larsson, E. G. and Li, J., "Preamble Design for Multiple-Antenna OFDM-Based WLANs With Null Subcarriers," *IEEE Signal Processing Lett.*, vol. 8, pp. 285–288, Nov. 2001.

[45] Larsson, E. G., Liu, G., Li, J., and Giannakis, G. B., "Joint Symbol Timing and Channel Estimation for OFDM Based WLANs," *IEEE Commun. Lett.*, vol. 5, pp. 325–327, Aug. 2001.

[46] Lee, W. and Zhu, J., "Channel Estimation for High-Speed Packet-Based OFDM Communication Systems," in *Wireless Personal and Multimedia Communications*, vol. 3, pp. 1293–1298, Oct. 2002.

[47] Li, J., Liu, G., Li, J., and Giannakis, G. B., "Carrier Frequency Offset for OFDM Based WLANs," *IEEE Signal Processing Lett.*, vol. 8, pp. 80–82, Mar. 2001.

[48] Li, Y. G., "Optimal Training for OFDM Systems with Multiple Transmit Antennas," in *Global Telecommunications Conference, GLOBECOM '2000*, vol. 3, pp. 1478–1482, Nov. 2000.

[49] Li, Y. G., "Pilot Symbol Aided Channel Estimation for OFDM in Wireless Systems," *IEEE Trans. Veh. Technol.*, vol. 49, pp. 1207–1215, July 2000.

[50] Li, Y. G., "Simplified Channel Estimation for OFDM Systems with Multiple Transmit Antennas," *IEEE Trans. Wireless Commun.*, vol. 1, pp. 67–75, Jan. 2002.

[51] Li, Y. G. and Ariyavisitakul, S., "Channel Estimation for Transmitter Diversity in OFDM Systems with Mobile Wireless Channels," *IEEE J. Select. Areas Commun.*, vol. 17, pp. 461–471, Mar. 1999.

[52] Li, Y. G., Seshadri, N., and Ariyavisitakul, S., "Channel Estimation for OFDM Systems with Diversity in Mobile Wireless Channels," *IEEE J. Select. Areas Commun.*, pp. 461–471, Mar. 1999.

[53] Li, Y. G., Winters, J. H., and Sollenberger, N. R., "MIMO-OFDM for Wireless Communications: Signal Detection with Enhanced Channel Estimation," *IEEE Trans. Commun.*, vol. 50, pp. 1471–1477, Sept. 2002.

[54] MacKay, D. J. C., "Good Error-Correcting Codes Based on Very Sparce Matrices," *IEEE Trans. Inform. Theory*, vol. 45, pp. 399–431, Mar. 1999.

[55] Manton, J. H., "Optimal Training Sequences and Pilot Tones for OFDM Systems," *IEEE Commun. Lett.*, vol. 5, Apr. 2001.

[56] Marzetta, T. L., "BLAST Training: Estimating Channel Capacity for High Capacity Space-Time Wireless," in *in Proc. 37$^{\text{th}}$ Annual Allerton Conference on Communication, Control and Computing*, (Monticello, IL), 1999.

[57] Mignone, V. and Morello, A., "CD3-OFDM: A Novel Demodulation Scheme for Fixed and Mobile Receivers," *IEEE Trans. Commun.*, vol. 44, pp. 1144–1151, Sept. 1996.

[58] Milewski, A., "Periodic Sequences with Optimal Properties for Channel Estimation and Fast Start-Up Equalization," *IBM J. Res. Develop.*, vol. 27, no. 5, pp. 426–431, 1983.

[59] Minn, H., Bhargava, V. K., and Letaief, K. B., "A Robust Timing and Frequency Synchronization for OFDM Systems," *IEEE Trans. Wireless Commun.*, vol. 2, pp. 822–839, July 2003.

[60] Mody, A. N., Raich, R., and Stüber, G. L., "Cramér-Rao Bounds for the Parameters Associated with SISO-OFDM Systems," *IEEE Trans. Signal Processing*, under preparation 2004.

[61] Mody, A. N. and Stüber, G. L., "Efficient Training and Synchronization Sequence Structures for MIMO OFDM Systems," in *Proceedings of The 6th OFDM Workshop*, no. 16 in 6, (Hamburg, Germany), 2001.

[62] Mody, A. N. and Stüber, G. L., "Parameter Estimation for OFDM with Tranmsit-Receive Diversity," in *Proceedings of The IEEE Vehicular Tech. Conf., (VTC 2001)*, vol. 2, (Rhodes, Greece), pp. 820–824, 2001.

[63] Mody, A. N. and Stüber, G. L., "Synchronization for MIMO OFDM Systems," in *Proceedings of The Global Communications Conference, (GLOBECOM 2001)*, (San Antonio, Texas), Nov. 2001.

[64] Mody, A. N. and Stüber, G. L., "Receiver Implementation for a MIMO OFDM System," in *Proceedings of The Global Communications Conference, (GLOBECOM 2002)*, (Taipei, Taiwan), pp. 716–720, Nov. 2002.

[65] Mody, A. N. and Stüber, G. L., "Open Loop Timing Recovery and Channel Estimation for MIMO OFDM Systems," in *Proceedings of The 8th International OFDM Workshop*, no. 16 in 8, (Hamburg, Germany), 2003.

[66] Mody, A. N. and Stüber, G. L., "Signal Acquisition and Tracking for Fixed Wireless Access MIMO-OFDM," *IEEE Trans. Wireless Commun.*, *submitted* 2004.

[67] Moose, P. H., "A Technique for Orthogonal Frequency Division Multiplexing Frequrncy Offset Correction," *IEEE Trans. Commun.*, vol. 42, pp. 2908–2914, Oct. 1994.

[68] Müller-Weinfurtner, S. H., "On Optimality of Metrics for Coarse Frame Synchronization in OFDM: A Comparison," in *Proceedings of IEEE PIMRC '98*, (Boston, MA), pp. 533–537, 1998.

[69] Narasimhan, R., "Performance of Diversity Schemes for OFDM Systems with Frequency Offset, Phase Noise and Channel Estimation Errors," *IEEE Trans. Commun.*, vol. 50, pp. 1561–1565, Oct. 2002.

[70] Necker, M. and Stüber, G. L., "Totally Blind Channel Estimation for OFDM Over Fast Varying Mobile Channels," *IEEE Trans. Wireless Commun.*, to appear.

[71] Nee, R. V. and Prasad, R., *OFDM Wireless Multimedia Communications*. Artech House, 2000.

[72] Negi, R. and Cioffi, J. M., "Blind OFDM Synchronization in ISI Channels," *IEEE Trans. Commun.*, vol. 40, pp. 1525–1534, Sept. 2002.

[73] Ng, J., Letaief, K. B., and Murch, R. D., "Complex Optimal Sequences with Constant Magnitude for Fast Channel Estimation Initialization," *IEEE Trans. Commun.*, vol. 46, Mar. 1998.

[74] Piazzo, L. and Mandarini, P., "Analysis of the Phase Noise Effects in OFDM Modems," *IEEE Trans. Commun.*, vol. 50, pp. 1696–1705, Oct. 2002.

[75] Pollet, T., Peeters, M., Moonen, M., and Vandendorpe, L., "Equalization for dmt-based broadband modems," *IEEE Commun. Mag.*, May 2000.

[76] Pollet, T., Steendam, H., and Moeneclaey, M., "Performance Degradation of Multi-carrier Systems Caused by an Insufficient Guard Interval Duration," *Proceedings of the International Workshop on Copper Wire Access Systems 'Bridging the Last Copper Drop,' CWAS '97*, pp. 265–270, 1997.

[77] Proakis, J. G., *Digital Communications*. New York: McGraw-Hill Inc., 1995.

[78] Raleigh, G. G. and Jones, V. K., "Channel Estimation for Wireless OFDM Systems," in *Proceedings of The IEEE Global Comm. Conf., GLOBECOM 1998*, vol. 2, pp. 980–985, Nov. 1998.

[79] Raleigh, G. G. and Jones, V. K., "Multivariate Modulation and Coding Wireless Communication," *IEEE J. Select. Areas Commun.*, vol. 17, pp. 851–866, May 1999.

[80] Russell, M. and Stüber, G. L., "Terrestrial Digital Video Broadcasting for Mobile Reception Using OFDM," in *Proceedings of The IEEE Vehicular Technology Conference, VTC 1992*, pp. 1694–1698, Dec. 1992.

[81] Ryu, H. G. and Lee, Y. S., "Phase Noise Analysis of OFDM Communication System by Standard Frequency Deviation," *IEEE Trans. Consumer Electron.*, vol. 49, pp. 41–47, Feb. 2003.

[82] Ryu, H. G., Li, Y. S., and Park, J. S., "Nonlinear Analysis of the Phase Noise in the OFDM Communication System," *IEEE Trans. Consumer Electron.*, vol. 50, pp. 54–63, Feb. 2004.

[83] Sandell, M., van de Beek, J. J., and Börjesson, P. O., "Timing and Frequency Synchronization in OFDM Systems Using Cyclic Prefix," in *Proceedings of IEEE Int. Symp. on Synchronization*, (Essen, Germany), pp. 16–19, Dec. 1995.

[84] Santella, G., "A Frequency and Symbol Synchronization System for OFDM Signals:Architecture and Simulation Results," *IEEE Trans. Veh. Technol.*, vol. 49, pp. 254–275, Jan. 2000.

[85] Sari, H., Karam, G., and Jeanclaude, I., "Transmission Techniques for Digital Terrestrial TV Broadcasting," *IEEE Commun. Mag.*, pp. 100–108, Feb. 1995.

[86] Scharf, L. L., *Statistical Signal Processing: Detection Estimation and Time Series Analysis*. Massachusetts: Addison-Wesley Publishing Company, 1990.

[87] Schmidl, T. M. and Cox, D. C., "Robust Frequency and Timing Synchronization for OFDM," *IEEE Trans. Commun.*, vol. 45, pp. 1613–1621, Dec. 1997.

[88] Shannon, C. E., "A Mathematical Theory of Communication," *Bell Labs Technical Journal*, vol. 27, pp. 623–656, Oct. 1948.

[89] Speth, M., Fechtel, S. A., Fock, G., and Meyr, H., "Optimum Receiver Design for Wireless Broad-Band Systems Using OFDM-Part I," *IEEE Trans. Commun.*, vol. 47, pp. 1668–1676, Nov. 1999.

[90] Speth, M., Fechtel, S. A., Fock, G., and Meyr, H., "Optimum Receiver Design for Wireless OFDM-Based Broadband Transmission-Part II: A Case Study," *IEEE Trans. Commun.*, vol. 49, pp. 571–578, Apr. 2001.

[91] Steendam, H. and Moeneclaey, M., "Analysis and Optimization of the Performance of OFDM on Frequency Selective Time Selective Fading Channels," *IEEE Trans. Commun.*, vol. 47, pp. 1811–1819, Dec. 1999.

[92] Strang, G., *Linear Algebra and its Applications*. New York: Saunders, Harcourt College Publishing, 3 ed., 1986.

[93] Stüber, G. L., *Principles of Mobile Communication*. Norwell, Massachusetts: Kluwer Academic Publishers, 2001.

[94] Stüber, G. L., Barry, J. R., Mclaughlin, S., Li, Y. G., Ingram, M. A., and Pratt, T. G., "Broadband MIMO-OFDM Wireless Communications," in *Proceedings of The IEEE*, vol. 91, pp. 271–294, Feb. 2004.

[95] Suehiro, N. and Hatori, M., "Modulatable Orthogonal Sequences and their Application to SSMA Systems," *IEEE Trans. Inform. Theory*, vol. 34, Jan. 1988.

[96] Sun, Q., Cox, D. C., Huang, H. C., and Lozano, A., "Estimation of Continuous Flat Fading MIMO channels," *IEEE Trans. Wireless Commun.*, vol. 1, Oct. 2002.

[97] Sung, J. G. and Barry, J. R., "Space Time Processing with the Channel Knowledge at the Transmitter," in *IEEE EUROCON*, July 2001.

[98] Tarokh, V. and Jafarkhani, H., "On Computation and Reduction of the Peak-to-Average Power Ratio in Multicarrier Communications," *IEEE Trans. Commun.*, vol. 48, pp. 37–44, Jan. 2000.

[99] Tarokh, V., Jafarkhani, H., and Calderbank, A. R., "Space-Time Block Codes from Orthogonal Designs," *IEEE Trans. Inform. Theory*, pp. 1456–1467, July 1999.

[100] Tarokh, V., Jafarkhani, H., and Calderbank, A. R., "Space-Time Block Coding for Wireless Communications: Performance Results," *IEEE J. Select. Areas Commun.*, vol. 17, pp. 451–460, Mar. 1999.

[101] Telatar, E., "Capacity of Multi-Antenna Gaussian Channels," *European Transactions on Telecommunications*, vol. 10, pp. 585–595, Nov. 1999.

[102] Tellambura, C., Parker, M. G., Guo, Y. J., Shepherd, S. J., and Barton, S. K., "Optimal Sequences for Channel Estimation Using Discrete Fourier Transform Techniques," *IEEE Trans. Commun.*, vol. 47, Feb. 1999.

[103] Tomba, L., "On the Effect of Wiener Phase Noise in OFDM Systems," *IEEE Trans. Commun.*, vol. 46, pp. 580–583, May 1998.

[104] Tufvesson, F., Edfors, O., and Faulkner, M., "Time and Frequency Synchronization OFDM Using PN-Sequence Preambles," in *Proceedings of The IEEE Vehicular Technology Conference 1999 (VTC '99)*, pp. 2203–2207, Sept. 1999.

[105] van de Beek, J. J. and et al., "A Time and Frequency Synchronization Scheme for Multiuser OFDM," *IEEE J. Select. Areas Commun.*, vol. 17, pp. 1900–1914, Nov. 1999.

[106] van de Beek, J. J., Sandell, M., and Börjesson, P. O., "ML Estimation of Time and Frequency Offsets in OFDM Systems," *IEEE Trans. Signal Processing*, vol. 45, pp. 1800–1805, July 1997.

[107] van de Beek, J. J., Sandell, M., Isaksson, M., and Börjesson, P. O., "Low Complexity Frame Synchronization in OFDM Systems," in *Proceedings of Int. Conf. on Universal Personal Comm.*, pp. 982–986, Nov. 1995.

[108] van Zelst, A. and Schenk, T. C. W., "Implementation of a MIMO OFDM-Based Wireless LAN System," *IEEE Trans. Signal Processing*, vol. 52, pp. 483–494, Feb. 2004.

[109] Vanbleu, K., Ysebaert, G., Cuypers, G., Moonen, M., and Acker, K. V., "Bitrate-maximizing time-domain equalizer design for DMT-based systems," *IEEE Trans. Commun.*, vol. 52, pp. 871–876, June 2004.

[110] Warner, W. D. and Leung, C., "OFDM/FM Frame Synchronization for Mobile Radio Data Communication," *IEEE Trans. Veh. Technol.*, vol. 42, pp. 302–313, Aug. 1993.

[111] Wei, L. and Schlegel, C., "Synchronization Requirements for Multi-User OFDM on Satellite Mobile and Two-Path Rayleigh Fading Channels," *IEEE Trans. Commun.*, vol. 43, pp. 887–895, Feb./Mar.Apr. 1995.

[112] Weinstein, S. B. and Ebert, P. M., "Data Transmission by Frequency Division Multiplexing Using Discrete Fourier Transform," *IEEE Trans. Commun.*, vol. COM-19, pp. 628–634, Oct. 1971.

[113] Winters, J. H., "Optimal Combining in Digital Mobile Radio with Cochannel Interference," *IEEE J. Select. Areas Commun.*, vol. sac-2, pp. 528–539, July 1984.

[114] Winters, J. H., "The Diversity Gain of Transmit Diversity in Wireless Systems with Rayleigh Fading," *IEEE Trans. Veh. Technol.*, vol. 47, pp. 119–123, Feb. 1998.

[115] Wu, S. and Bar-Ness, Y., "A Phase Noise Suppression Algorithm for OFDM-Based WLANs," *IEEE Commun. Lett.*, vol. 6, pp. 535–537, Dec. 2002.

[116] Wu, S. and Bar-Ness, Y., "OFDM Systems in Presence of Phase Noise:Consequences and Solutions," *IEEE Trans. Commun.*, vol. 52, May 2004.

[117] Yang, B., Cao, Z., and Letaief, K. B., "Analysis of Low-Complexity Windowed DFT-Based MMSE Estimator for OFDM Systems," *IEEE J. Select. Areas Commun.*, vol. 49, pp. 1977–1987, Nov. 2001.

[118] Yang, B., Letaief, K. B., Cheng, R. S., and Cao, Z., "Timing Recovery for OFDM Transmission," *IEEE J. Select. Areas Commun.*, vol. 18, pp. 2278–2291, Nov. 2000.

[119] Zhao, Y. and Huang, A., "A Novel Channel Estimation Method for OFDM Mobile Communication Systems Based on Pilot Signals and Transform-Domain Processing," in *Proceedings of The IEEE Vehicular Technology Conference 1997, VTC '97*, vol. 3, pp. 2089–2093, May 1997.

[120] Zogakis, T. N. and Cioffi, J. M., "The Effect of Timing Jitter on the Performance of a Discrete Multitone System," *IEEE Trans. Commun.*, vol. 44, July 1996.

[121] Zou, H., McNair, B., and Daneshrad, B., "Receiver for High-Speed Mobile Data Communications," in *Proceedings of The IEEE Global Communications Conference, GLOBECOM 2001*, pp. 3090–3094, Nov. 2001.

VITA

Apurva N. Mody received his B.S. degree in Electronics Engineering from the University of Bombay (Mumbai) in 1996 with First Class and Honors and M.S. degree Electrical Engineering with Highest Honors from the University of Texas at El Paso, in 1998. He is currently working on his Ph. D. in Electrical Engineering at Georgia Institute of Technology. His research interests are in the field of receiver design and signal processing for wireless and fiber optic communications. He is also involved in the wireless standardization process for the IEEE 802.16 standard for broadband wireless access. In the Summer of 1999, he worked with the optoelectronics group of Lucent Technologies in Breiningsville, Pennsylvania. During the coarse of his studies he received Cotton Memorial scholarship from the University of Texas at El Paso and President' s fellowship from Georgia Institute of Technology. He is a member of Eta Kappa Nu and Tau Beta Pi.